NTIS HC $7.00

The Effect of Gravity-Induced Free Convection Upon the Melting Phenomena of a Finite Paraffin Slab for Thermal Control

CSM-CPR-R172

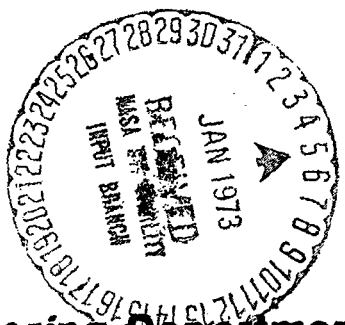

Chemical and Petroleum-Refining Engineering Department
Colorado School of Mines
Golden, Colorado 80401

THE EFFECT OF GRAVITY-INDUCED FREE CONVECTION UPON THE MELTING PHENOMENA OF A FINITE PARAFFIN SLAB FOR THERMAL CONTROL

By

R. L. Bain

F. J. Stermole

J. O. Golden

Annual Summary Report No. 1

21 Nov. 1968 - 30 June 1971

Contract NAS 8-30511, Mod 1

for

National Aeronautics and Space Administration

George C. Marshall Space Flight Center

Huntsville, Alabama 35812

CSM-CPR-R172

January 21, 1972

PREFACE

This work was prepared by Colorado School of Mines, Golden, Colorado, under contract NAS 8-30511, Mod 1 "Research in Phase Change Thermal Control Technology" and under Colorado School of Mines Foundation Contract F-6911 and F-6915. The work was administered under the direction of the Space Sciences Laboratory, George C. Marshall Space Flight Center, with Miss Barbara Richard acting as the contracting officers' technical representative.

This report covers work from 21 November, 1968, to 30 June, 1971.

The work at Colorado School of Mines was carried out by R. L. Bain under the direction of F. J. Stermole and J. O. Golden, principle investigators.

ABSTRACT

The goal of this study was to investigate the importance of gravity-induced free convection in phase-change materials and thereby contribute to the understanding of the behavior and performance of phase-change thermal control devices.

Two theoretical models were developed to predict the thermal response of the phase-change material to a given hot plate temperature. A two-dimensional pure-conduction model was developed to predict the melting of the phase-change material when heat transfer was a function of conduction. A combined conduction-convection model, also two-dimensional, was developed to predict the phase change phenomena when heat transfer was a function of conduction and gravity-induced free convection. Both models were solved using explicit finite difference approximations on a Digital Equipment Corporation, Model PDP-10, digital computer.

The experimental equipment consisted of a rectangular cell utilizing a heating chamber, an expansion chamber, and a test chamber; a sixteen-channel multipoint recorder, and a fluid flow system. The recorder monitered hot and cold plate temperatures and interior node temperatures at two second intervals.

A comparison of theoretical temperature profiles and experimental temperature profiles is presented for six runs at various angles of inclination of the test cell with respect to the horizontal direction. A detailed discussion of results is presented. As expected, since the pure conduction model neglects convection, variation exists between experimental results and theoretical results calculated using the pure conduction model at angles of inclination other than zero. At an angle of inclination of zero degrees good agreement is obtained between experimental data and the pure conduction model. Good agreement is obtained between experimental data and theoretical temperature profiles using the conduction-convection model. The results show that gravity-induced free convection is an important factor in the melting process and can be predicted using the theoretical convection model developed in this study.

TABLE OF CONTENTS

LIST OF FIGURES

List of Figures (Continued)

LIST OF TABLES

INTRODUCTION

Phase change thermal control techniques have received increasing attention, (references 1, 23, 24, 25) in the last several years for spacecraft thermal design. Because of inherent advantages of simplicity and reliability a passive solid-liquid phase change material can be used in the walls of spacecraft as packaging around sensitive electronic equipment to absorb or release energy to maintain constant temperature of the electronic equipment. However, this system is limited by the heat rejection or absorption capacity of the material used.

A previous study[2] has determined the property requirements of phase change materials in order that they be good thermal control devices. The material should be non-toxic, chemically-inert and stable, noncorrosive, have small density variations, and have a high latent heat of fusion. The material should also melt in the 50- to 150° F range; n-paraffins with an even number of carbon atoms are the most widely used materials for this purpose. In this study n-octadecane was used.

An earlier study[1] at the Colorado School of Mines dealt with an unidimensial melting investigation of a finite paraffin slab. It was concluded that the pure conduction model used did not completely solve the phase change problem. Therefore, the present study concerns the effects of gravity-induced free convection upon the melting phenomena.

All phase-change experiments, such as ground tests made in high gravity fields, must take into account the effect of gravity-induced free convection. Either the experiments must be designed to eliminate convection or the convection must be mathematically modeled. It is important to determine at what gravity level gravity-induced free convection may be neglected. This will enable designers of phase-change thermal control devices for spacecraft to determine whether or not gravity-induced free convection is an important design factor under low gravity conditions such as periods of thrust.

Other effects, such as electrically-induced convection or magnetically-induced convection, may also be important design factors. Since experiments to study other effects will be made in a high gravity field, the effect of gravity must be determined before effects of other forces can be studied completely and modeled accurately.

LITERATURE SURVEY

There has been a large amount of literature published on the subject of melting phenomena and gravity-induced free convection. This literature survey deals with only a small portion of the published material. One of the main references used in this study is the thesis of P. R. Pujado[1]. In his thesis Mr. Pujado presented a theoretical model for the unidimensional melting of a finite paraffin slab. The theoretical model was developed using finite difference methods to approximate the solution of the partial differential equations governing the physical system. The finite difference approximations were solved on an IBM-Model 360 digital computer. The model solved two-phase, unidimensional heat conduction equations with a moving interface and variable thermal properties. Mr. Pujado stated that the theoretical model neglected free convection in the liquid phase portion of the system and concluded that the errors in his results were probably due to the existence of free convection in the cell.

Earlier, Northrup Corporation[2] conducted a similar study and obtained results which compared very closely with the work Mr. Pujado did.

Some of the texts which are good theoretical references for heat transfer and fluid flow are Carslaw and Jaeger[3], Rohsenow and Choi[4], and Schlicting[5]. Longwell[6] was used as the basic theoretical reference for developing the boundary layer equations in this study. Dusinberre[7] was used for development of the interface phase-change equation used in the finite difference approximations of the theoretical equations. Bird, Stewart, and Lightfoot[8] was used as the reference for free convection between infinite parallel plates. Vallentine[9] was used as the basic ideal flow reference for the development of the ideal-viscous flow model.

Grodzka and Fan[10] listed various areas of study when attempting to solve the problem of free convection in phase change thermal control equipment. They stated that free convection might be induced through the following forces: gravity, surface tension, electricity, and magnetism.

The majority of work on free convection effects in liquids and gases has been done for infinite plate systems. Models for this type of system have been developed by Bodoia and Osterle[11], Dropkin and Globe[12], Dropkin and Somerscales[13], Gebhart[14], Kohand Price[15], and Samuels and Churchill[16].

Wilkes and Churchill[17] made a study of temperature profiles in a closed rectangular system to determine the effects of gravity induced convection. The theoretical model was developed from the basic equations of motion, energy, and continuity; a two-dimensional approach precluded the study of turbulent flow. The system of equations was solved by an implicit alternating-direction technique developed by Peaceman and Rachford[18]. Instabilities in the numerical solutions were noticed above certain Grashoff numbers.

Other closed cell convection studies have been made by Bellamy-Knights[19] and Fromm[20].

Various papers have also been published which deal with the melting of finite slabs. Chi-Tien and Yin-Chao Yen[21] developed approximate theoretical solutions for temperature distributions and melting rates when the mode of heat transfer was natural convection induced by buoyancy forces. Numerical solutions for various ice-water systems were given. Goodman and Shea[22] used a series solution to solve the problem of unidimensional melting in a finite slab. Other works on phase change phenomena include Bannister and Bentilla[23]; Ukanwa, Stermole, and Golden[24]; and Shah[25].

Papers have also been published which discussed other courses of free convection besides gravity-induced convection. Emery[26] has studied magnetically induced convection. Pearson[27] and Nield[28] have studied the effects of interfacial tension upon convection. Chandrasekar[29] studied surface tension effects, rotational effects, and magnetic effects on convection patterns.

THEORY

Two separate theoretical models are developed in this study. The first model predicts the transient temperature distribution in the system when heat transfer is a function of conduction. The second model predicts the transient temperature distribution in the system when heat transfer is a combined function of conduction and of gravity-induced free convection.

The test material used in the research was n-octadecane. The physical properties of n-octadecane are given below and in figure 1. The values were obtained from Pujado's thesis[1], Northrup's Final Report[2], and the Data Book on Hydrocarbons.[30]

Density
Solid phase = (-.0008336) T + 1.0918, gm/cc
Liquid phase = (-.0012505) T + 1.1316, gm/cc

Heat capacity
Solid phase = 2.164, watt·sec/gm ^{o}K
Liquid phase = (.008213) T - 0.14237, watt·sec/gm ^{o}K

Conductivity
Solid phase = $(-0.50054 \times 10^{-5})$ T + .002914, watts/cm ^{o}K
Liquid phase = $(-0.50054 \times 10^{-5})$ T + .002914, watts/cm ^{o}K

Melting point = 300.60 ^{o}K

Liquefaction enthalpy = 243.893 watt·sec/gm

A diagram of the system is given in figure 2.

Pure Conduction Model

The equations governing the two-dimensional problem have been developed by Carslaw and Jaeger[3]. These equations are given below.

Solid phase

$$T_t = \frac{k_s}{\rho_s C_{ps}} \left(T_{xx} + T_{yy} \right) \qquad (1)$$

Liquid phase

$$T_t = \frac{k_\ell}{\rho_\ell C_{p_\ell}} \left(T_{xx} + T_{yy} \right) \qquad (2)$$

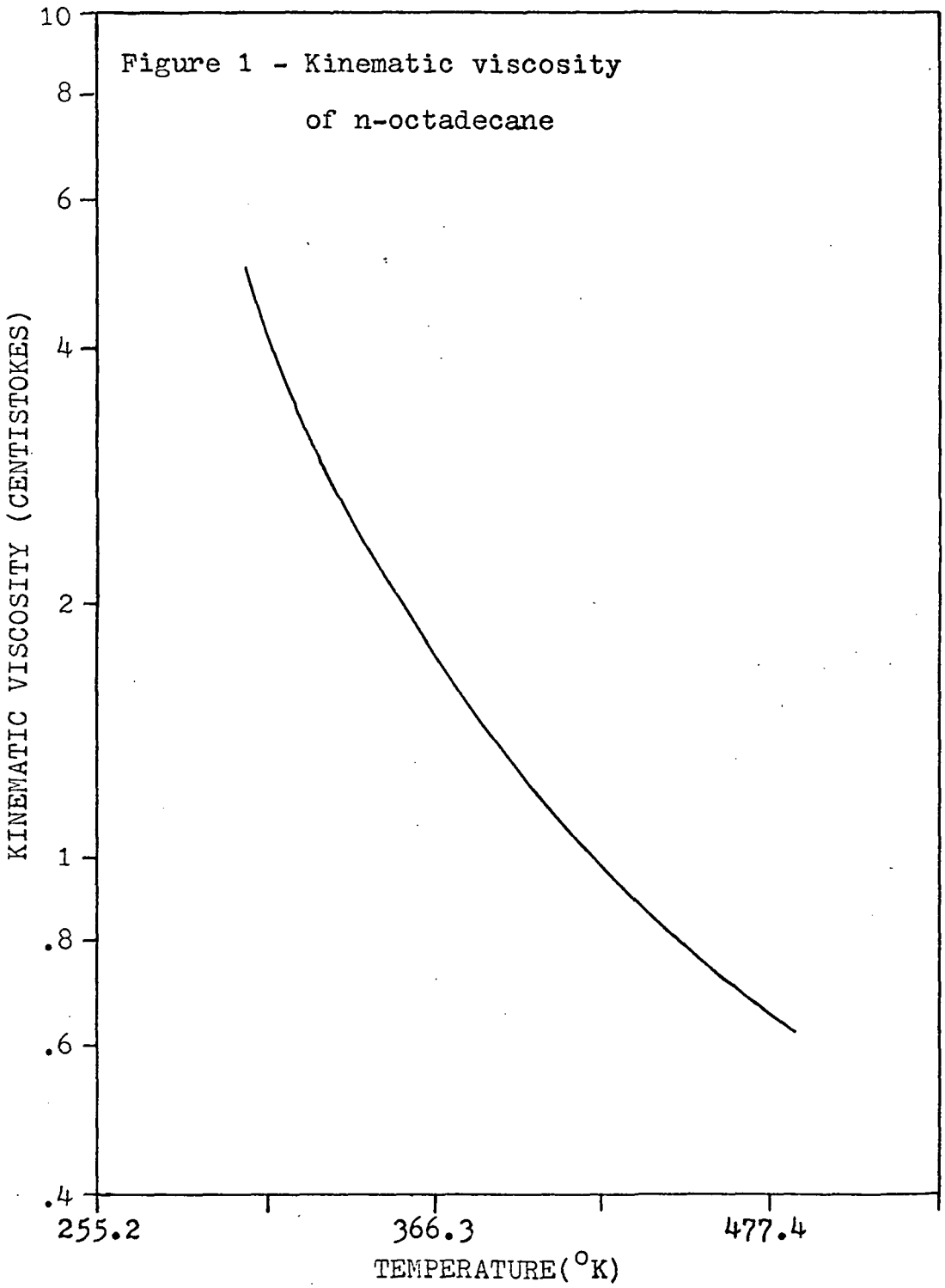

Figure 1 - Kinematic viscosity of n-octadecane

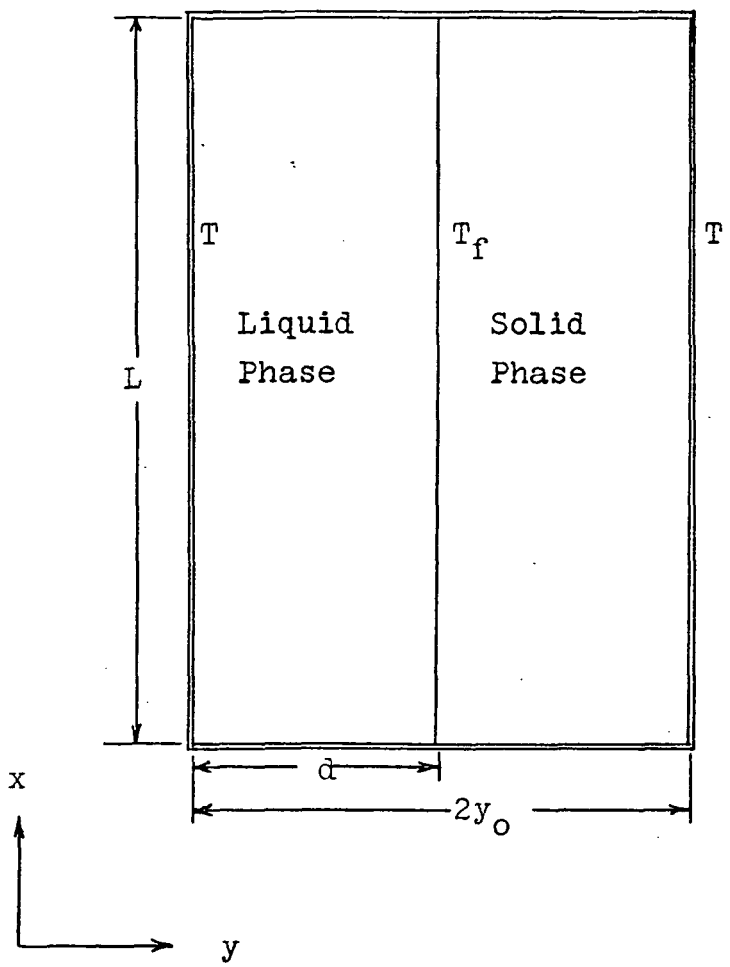

Figure 2 - Diagram of Cell

The boundary conditions for the system under study are

@ $y = 0$, $T = T_p$
@ $y = d$, $T = T_f$
@ $y = 2y_o$, $T = T_o$
@ $x = L$ and $x = 0$

Liquid phase

$$T = \frac{y}{d} (T_p - T_f) + T_f$$

Solid phase

$$T = \frac{y - d}{2y_o - d} (T_f - T_o) + T_o$$

The initial condition is

$$@ \theta = 0, \quad T (x,y,0) = T_i$$

The method of excess degrees is used to predict the phase change phenomena. When the theoretical solid phase temperature of a volume element exceeds the melt temperature a fictitious temperature, (T_s-T_f), is calculated; when the fictitious temperature, summed over time and multiplied by the heat capacity at the phase change temperature, has a larger magnitude than the liquefaction enthalpy, then the volume element has changed phase. Figure 3 gives the nodal network diagram.

An explicit, forward-difference finite-difference method is used to approximate the partial differential equations. The finite difference operators are

$$T_t = \frac{T^* (n,m) - T(n,m)}{\Delta\theta}$$

$$T_{xx} = \frac{T(n+1,m) - 2T(n,m) + T(n-1,m)}{(\Delta x)^2}$$

$$T_{yy} = \frac{T(n,m+1) - 2T(n,m) + T(n,m-1)}{(\Delta y)^2}$$

The finite difference operators are substituted into equations (1) and (2), and the resulting equations are rearranged to the final form given below:

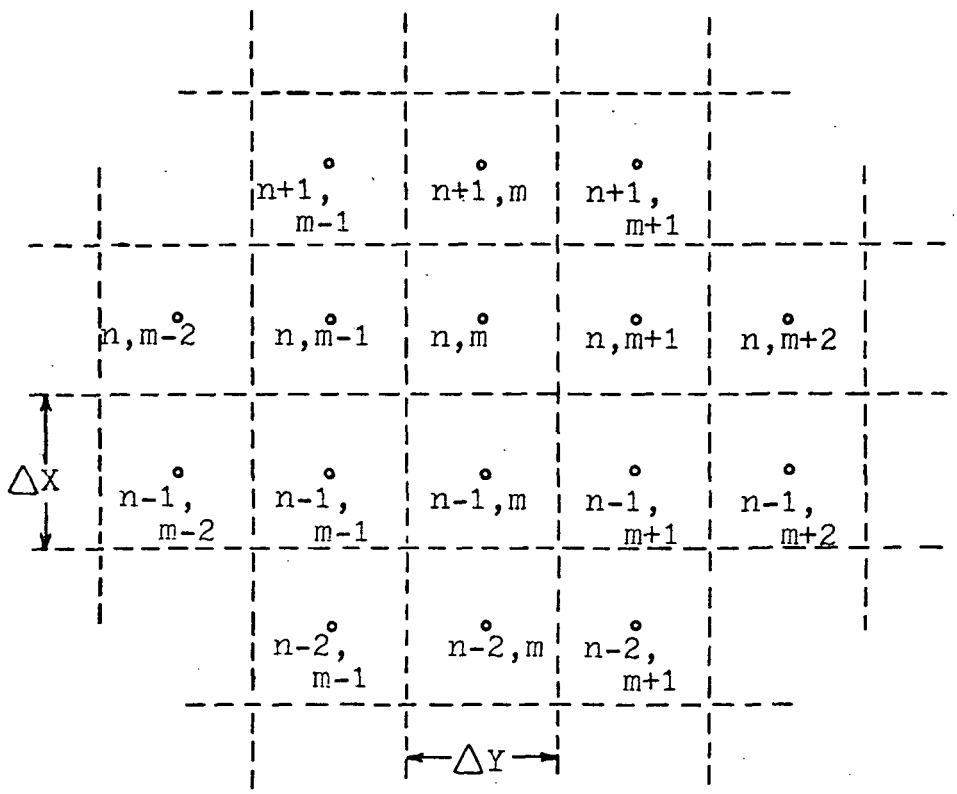

Figure 3 - Nodal Network Diagram

Solid phase

$$T^*(n,m) = T(n,m)\left(1 - \frac{2\Delta\theta k_s}{(\Delta x)^2 \rho_s C_{ps}} - \frac{2\Delta\theta k_s}{(\Delta y)^2 \rho_s C_{ps}}\right) +$$

$$\frac{k_s \Delta\theta}{\rho_s C_{ps}(\Delta x)^2} T(n+1,m) + \frac{k_s \Delta\theta}{\rho_s C_{ps}(\Delta x)^2} T(n-1,m) +$$

$$\frac{k_s \Delta\theta}{\rho_s C_{ps}(\Delta y)^2} T(n,m+1) + \frac{k_s \Delta\theta}{\rho_s C_{ps}(\Delta y)^2} T(n,m-1) \qquad (3)$$

Liquid phase

$$T^*(n,m) = T(n,m)\left(1 - \frac{2\Delta\theta k_\ell}{(\Delta x)^2 \rho_\ell C_{p\ell}} - \frac{2\Delta\theta k_\ell}{(\Delta y)^2 \rho_\ell C_{p\ell}}\right) +$$

$$\frac{k_\ell \Delta\theta}{\rho_\ell C_{p\ell}(\Delta x)^2} T(n+1,m) + \frac{k_\ell \Delta\theta}{\rho_\ell C_{p\ell}(\Delta x)^2} T(n-1,m) +$$

$$\frac{k_\ell \Delta\theta}{\rho_\ell C_{p\ell}(\Delta y)^2} T(n,m+1) + \frac{k_\ell \Delta\theta}{\rho_\ell C_{p\ell}(\Delta y)^2} T(n,m-1) \qquad (4)$$

The following two equations give the stability requirements for the finite-difference solution:

Solid phase

$$1 - \frac{2\Delta\theta k_s}{\rho_s C_{ps}(\Delta x)^2} - \frac{2\Delta\theta k_s}{\rho_s C_{ps}(\Delta y)^2} \geq 0 \qquad (5)$$

Liquid phase

$$1 - \frac{2\Delta\theta k_\ell}{\rho_\ell C_{p\ell}(\Delta x)^2} - \frac{2\Delta\theta k_\ell}{\rho_\ell C_{p\ell}(\Delta y)^2} \geq 0 \qquad (6)$$

The listing of the computer program solving the finite difference equations is given in Appendix D.

Combined Conduction and Convection Model

Gravity-induced free convection affects the heat transfer in the liquid phase of the test material. The changes are caused by flow due to density variations resulting from the temperature gradient.

The physical situation under consideration is completely described by the following equations with appropriate boundary conditions: momentum equation, energy equation, continuity equation, and an equation of state.

The initial theoretical work was directed toward a numerical solution of the above equations and of modified forms of the above equations.

However, stability problems were encountered in all numerical solutions. Because of these problems an approximate theoretical model has been developed. The development of the above equations and a discussion of the numerical solutions investigated is given in Appendix B.

The energy equation for the solid phase is given by equation (1). The energy equation for the liquid phase is

$$\frac{DT}{D\theta} = \frac{k_\ell}{\rho_\ell C_{p_\ell}} \left(T_{xx} + T_{yy} \right) \tag{7}$$

In expanded form the energy equation is

$$T_t + u\,T_x + v\,T_y = \frac{k_\ell}{\rho_\ell C_{p_\ell}} \left(T_{xx} + T_{yy} \right) \tag{8}$$

Substituting in finite difference operators, making the assumption that velocity values are those at the node being solved, and rearranging, the energy equation becomes

$$\begin{aligned} T^*(n,m) = T(n,m) \left(1 - \frac{2\,k_\ell\,\Delta\theta}{\rho_\ell C_{p_\ell} (\Delta x)^2} - \frac{2k_\ell\,\Delta\theta}{\rho_\ell C_{p_\ell} (\Delta y)^2}\right) \\ + T(n+1,m) \left(\frac{k_\ell\,\Delta\theta}{(\Delta x)^2} - \frac{u(n,m)\,\Delta\theta}{2\,\Delta x}\right) \\ + T(n-1,m) \left(\frac{k_\ell\,\Delta\theta}{(\Delta x)^2} + \frac{u(n,m)\,\Delta\theta}{2\,\Delta x}\right) \\ + T(n,m+1) \left(\frac{k_\ell\,\Delta\theta}{(\Delta y)^2} - \frac{v(n,m)\,\Delta\theta}{2\,\Delta y}\right) \\ + T(n,m-1) \left(\frac{k_\ell\,\Delta\theta}{(\Delta y)^2} + \frac{v(n,m)\,\Delta\theta}{2\,\Delta y}\right) \end{aligned} \tag{9}$$

The stability criterion from the solid-phase energy equation is

$$1 - \frac{2\,\Delta\theta\,k_s}{\rho_s C_{ps} (\Delta x)^2} - \frac{2\,\Delta\theta\,k_s}{\rho_s C_{ps} (\Delta y)^2} \geq 0 \tag{10}$$

The stability criterion from the liquid-phase energy equation

$$1 - \frac{2\,\Delta\theta\,k_\ell}{\rho_\ell C_{p_\ell} (\Delta x)^2} - \frac{2\,\Delta\theta\,k_\ell}{\rho_\ell C_{p_\ell} (\Delta y)^2} \geq 0 \tag{11}$$

$$u_{(n,m)} - \frac{2k_\ell}{\rho_\ell C_{p_\ell} \Delta x} \geq 0 \qquad (12)$$

$$v_{(n,m)} - \frac{2k_\ell}{\rho_\ell C_{p_\ell} \Delta y} \geq 0 \qquad (13)$$

Equations (12) and (13) give maximum stable values of velocity that can be used in the finite difference solution of the liquid-phase energy equation. Table I gives tabulated stability criteria for various values of Δx and Δy.

Table I

Stability Criteria

(Δx) CM	(Δy) CM	$\Delta\theta_\ell$ Sec	$\Delta\theta_s$ Sec	u CM/Sec	v CM/Sec
.3175	.15875	12.57	12.25	.00570	.01112
.2539	.2539	18.26	18.17	.00695	.00695
.2539	.15875	10.263	10.00	.00695	.0112
.15875	.079375	2.855	2.781	.01112	.02224
.079375	.079375	1.78	1.74	.02224	.02224

The velocity profile used in the convection model is an approximate profile obtained by combining an ideal flow solution for flow in a cul-de-sac region[9] with a viscous flow solution for flow between infinite parallel plates. A maximum velocity is imposed on the ideal-viscous flow pattern, using either a driving velocity calculated from the buoyancy force term or the maximum velocity calculated from the liquid-phase energy equation stability criteria.

The velocity profile for unidimensional flow between infinite vertical plates is developed by Bird, Stewart, and Lightfoot.[8] The velocity profile is

$$v = \frac{\rho\beta g b^2 \Delta T}{12\mu} (\eta^3 - \eta) \qquad (14)$$

where $\eta = y/b$

Since a maximum velocity has been determined the velocity profile should be given as a function of the maximum velocity. The equation for velocity now becomes

$$v = v_{max} \left(\frac{\eta^3 - \eta}{\eta_0^3 - \eta_0}\right) \tag{15}$$

where $\eta_0 = \pm \frac{1}{\sqrt{3}}$ (from centerline)

The ideal flow velocity profiles are developed by the use of complex variable transformations; the flow pattern under consideration is shown in the following diagram

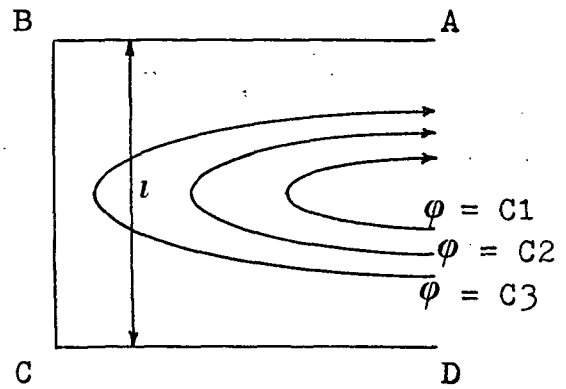

The basic assumptions made in the conformal transformation process are that (1) the flow pattern being studied is irrotational flow of a perfect fluid and that (2) the complicated flow pattern can be transformed by use of complex variables into parallel, uniform flow.

The flow pattern shown above is assumed to be a complex z-plane flow within straight-wall boundaries. Since we are investigating ideal flow with a simple polygon, a Schwarz-Christoffel transformation[9] may be used to obtain a parallel uniform flow pattern.

If the polygon is in the z-plane and the new plane is the t-plane, then

$$\frac{dz}{dt} = A^1(a-t)^{-\gamma/\pi}(b-t)^{-\epsilon/\pi}(c-t)^{-\zeta/\pi}\ldots \tag{16}$$

where A^1 = complex constant

a,b,c = real constants in ascending order of magnitude

γ, ϵ, ζ = external deflection angles of the polygon

for the flow pattern under study

$$-\gamma/\pi = -\epsilon/\pi = -\zeta/\pi = -\tfrac{1}{2}$$

The boundary conditions for the transformation are

@A, $t = -\infty$
@B, $t = -1$
@C, $t = +1$
@D, $t = +\infty$

Therefore

$$z = A^1 \int \frac{dt}{\sqrt{(1-t)\ (-1-t)}} + B^1 \qquad (17)$$

or $$z = A^1 \cosh^{-1} t + B^1 \qquad (18)$$

Applying the boundary conditions

@c $t = 1$, $z = 0$

$0 = A^1 \cosh^{-1} (1) + B^1$

$0 = B^1$

@B, $t = -1$, $z = i\ell$

$i\ell = A^1 \cosh^{-1} (-1)$

$i\ell = A^1 i\pi$

$A^1 = \ell/\pi$

Therefore

$$z = \ell/\pi \cosh^{-1} (t) \qquad (19)$$

According to definition as given by Vallentine [9] parallel, uniform ideal flow should have a source at $-\infty$ and a sink at $+\infty$. However, the above t-plane flow pattern gives a source at $+\infty$ and sink at $-\infty$. Therefore $w = -t$, where w is a new complex plane, and

$$w = -\cosh \frac{(\pi z)}{\ell}$$

, where $z = x+iy$

$$W = -\cosh \left(\frac{\pi x}{\ell} \quad i\frac{\pi y}{\ell}\right)$$

or $$w = -\cosh\left(\frac{\pi x}{\ell}\right)\cos\left(\frac{\pi y}{\ell}\right) - i \sinh\left(\frac{\pi x}{\ell}\right)\sin\left(\frac{\pi y}{\ell}\right) \qquad (20)$$

By definition of complex flow

$$\varphi = -\cosh\frac{\pi x}{\ell}\cos\frac{\pi y}{\ell} \tag{21}$$

$$\psi = -\sinh\frac{\pi x}{\ell}\sin\frac{\pi y}{\ell} \tag{22}$$

The stream function is defined by the following equations

$$u = \psi_y \tag{23}$$

$$v = -\psi_x \tag{24}$$

Substituting into equation (22) and differentiating we obtain

$$u = -\frac{\pi}{\ell}\sinh\left(\frac{\pi}{\ell}x\right)\cos\left(\frac{\pi}{\ell}y\right) \tag{25}$$

and

$$v = \frac{\pi}{\ell}\cosh\left(\frac{\pi}{\ell}x\right)\sin\left(\frac{\pi}{\ell}y\right) \tag{26}$$

The liquid phase is split into three regions; as shown below.

Region I	Region II	Region III
IDEAL FLOW	VISCOUS FLOW	IDEAL FLOW

Region I flow is governed by equations (22), (25), and (26) with appropriate boundary conditions. Region II is governed by equation (15) with a given maximum velocity. Region III is governed by another set of ideal flow equations; but assuming symmetrical flow it is not necessary to develop the equations for this region.

The ideal flow regions are coupled to the viscous flow region by assuming that the velocities in the viscous flow region are the boundary velocities for the ideal flow region. All y velocities are zero at this boundary. By use of equation (22) values of the stream function may be calculated at the ideal flow-viscous flow boundary. Since there can be no flow across a line of constant stream function, velocities in the ideal flow region can be related to boundary velocities at calculated values of the stream function at the boundary. By this method a pseudo-viscous flow pattern can be imposed on the ideal flow regions.

The actual liquid phase in the test cell does not have a constant depth. The velocities calculated by the ideal flow-viscous flow model are imposed on the liquid phase at a point by assuming the depth of the liquid phase at that point to be the depth of the cell in the ideal flow-viscous flow model.

The flow pattern calculated is only an approximation, but with the small magnitude of allowable velocities calculated by stability criteria

the velocities calculated should give fairly accurate flow patterns in the liquid phase.

A listing of the conduction-convection model computer program is given in Appendix E.

An additional source of error exists in the finite difference solution of equation (8). The finite difference approximation neglects the second order partial differential with respect to time, and considers it be a truncation error to be included with higher order truncation errors.

If the second order partial is kept equation (8) now becomes

$$T_t + \frac{\Delta t}{2} T_{tt} + u T_x + v T_y = \frac{k}{\rho c_p} (T_{xx} + T_{yy}) \qquad (27)$$

When equation (8) is rearranged to solve for T_t and then substituted into equation (27) the resulting equation is

$$T_t + u T_x + v T_y = \left(\frac{k}{\rho c_p} - \frac{\Delta t u^2}{2} \right) T_{xx} + \left(\frac{k}{\rho c_p} - \frac{\Delta t v^2}{2} \right) T_{yy} - \Delta t\, uv\, T_{yx} \qquad (28)$$

The magnitude of the numerical dispersion coefficient is approximately one-half the value of the thermal diffusivity coefficient for values of physical properties, time step, and velocity levels used in the numerical solution.

EQUIPMENT AND PROCEDURE

The test cell, figure 4, consisted of a rectangular test chamber, a heating chamber, and an expansion chamber. The test chamber was 2.54 cm by 12.7 cm by 12.7 cm. Fourteen iron-constantan thermocouples were placed in the test chamber for the purpose of recording temperatures. A valve was placed in the heating chamber, which connected the test chamber and expansion chamber. The expansion chamber was included in the cell design because the cell was originally designed for use in a vacuum; this fact necessitated the use of a completely closed system. The heating chamber consisted of a rectangular copper cell with an entrance port on each of the vertical walls and two exit ports through the top plate of the chamber.

Although the cell was designed and built as a completely closed system, with all edges sealed, leaks were encountered when the cell was first used. The problem was overcome by the use of an epoxy coating on all joints, and by making experimental runs at lower temperatures than originally planned.

The heating system, figure 5, consisted of a constant temperature bath, a centrifugal pump, 6 tygon lines connecting the bath, pump, and test cell. The constant temperature bath was a 5-liter glass tank, two immersion heaters, and a stirrer. The heating fluid used was water.

The recorder used was a Bristol multipoint recorder. Sixteen channels were used, with a two-second interval between points recorded. The accuracy of the recorder was $\pm 0.417^{o}K$. The leads from the test cell were connected directly into the recorder.

The cell filling apparatus, figure 6, consisted of a cell filler and a constant temperature bath. The test material was heated by running water in coils from the constant temperature bath through the cell filler. The bath was kept at $305^{o}K$; this temperature was used because a small solid-liquid density change in the test material was desired when filling the cell. The test material was degassed by the use of a magnetic stirrer.

Experimental runs were made using the following procedure:

1. The constant temperature bath was allowed to heat to approximately $2.22^{o}K$ higher than the desired hot plate temperature; this procedure allowed for the small cooling effect of the cold water present in the expansion chamber of the test cell.

2. The recorder was allowed to run during the heating period in order to check the initial steady state temperatures and to monitor the heating tank temperature.

3. When the tank was at the desired temperature the run was initiated by turning on the pump.

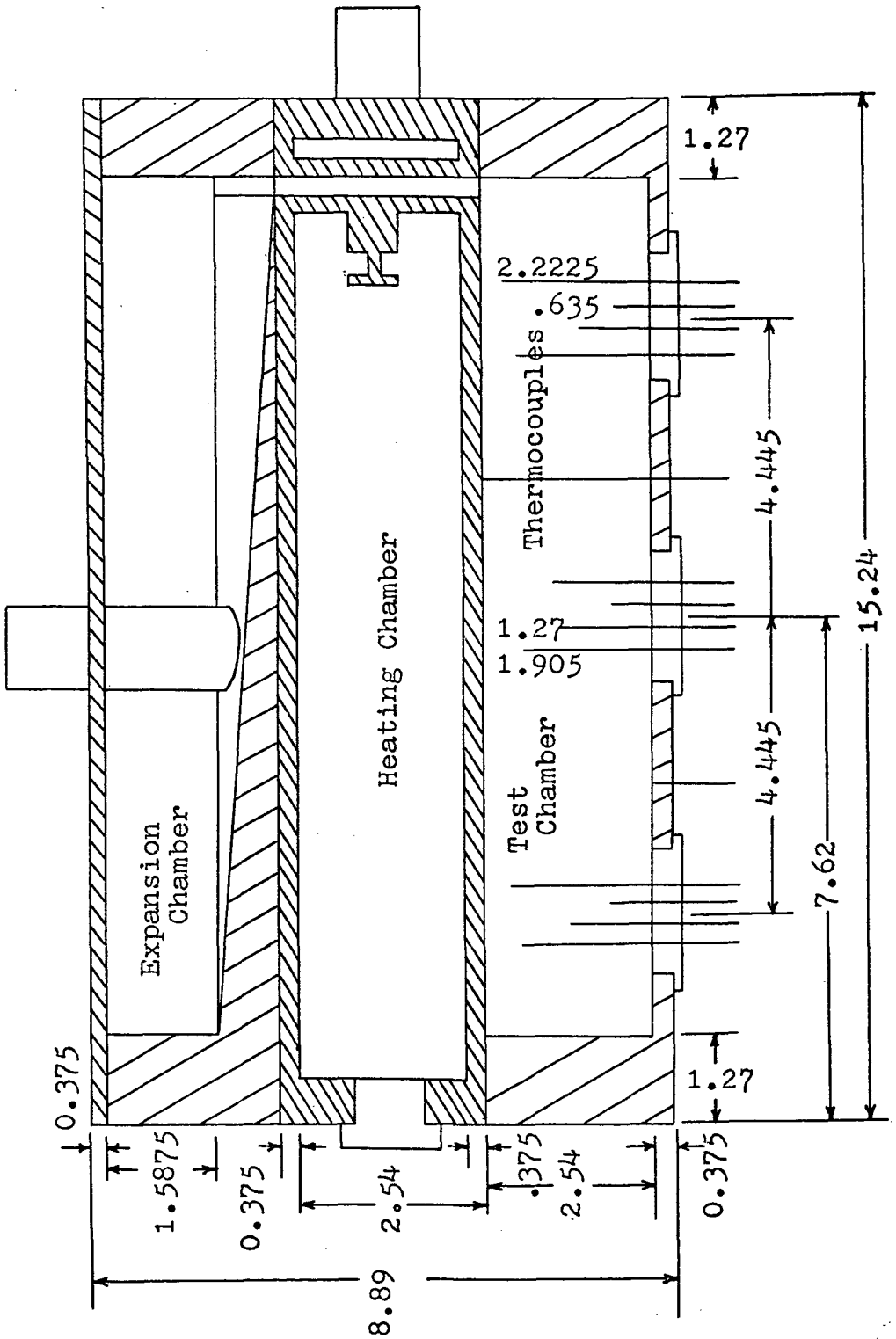

Note: All dimensions are in cm

Figure 4 - Pseudosection of Test Cell: Scale 1cm:1cm

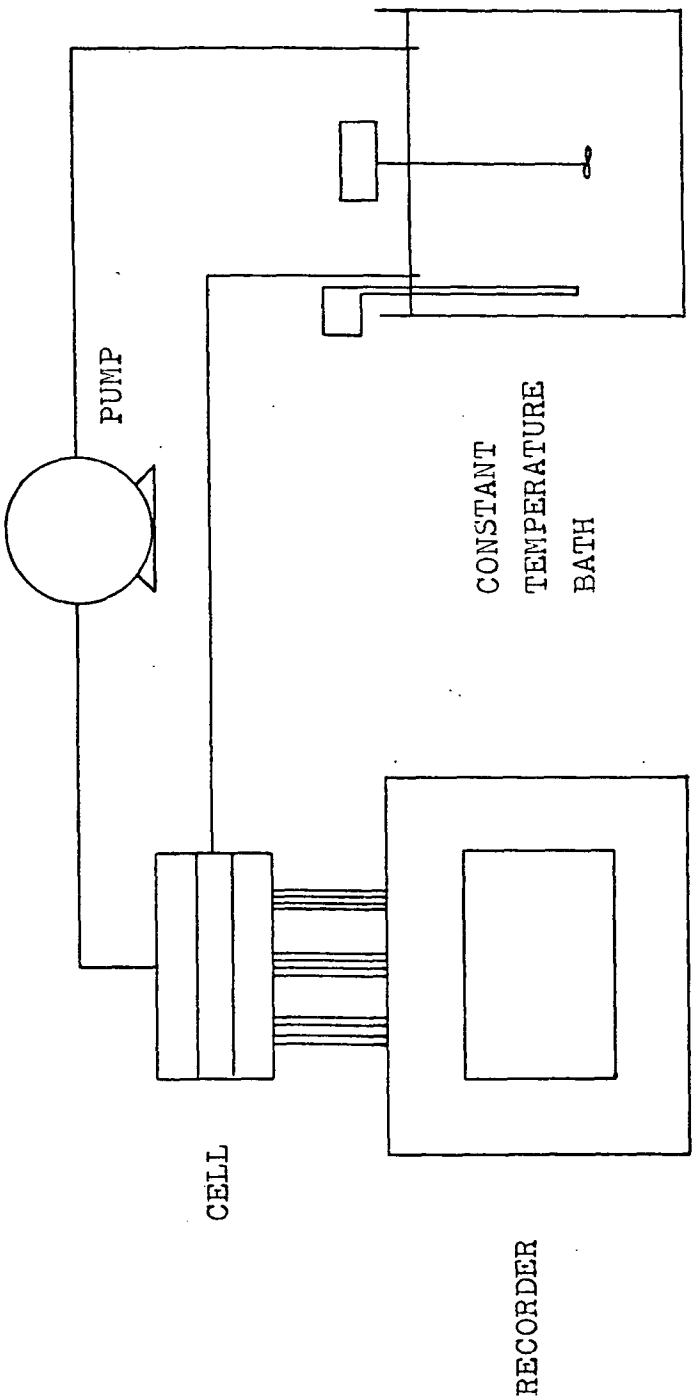

Figure 5 - Equipment Flowchart

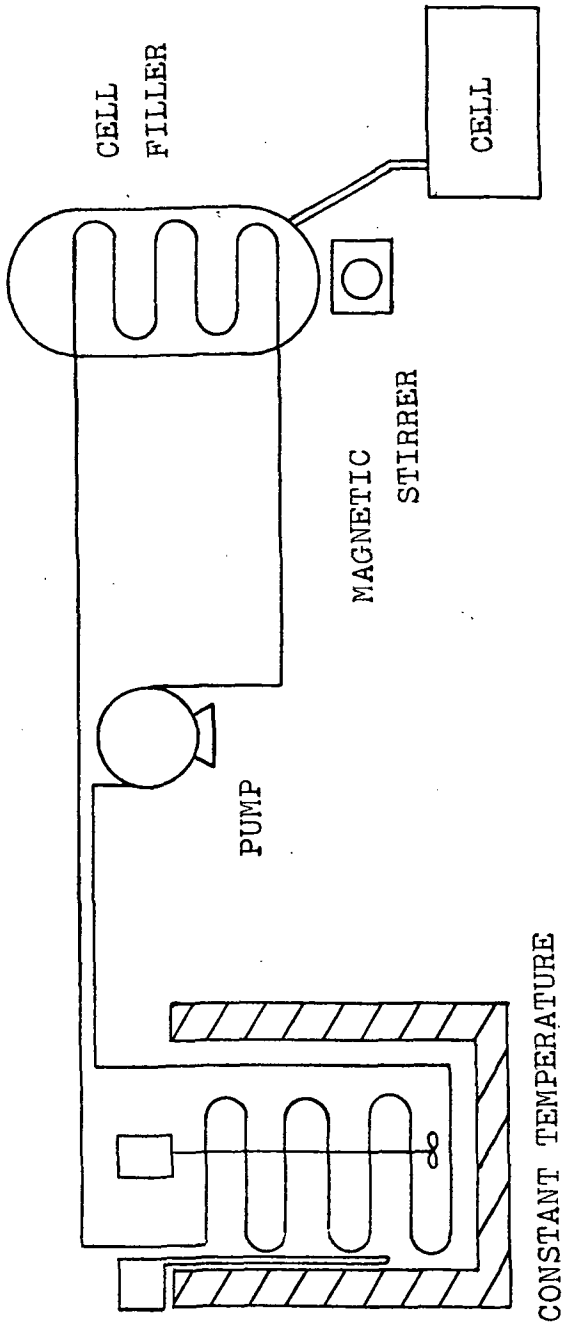

Figure 6 - Cell Filling Apparatus

4. The duration of the run was approximately 40 minutes.

Runs were made at angles of inclination of 0-, 30-, and 60- degrees. Runs were not made at higher angles of inclination because the phase-change material melted completely in the top part of the test cell.

DISCUSSION OF RESULTS

The results from six data runs have been compared with the theoretical temperature profiles predicted by the pure conduction model program and the conduction-convection model program. The results obtained show the effect that gravity has upon the phase change process. The results show that the pure conduction model cannot predict actual temperature profiles in the phase change material if gravity-induced free convection is present. However, good agreement is obtained for results comparing experimental data and the conduction-convection model.

Figure 7 presents results for y = 0.635 cm at an angle of inclination of 0^{o}. The spread in experimental results is due to the presence of air bubbles in the liquid phase. At an angle of inclination of 0^{o} the pure conduction model predicts the experimental temperature profiles closely, considering that the air bubbles do affect the experimental temperature profiles.

Figure 8 shows results for y = 1.27 cm at an angle of inclination of 0^{o}. Good agreement is obtained between experimental data and the pure conduction model temperature profile. Figure 9 presents a comparison of experimental data to the pure conduction temperature profile for the same run at y = 1.905. Again good agreement is obtained between the theoretical temperature profile and experimentally measured temperatures.

Figures 10, 11, and 12 present comparions of experimental data to theoretical pure conduction temperature profiles for Run 7 at y equal 0.635 cm, 1.27 cm, and 1.905 cm, respectively. The angle of inclination is again 0^{o}. The 0.635 cm results again show spread. The main cause of thy spread is due to air bubbles. In figure 7 and figure 10 the thermocouple at the middle of the cell records a lower temperature than the thermocouples at the ends of the cell. Part of this difference may be due to the fact that the plexiglas has a slightly higher thermal diffusivity than the n-octadecane. Therefore, the results are also showing end effects due to higher temperatures in the plexiglas walls. The 1.27 cm and 1.905 cm results again present good agreement between experimental results and theoretical prediction.

Figures 13, 14, and 15 present a comparison of experimental data to pure conduction temperature profiles for Run 3 at y equal 0.3175 cm, 0.635 cm, and 1.27 cm, respectively. These results are presented to show qualitatively the effects of free convection. In figure 13, the thermocouple at x = 2.8575 cm takes the longest time to melt; the thermocouple at x = 11.1125 cm takes the shortest time to melt. The thermocouple at x = 6.6675 cm melts at an intermediate time. This trend is to be expected when gravity-induced free convection is present. The depth of liquid should be larger at the top of the cell than at the bottom; as measured along the long axis of the cell the large x-positions will be referred to as the top of the cell, intermediate x-positions

as the middle of the cell, and small x-positions as the bottom of the cell. Since the pure conduction model predicts the same temperature profile for all three x-positions it is evident that the model cannot predict the experimental temperature profiles obtained.

The same trend is present in figure 14; but in this case only the thermocouple at x = 10.16 cm deviates from the others during the duration of the experimental run. The pure conduction model cannot predict this deviation in experimental temperatures.

Figure 15 again shows the deviation of experimental results from the pure conduction model prediction. At this y position the time required for the deviation in temperature to occur is longer than in figures 13 and 14; but still it is evident that the pure conduction model does not predict the temperature profiles when convection is present.

Figures 16 and 17 present theoretical and experimental comparisons for Run 4 at y = 0.3175 cm and y = 0.635 cm. These results show the same trends as figures 13 and 14. They are presented to show that convection occurs in more than just one run. The pure conduction model does not predict the effect of convection evident in experimental data.

The results presented in figures 7 through 17 show that the pure conduction model will predict experimental temperature profiles when convection is not present, but will not predict experimental temperature profiles when convection is present.

Figures 18 through 44 present a comparison of experimental data to both the convection model and pure conduction model for angles of inclination of 30^{o} and 60^{o}. If only one theoretical curve is shown in a figure it indicates that both theoretical models predict approximately the same temperature profile.

Figures 18 through 26 show results for Runs 8 and 10, both made at an angle of inclination 60^{o}. Some spread in experimental results is evident; the spread is due to the presence of air bubbles. Figures 18, 19, and 20 give results at small x-positions. Figure 19 shows that the convection model predicts the experimental results more closely than the pure conduction model. It should also be noticed that the convection model predicts a lower temperaturyprofile than the pure conduction model. Figures 20 and 21 show good agreement between both theoretical models and experimental data.

Figures 21, 22, and 23 present results at intermediate x-positions. Both models predict approximately the same temperature profile; there is a small difference in figure 21, due to different nodal sizes used in the models. Both models predict the experimental results, taking into account some spread in experimental results, due to air bubbles (see Figure 21).

Figures 24, 25, and 26, at the larger x-positions, show the largest deviations between the pure conduction model and the convection model. In all three figures the convection model has better agreement with experimental data than does the pure conduction model. Deviation between figure 19 shows that the convection model predicts the experimental results more closely than the pure conduction model. It should also be noticed that the convection model predicts a lower temperature profile than the pure conduction model. Figures 20 and 21 show good agreement between both theoretical models and experimental data.

Figures 21, 22, and 23 present results at intermediate x-positions. Both models predict approximately the same temperature profile; there is a small difference in figure 21, due to different nodal sizes used in the models. Both models predict the experimental results, taking into account some spread in experimental results, due to air bubbles (see figure 21).

Figures 24, 25, and 26, at the larger x-positions, show the largest deviations between the pure conduction model and the convection model. In all three figures the convection model has better agreement with experimental data than does the pure conduction model. Deviation between experimental data and the convection model is caused by the reduced gravity field used in the convection model and imposed by velocity stability criteria in the energy equation for the model At this end of the cell the convection model predicts higher temperatures than predicted by the pure conduction model. This trend agrees with experimental results obtained.

Figures 27 through 35 present results obtained for a 30^{o} run. Figures 27, 28, and 29 represent thermocouples located at small x-positions. The y = 1.27 cm and y = 1.905 cm theoretical curve, both convection and conduction models, agrees very closely with the experimental results. At y = 0.635 cm the convection model agrees closely with experimental data; the pure conduction model deviates from the experimental data and predicts higher temperatures than obtained experimentally. Figures 30, 31, and 32 present a comparison of theoretical and experimental results at intermediate x-positions. At all y positions good agreement is obtained between theory and data; both models predict the same temperature profiles at all y positions. Figures 33, 34, and 35 represent thermocouples located at large x-positions. The convection predicts all temperature profiles closely; while deviation occurs between the pure conduction model and experimental data at y = 0.635 cm and y = 1.27 cm. The convection model predicts higher temperatures than does the pure conduction model.

Figures 36 through 43 present results obtained for another 30° angle of inclination run. The results from this run are presented separately because the initial temperature is different from run 4. Figure 36, 37, and 38 show a comparison of experimental data and theoretical temperature profiles for small x-positons. As in the previous cases the y = 1.27 cm and y = 1.905 cm results show good agreement between theory and data. At y = 0.635 cm the convection model predicts a lower temperature profile than does the pure conduction model; again the convection model temperature profile is closer to the experimental data than the conduction model temperature profile. Figures 39, 40, and 41 present a comparison of theoretical and experimental results at intermediate x-positions. The theoretical results, both conduction and convection, agree very closely with experimental data. There is some deviation, at y = 0.635 cm, due to air bubbles.

Figures 42, 43, and 44 show comparisons of theory and data for large x-positions. At all y-positions the convection model more closely predicts the experimental data than does the pure conduction model. At y = 0.635 cm and at y = 1.905 cm the experimental phase change takes place sooner than theoretically predicted by the convection model; the deviation is due to stability limitations and numerical dispersion effects.

Figures 45, 46, and 47 present theoretical results showing the effect of velocity level upon the shape of the solid-liquid interface. At v_{max} = 0.0107 cm/sec the maximum difference in interface position between the top, x = 10.16 cm, and bottom, x = 2.54 cm, is 0.762 cm. At v_{max} = 0.00535 cm the maximum difference is 0.278 cm. At v_{max} = 0.002675 cm the maximum difference is 0.056 cm; this difference is negligible since the y used in the calculation was 0.076 cm. At this theoretical velocity level the pure conduction model can be used to predict temperature profiles and gravity level.

Figure 48 is included to show the effect of velocity level upon temperature profiles. At x = 10.16 cm, y = 0.635 cm the pure conduction model has the largest deviation from a typical experimental temperature profile. As the velocity level increases the convection effect becomes larger and the theoretical profiles more closely predict the experimental profile. Since, due to stability criteria, 0.0107 cm/sec is the largest allowable maximum velocity the experimental profile cannot be exactly predicted. There is no effect due to convection at the intermediate x-position, figure 48-b. At the low x-position, figure 48-c, the results show that the convection model will predict the experimental results closely even at low velocity levels.

Figure 49 presents results from theoretical computer runs made to determine numerical dispersion effects.

At the middle of the test cell, figure 49-b, there is no apparent effect of numerical dispersion. At the top and bottom of the cell, figures 49-a and 49-c, the effect shows the same trends as varying the velocity level, but with the time step range used in this study the effect is smaller than

varying the velocity. The solutions are not convergent with the time steps used, but due to computer limitations smaller time steps could not be used.

No comparisons between experimental data and the convection model is presented for y = 0.3175 cm in this discussion of results. Because of air bubbles large deviations occur between data and theory. These results are presented in Appendix C.

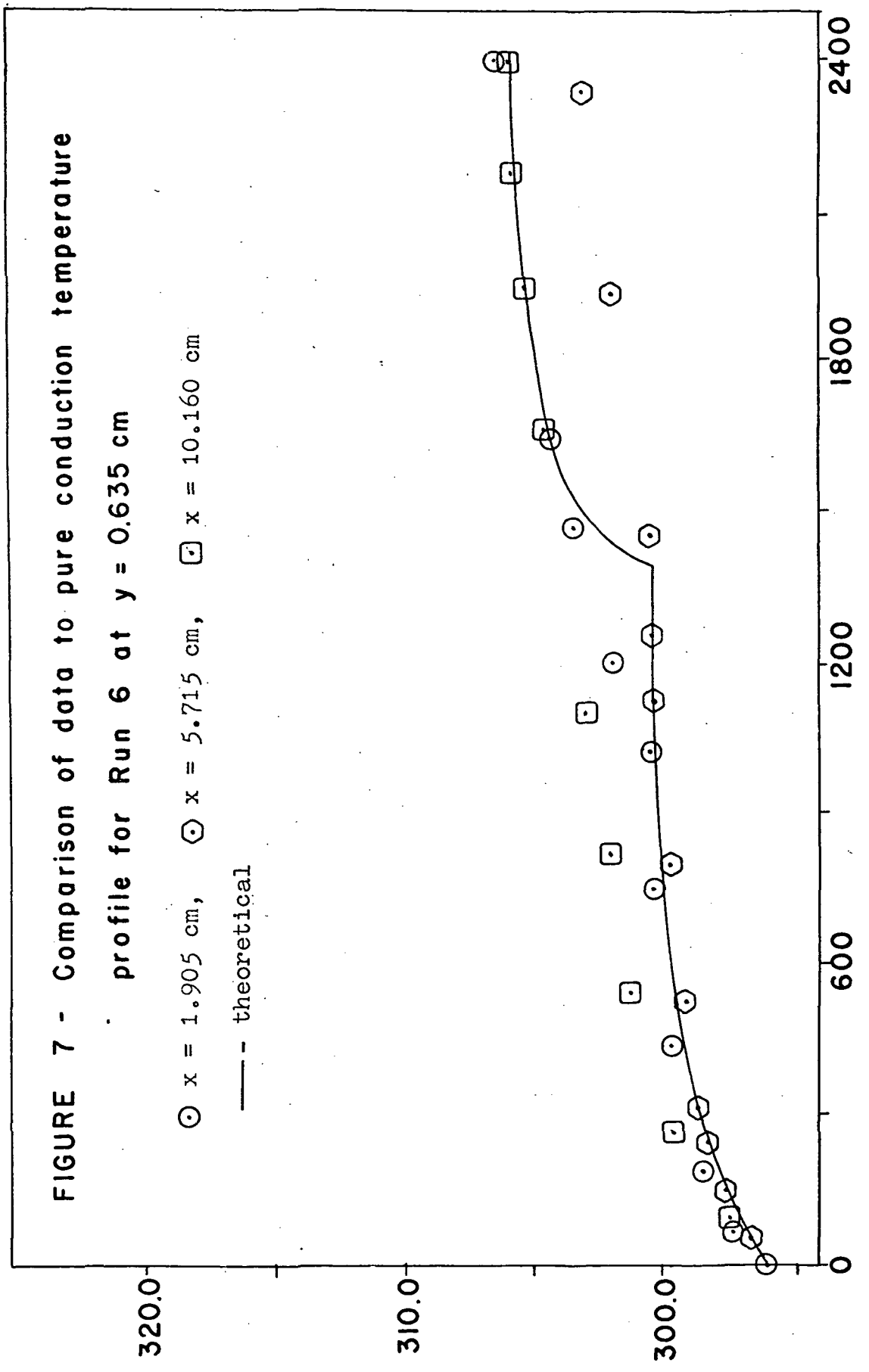
FIGURE 7 - Comparison of data to pure conduction temperature profile for Run 6 at y = 0.635 cm
⊙ x = 1.905 cm, ⊙ x = 5.715 cm, ⊡ x = 10.160 cm
—— - theoretical
TEMPERATURE (°K)
320.0
310.0
300.0
0
600
1200
1800
2400
TIME (SEC)

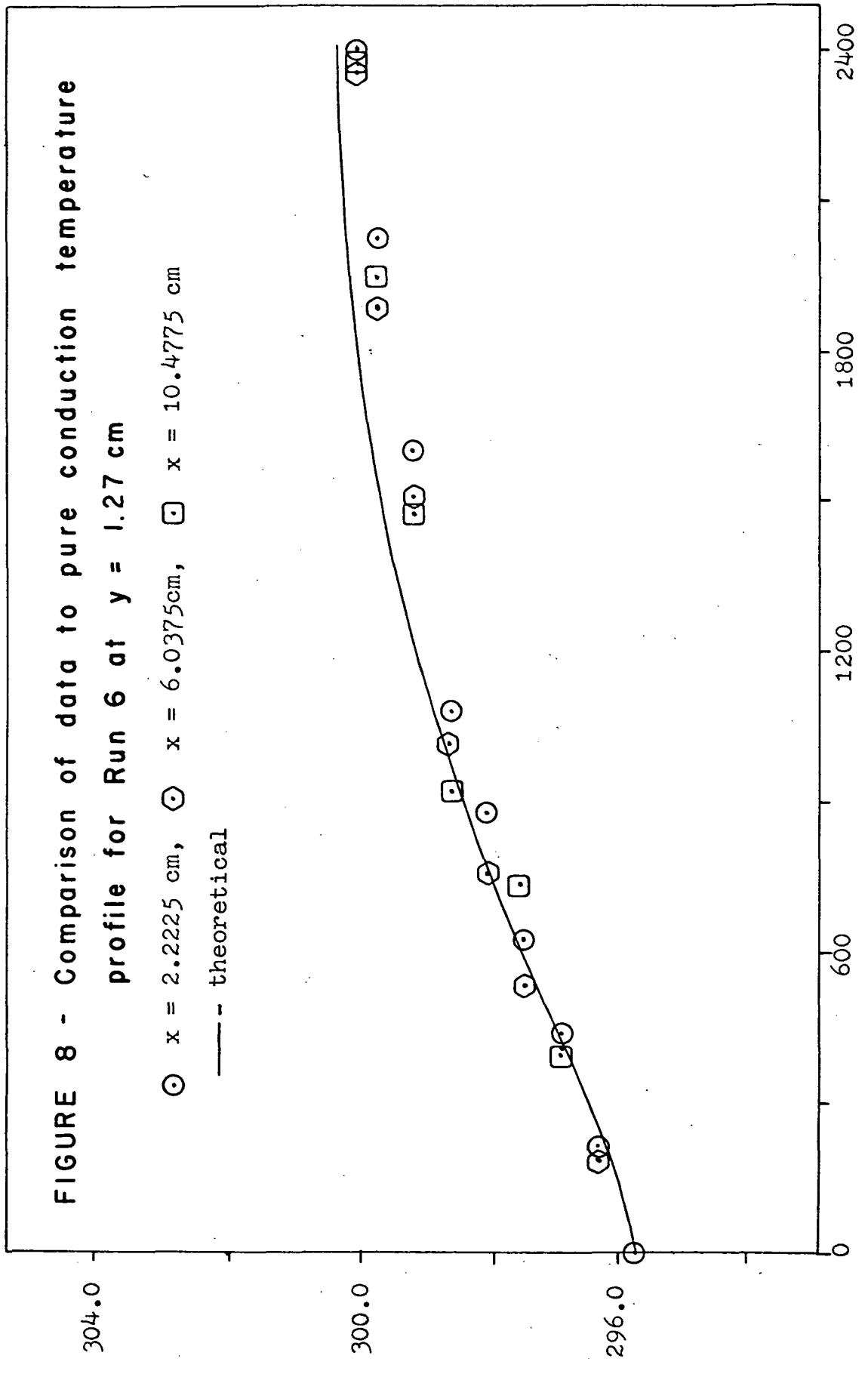
FIGURE 8 - Comparison of data to pure conduction temperature profile for Run 6 at y = 1.27 cm
x = 2.2225 cm, x = 6.0375cm, x = 10.4775 cm
theoretical
TEMPERATURE (°K)
304.0
300.0
296.0
0
600
1200
1800
2400
TIME (SEC)

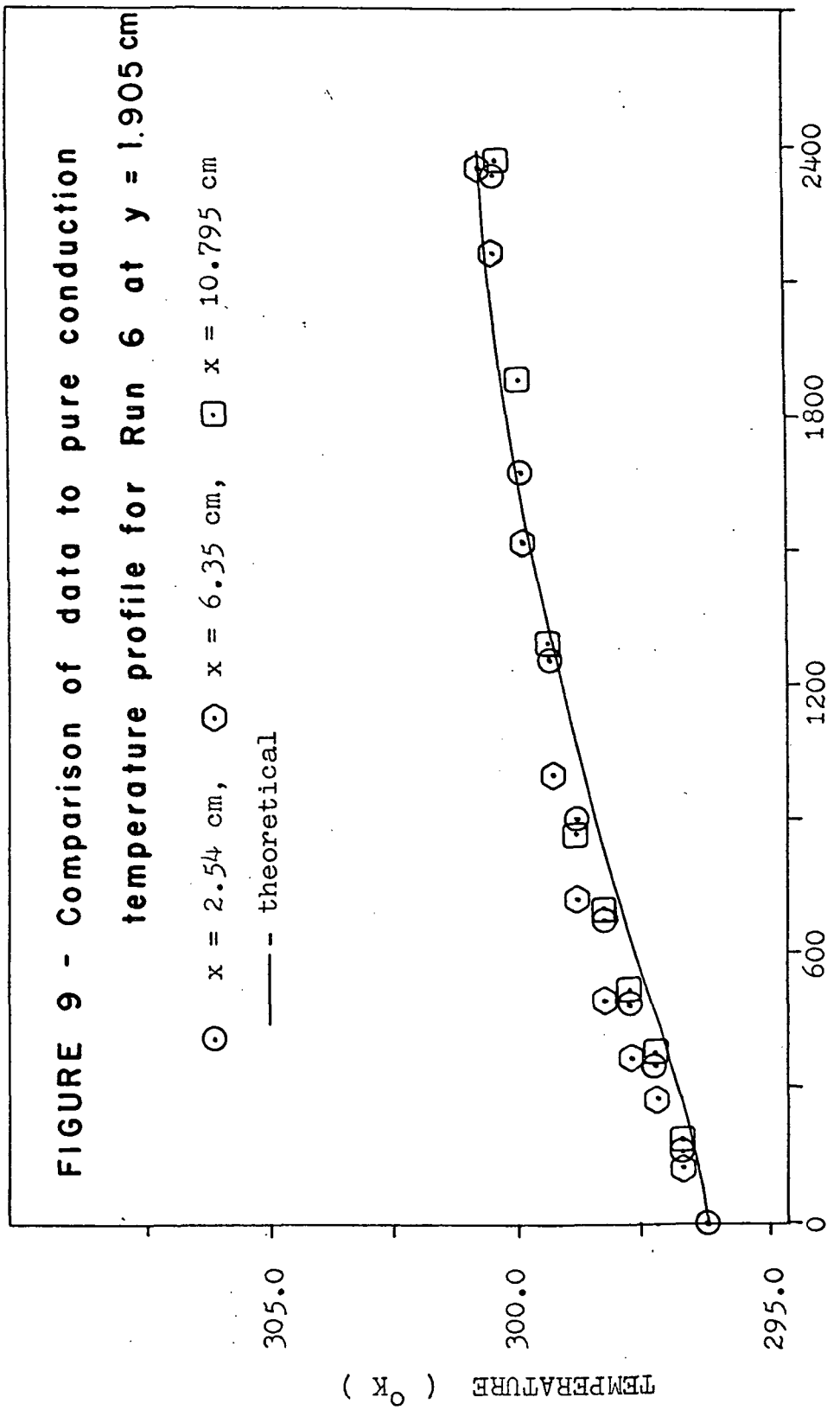
FIGURE 9 - Comparison of data to pure conduction temperature profile for Run 6 at y = 1.905 cm
⊙ x = 2.54 cm, ⊙ x = 6.35 cm, ⊡ x = 10.795 cm
—— - theoretical
TEMPERATURE (°K)
305.0
300.0
295.0
0
600
1200
1800
2400
TIME (SEC)

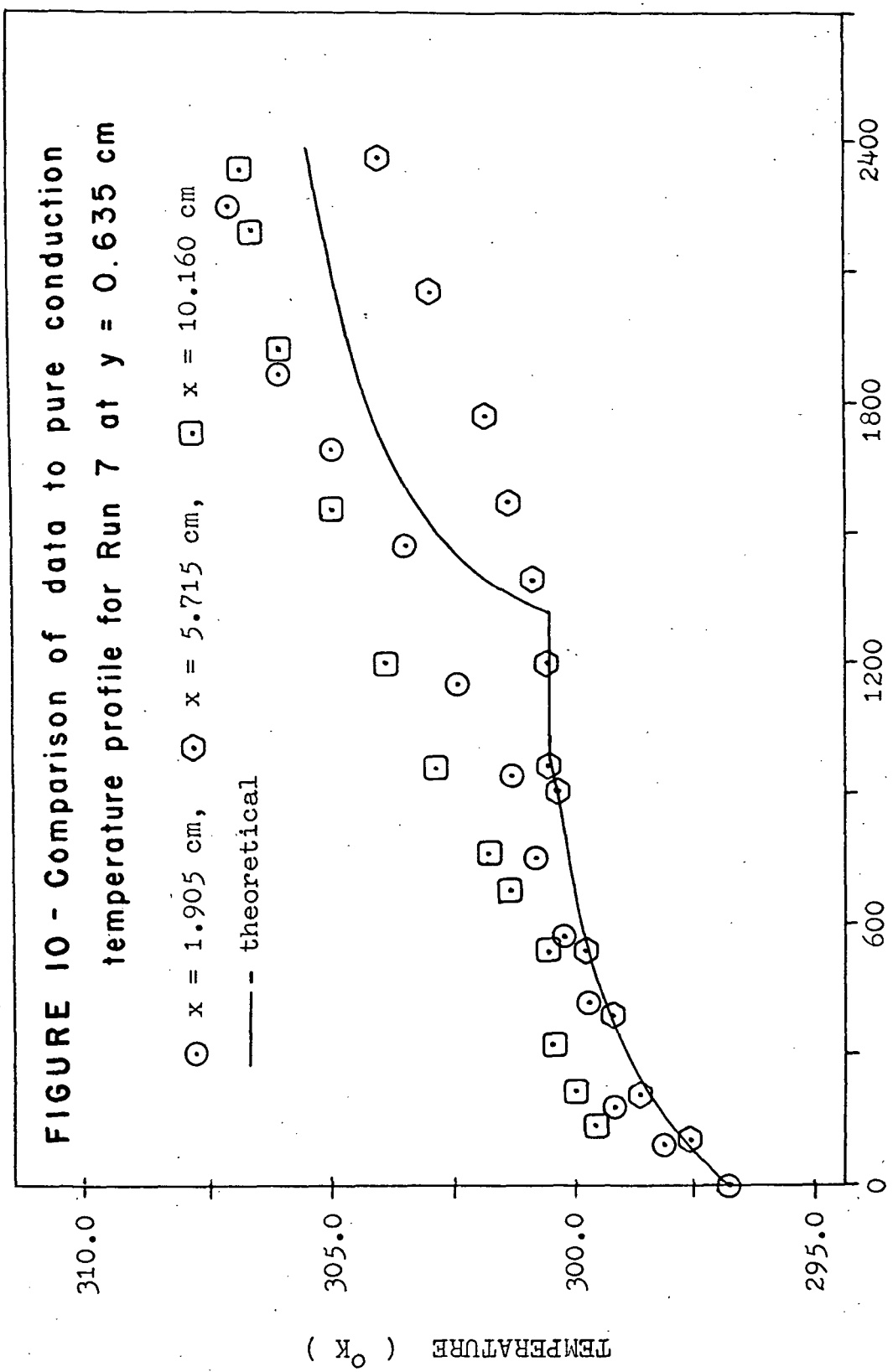
FIGURE 10 - Comparison of data to pure conduction temperature profile for Run 7 at y = 0.635 cm
x = 1.905 cm, x = 5.715 cm, x = 10.160 cm
theoretical
TEMPERATURE (°K)
310.0
305.0
300.0
295.0
0
600
1200
1800
2400
TIME (SEC)

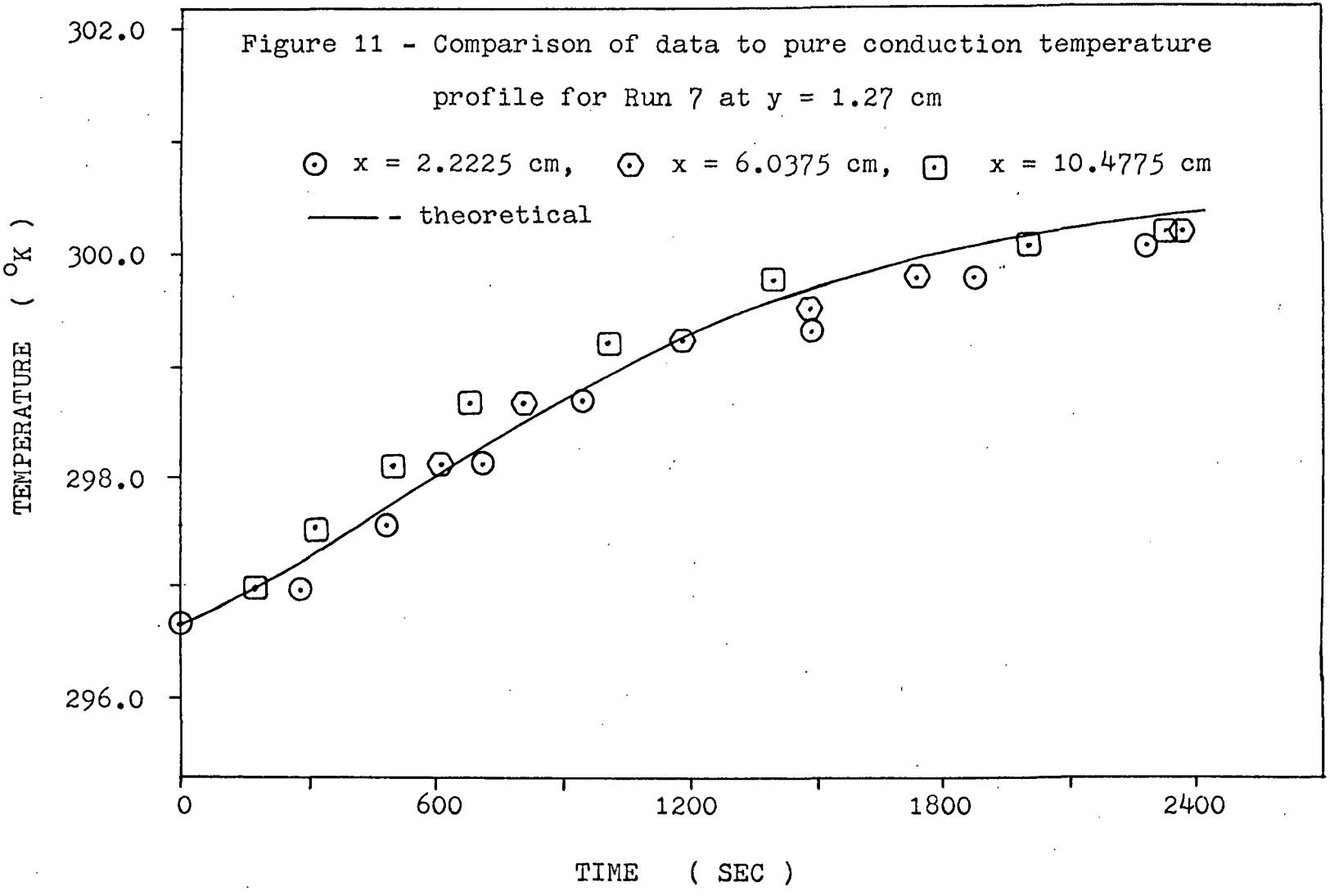

Figure 11 - Comparison of data to pure conduction temperature profile for Run 7 at y = 1.27 cm

⊙ x = 2.2225 cm, ⊙ x = 6.0375 cm, ⊡ x = 10.4775 cm

——— - theoretical

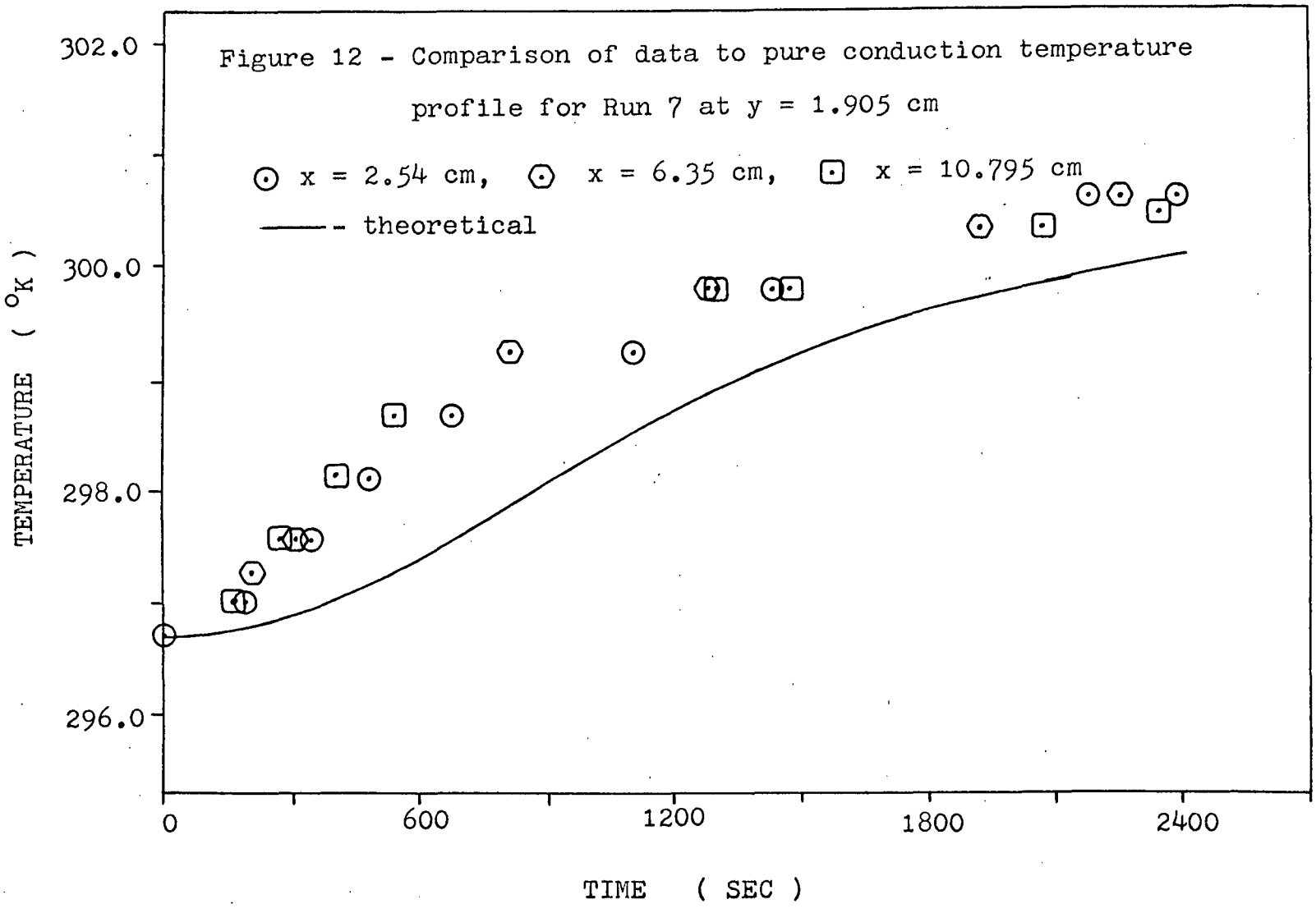
Figure 12 - Comparison of data to pure conduction temperature profile for Run 7 at y = 1.905 cm
x = 2.54 cm, x = 6.35 cm, x = 10.795 cm
theoretical
302.0
300.0
298.0
296.0
TEMPERATURE (°K)
0
600
1200
1800
2400
TIME (SEC)

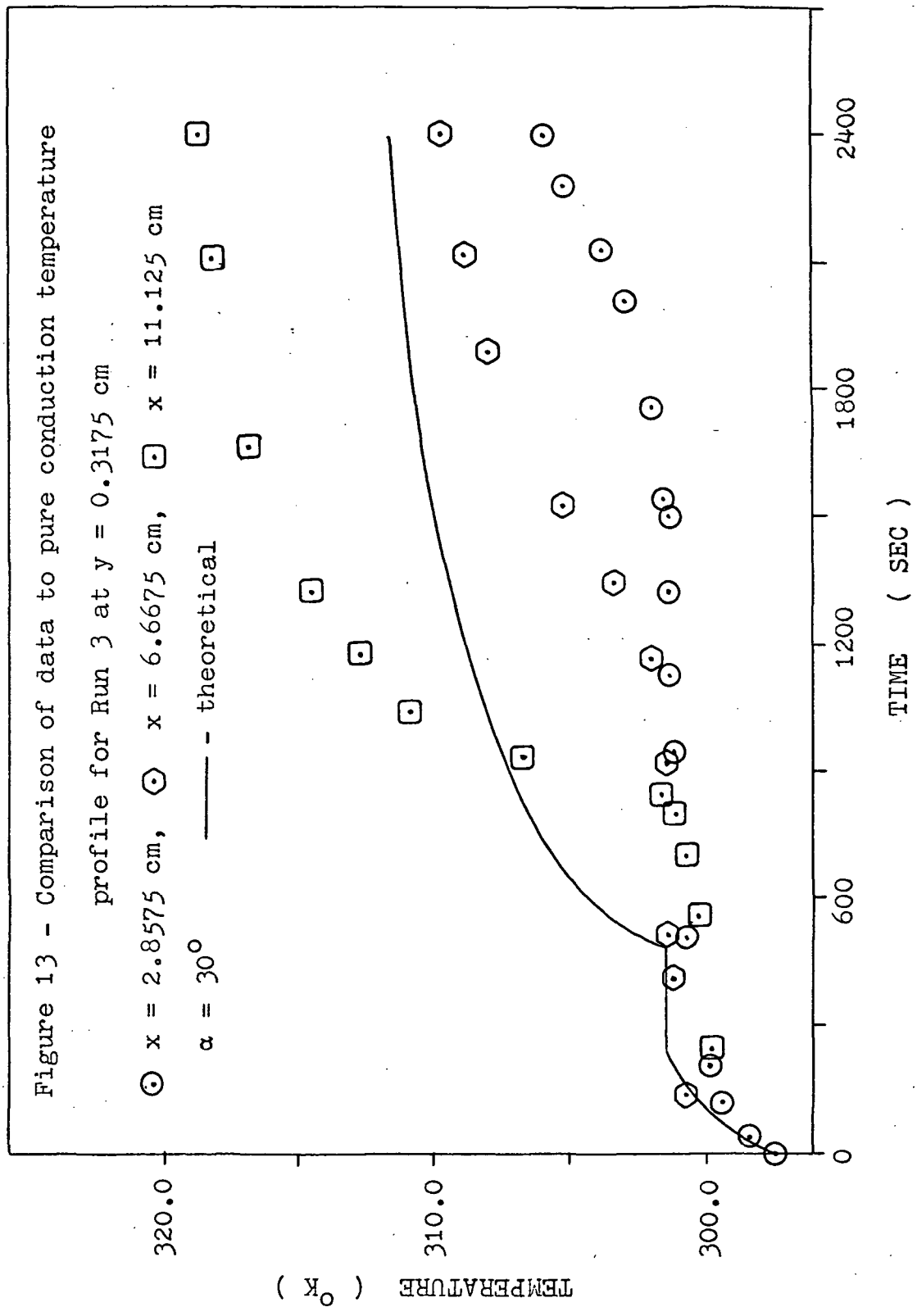
Figure 13 - Comparison of data to pure conduction temperature
profile for Run 3 at y = 0.3175 cm
x = 2.8575 cm, x = 6.6675 cm, x = 11.125 cm
α = 30°
- theoretical
TEMPERATURE (°K)
320.0
310.0
300.0
0
600
1200
1800
2400
TIME (SEC)

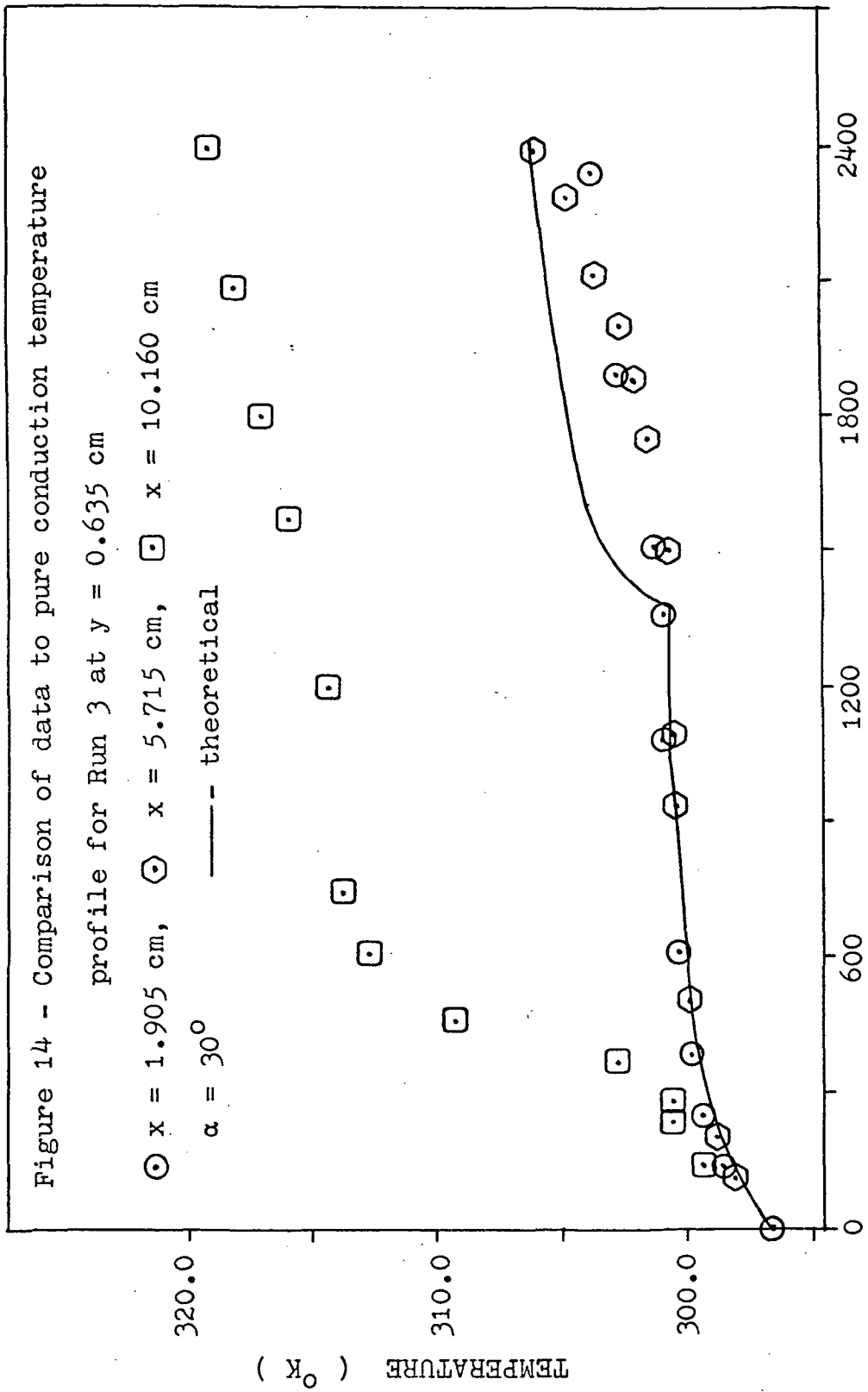
Figure 14 - Comparison of data to pure conduction temperature
profile for Run 3 at y = 0.635 cm
⊙ x = 1.905 cm, ⊙ x = 5.715 cm, ⊡ x = 10.160 cm
α = 30°
—— theoretical
TEMPERATURE (°K)
320.0
310.0
300.0
0
600
1200
1800
2400
TIME (SEC)

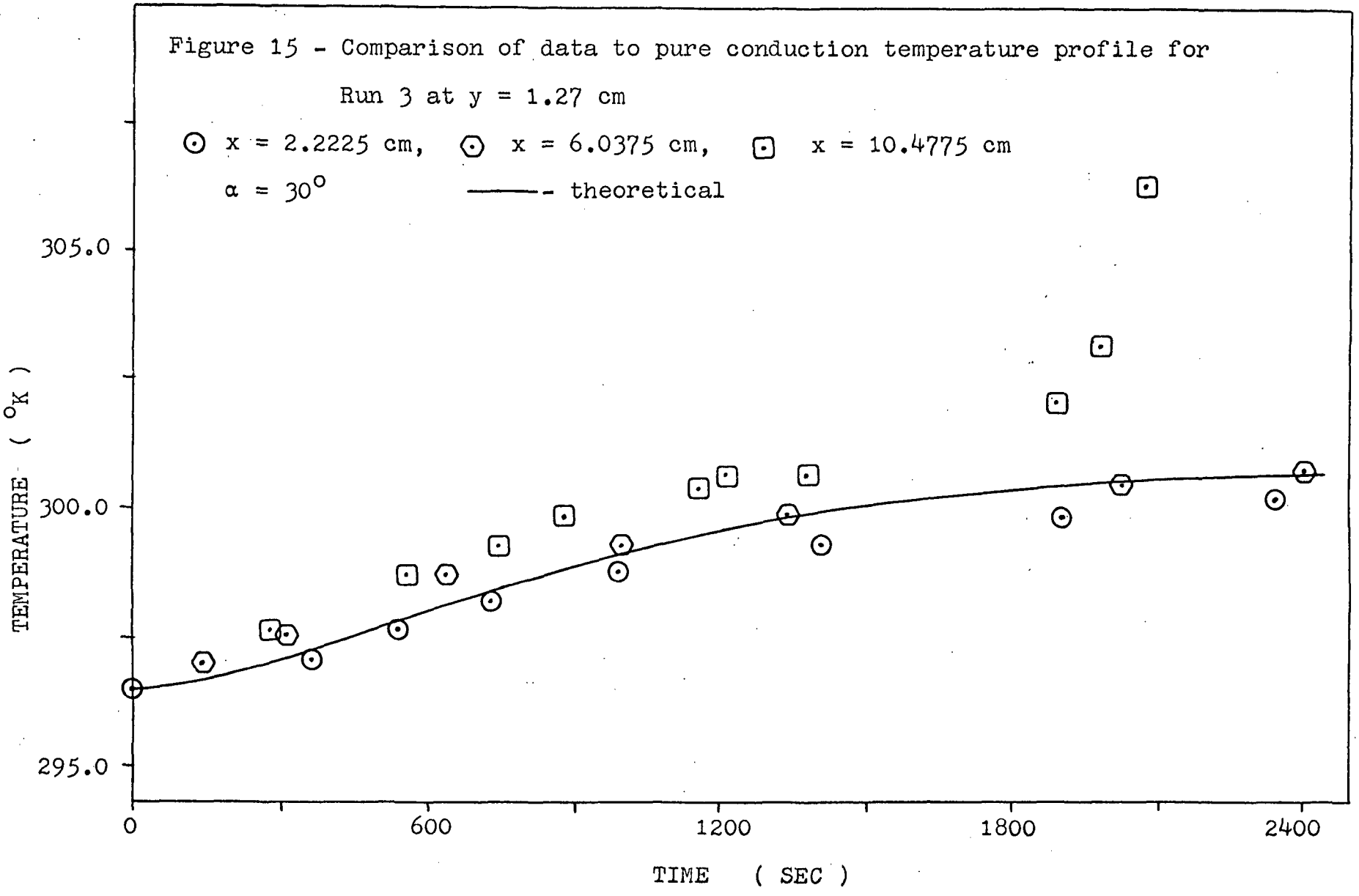
Figure 15 - Comparison of data to pure conduction temperature profile for
Run 3 at y = 1.27 cm
x = 2.2225 cm, x = 6.0375 cm, x = 10.4775 cm
α = 30°
theoretical
305.0
300.0
295.0
TEMPERATURE (°K)
0
600
1200
1800
2400
TIME (SEC)

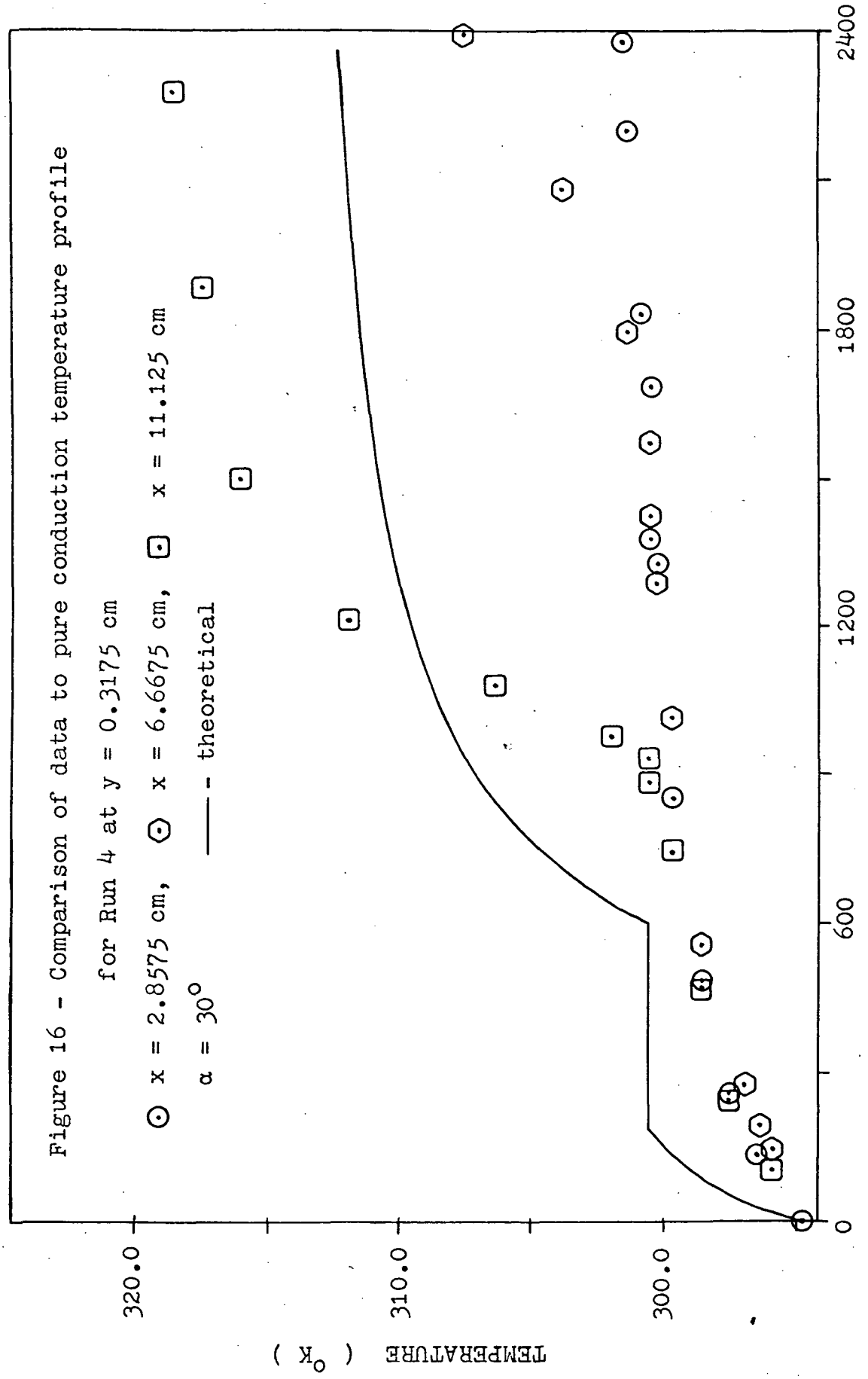
Figure 16 - Comparison of data to pure conduction temperature profile
for Run 4 at y = 0.3175 cm
x = 2.8575 cm, x = 6.6675 cm, x = 11.125 cm
α = 30°
- theoretical
TEMPERATURE (°K)
320.0
310.0
300.0
0
600
1200
1800
2400
TIME (SEC)

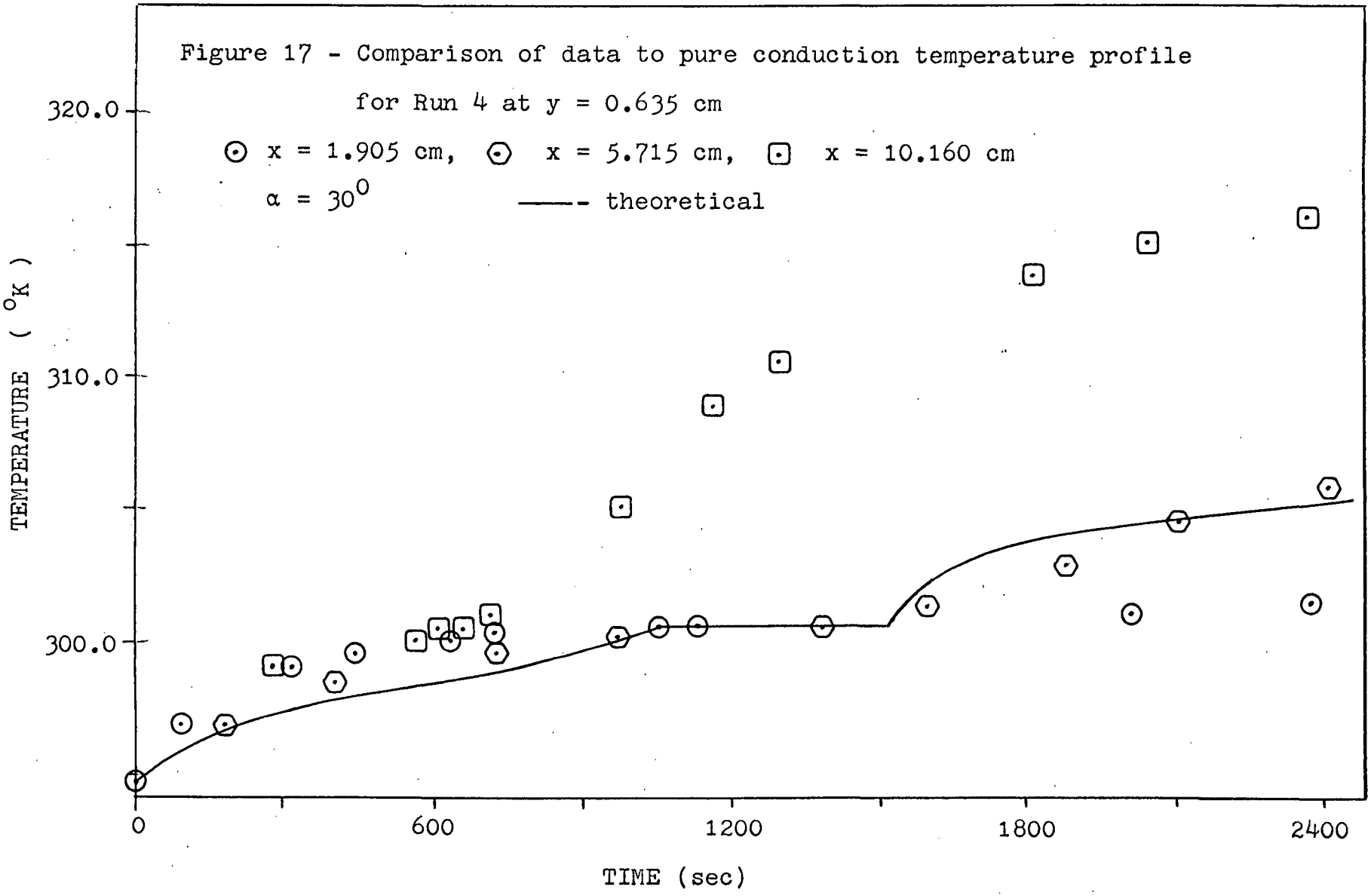
Figure 17 - Comparison of data to pure conduction temperature profile
for Run 4 at y = 0.635 cm
⊙ x = 1.905 cm, ⊙ x = 5.715 cm, ⊡ x = 10.160 cm
α = 30°
—— theoretical
320.0
310.0
300.0
TEMPERATURE (°K)
0
600
1200
1800
2400
TIME (sec)

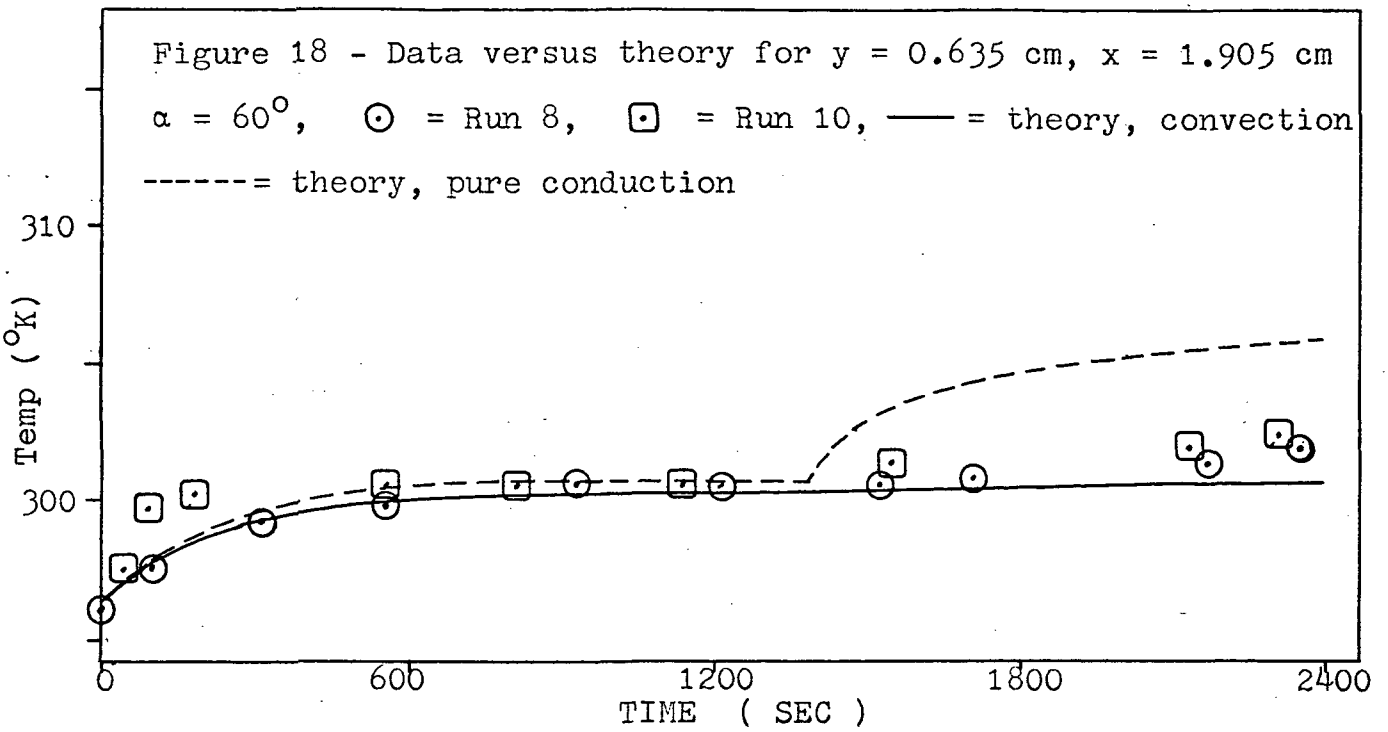
Figure 18 - Data versus theory for y = 0.635 cm, x = 1.905 cm
α = 60°, ⊙ = Run 8, ⊡ = Run 10, —— = theory, convection
------ = theory, pure conduction
310
300
Temp (°K)
0
600
1200
1800
2400
TIME (SEC)

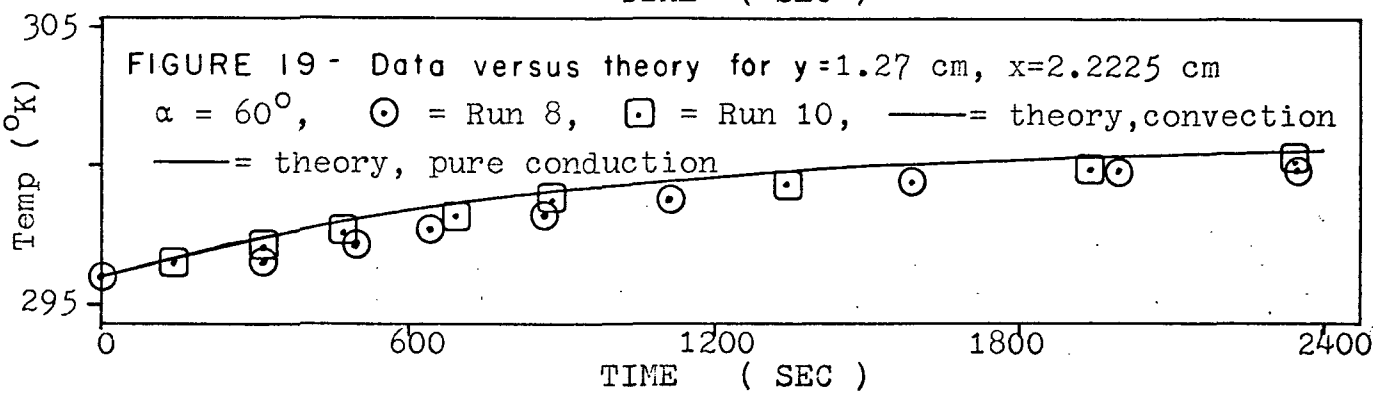
FIGURE 19 - Data versus theory for y=1.27 cm, x=2.2225 cm
α = 60°, ⊙ = Run 8, ⊡ = Run 10, ——= theory,convection
——= theory, pure conduction
305
295
Temp (°K)
0
600
1200
1800
2400
TIME (SEC)

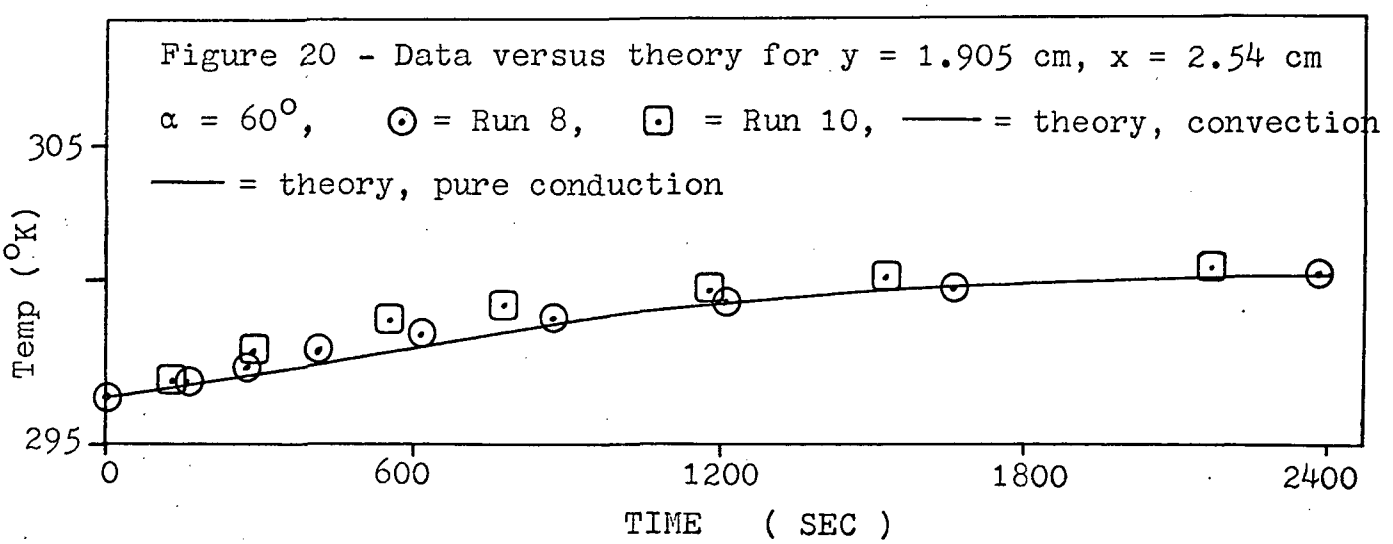
Figure 20 - Data versus theory for y = 1.905 cm, x = 2.54 cm
α = 60°, ⊙ = Run 8, ⊡ = Run 10, —— = theory, convection
—— = theory, pure conduction
305
295
Temp (°K)
0
600
1200
1800
2400
TIME (SEC)

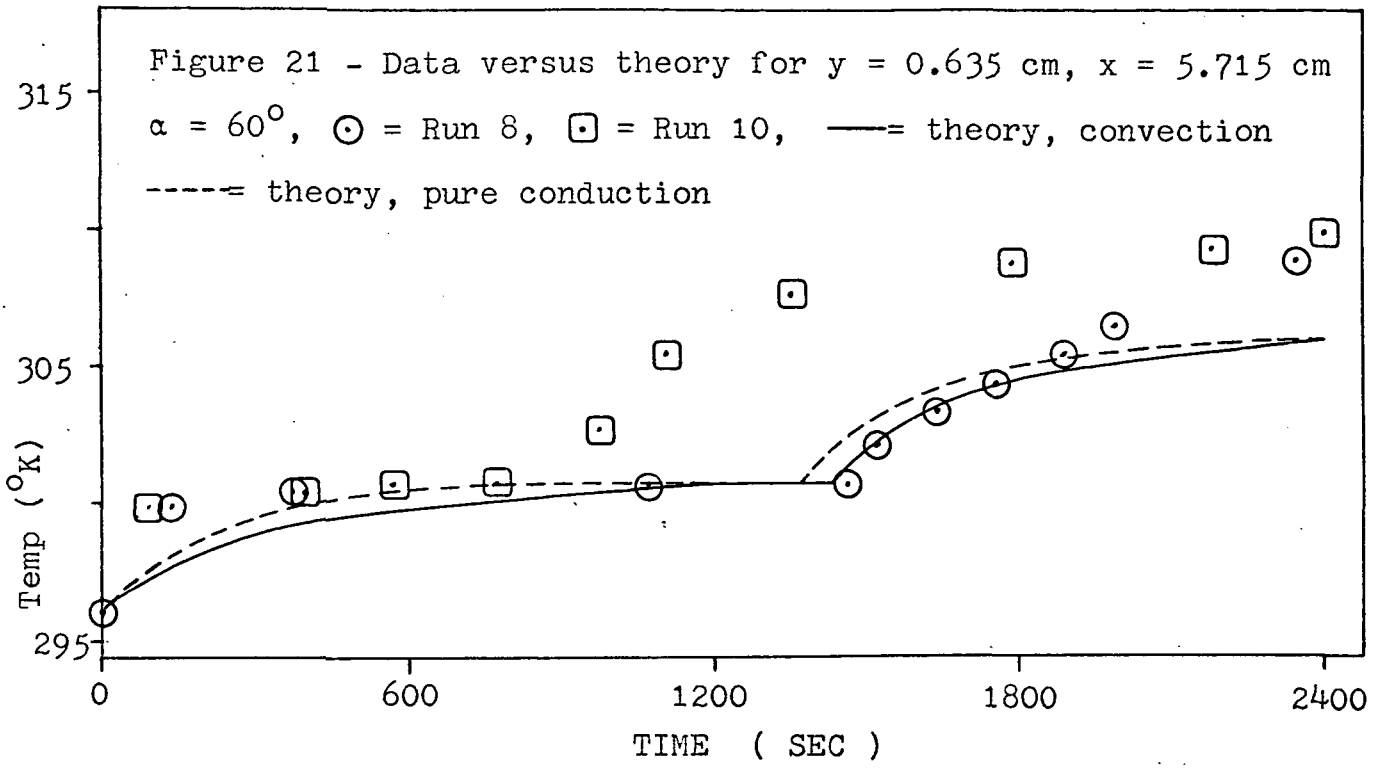

Figure 21 - Data versus theory for y = 0.635 cm, x = 5.715 cm
$\alpha = 60^{\circ}$, ⊙ = Run 8, ⊡ = Run 10, ——= theory, convection
-----= theory, pure conduction

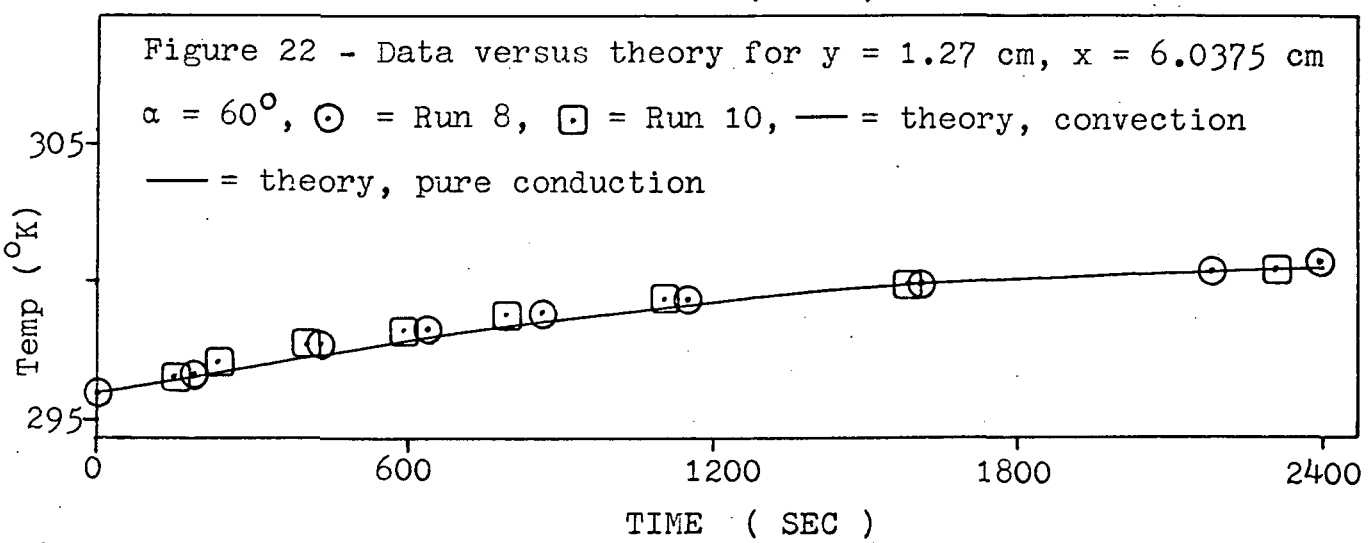

Figure 22 - Data versus theory for y = 1.27 cm, x = 6.0375 cm
$\alpha = 60^{\circ}$, ⊙ = Run 8, ⊡ = Run 10, —— = theory, convection
—— = theory, pure conduction

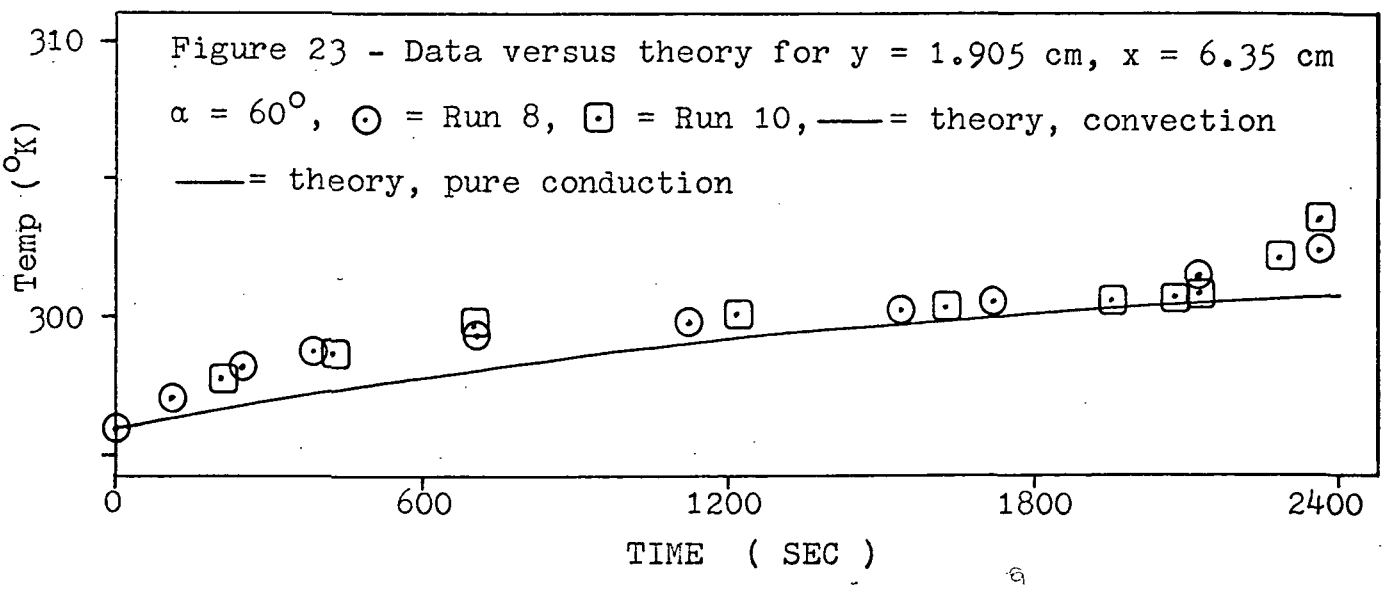

Figure 23 - Data versus theory for y = 1.905 cm, x = 6.35 cm
$\alpha = 60^{\circ}$, ⊙ = Run 8, ⊡ = Run 10, ——= theory, convection
——= theory, pure conduction

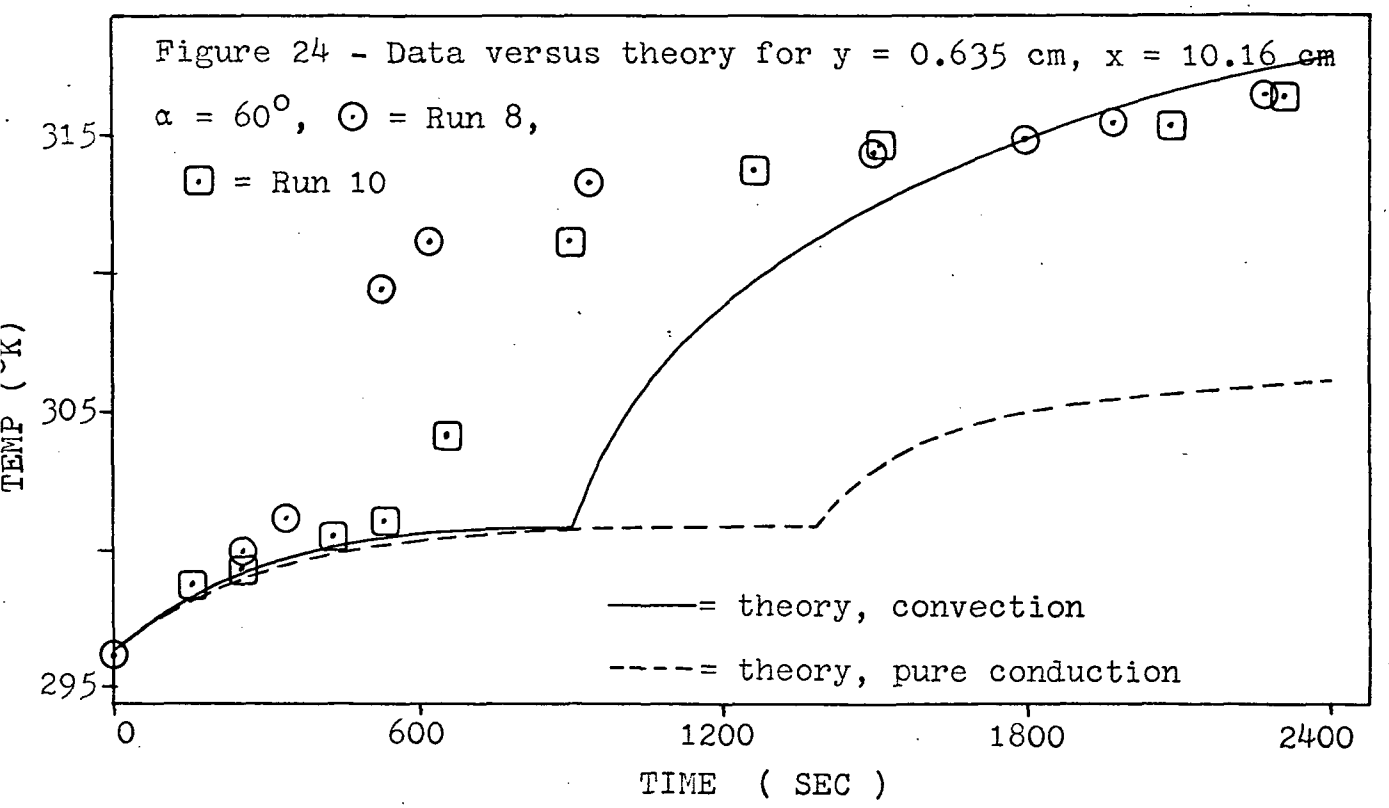

Figure 24 - Data versus theory for y = 0.635 cm, x = 10.16 cm
$\alpha = 60^{\circ}$, ⊙ = Run 8, ⊡ = Run 10

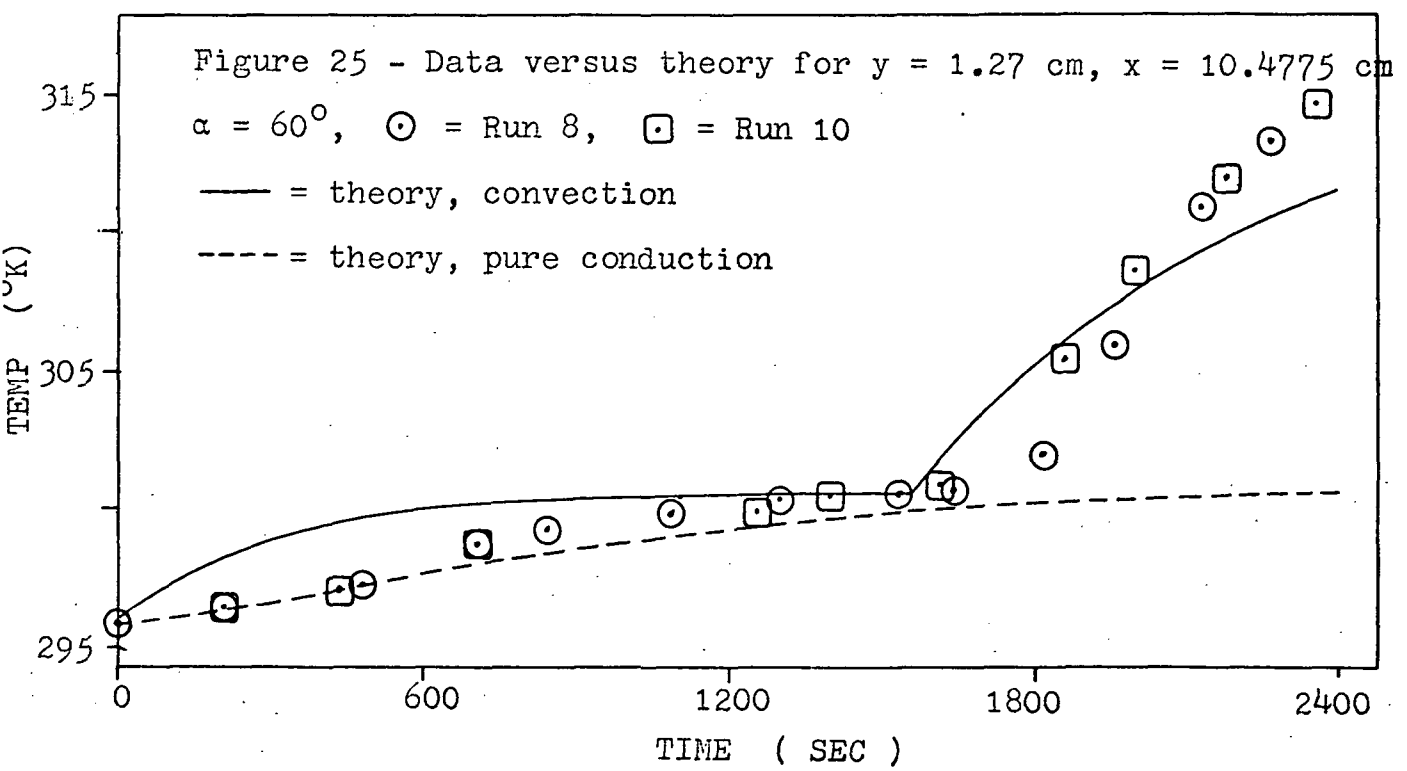

Figure 25 - Data versus theory for y = 1.27 cm, x = 10.4775 cm
$\alpha = 60^{\circ}$, ⊙ = Run 8, ⊡ = Run 10

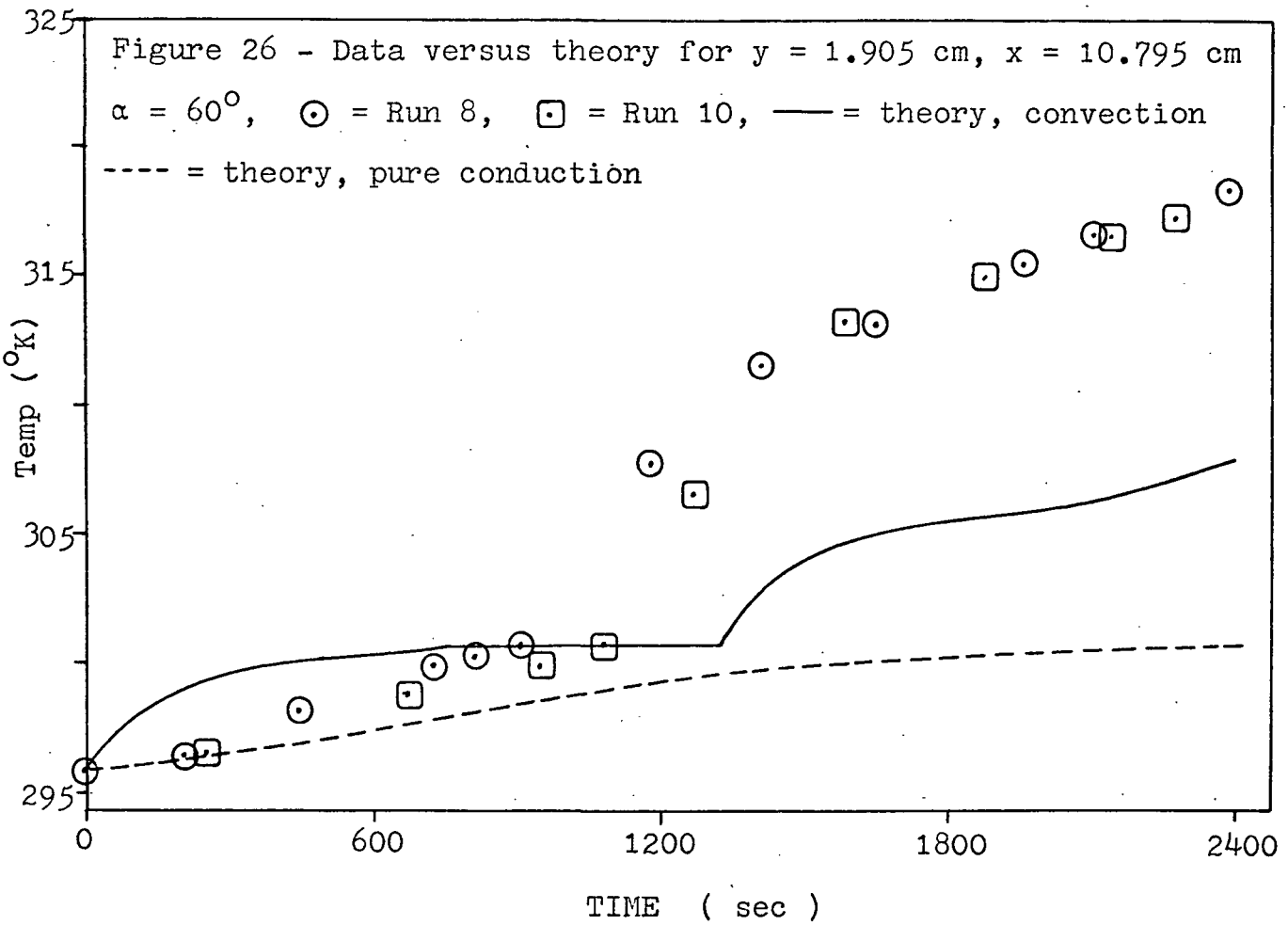

Figure 26 - Data versus theory for y = 1.905 cm, x = 10.795 cm
$\alpha = 60^{\circ}$, ⊙ = Run 8, ⊡ = Run 10, —— = theory, convection
---- = theory, pure conduction

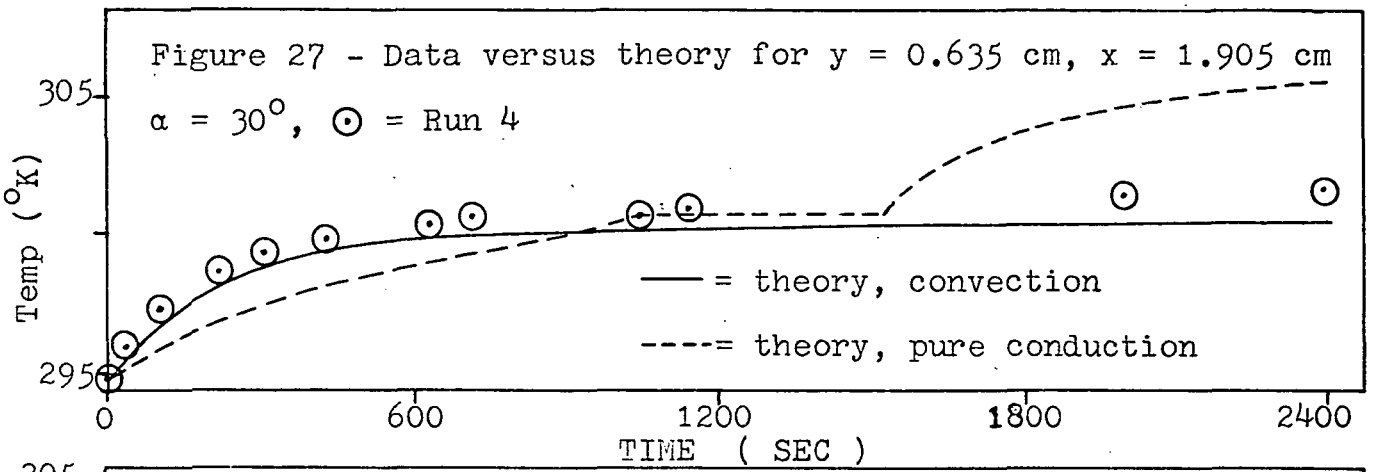

Figure 27 - Data versus theory for y = 0.635 cm, x = 1.905 cm
$\alpha = 30^{\circ}$, ⊙ = Run 4

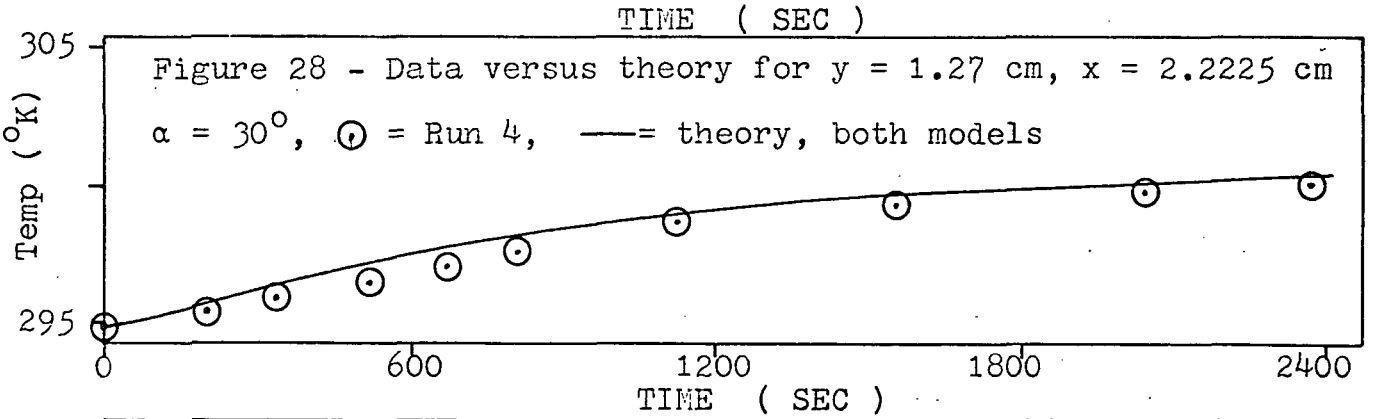

Figure 28 - Data versus theory for y = 1.27 cm, x = 2.2225 cm
$\alpha = 30^{\circ}$, ⊙ = Run 4, —— = theory, both models

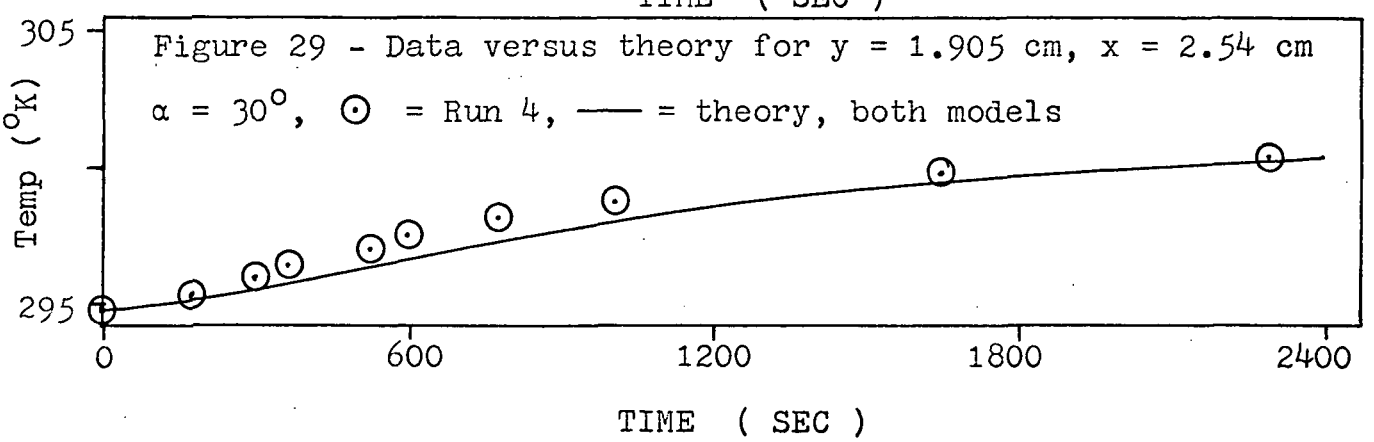

Figure 29 - Data versus theory for y = 1.905 cm, x = 2.54 cm
$\alpha = 30^{\circ}$, ⊙ = Run 4, —— = theory, both models

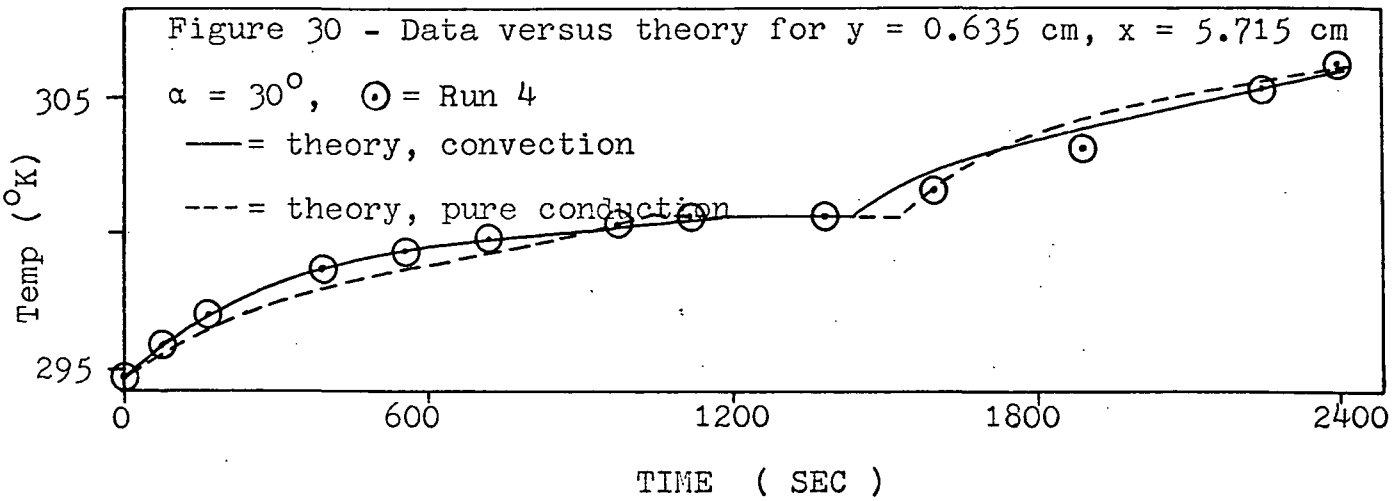
Figure 30 - Data versus theory for y = 0.635 cm, x = 5.715 cm
α = 30°, ⊙ = Run 4
—— = theory, convection
--- = theory, pure conduction
305
295
Temp (°K)
0
600
1200
1800
2400
TIME (SEC)

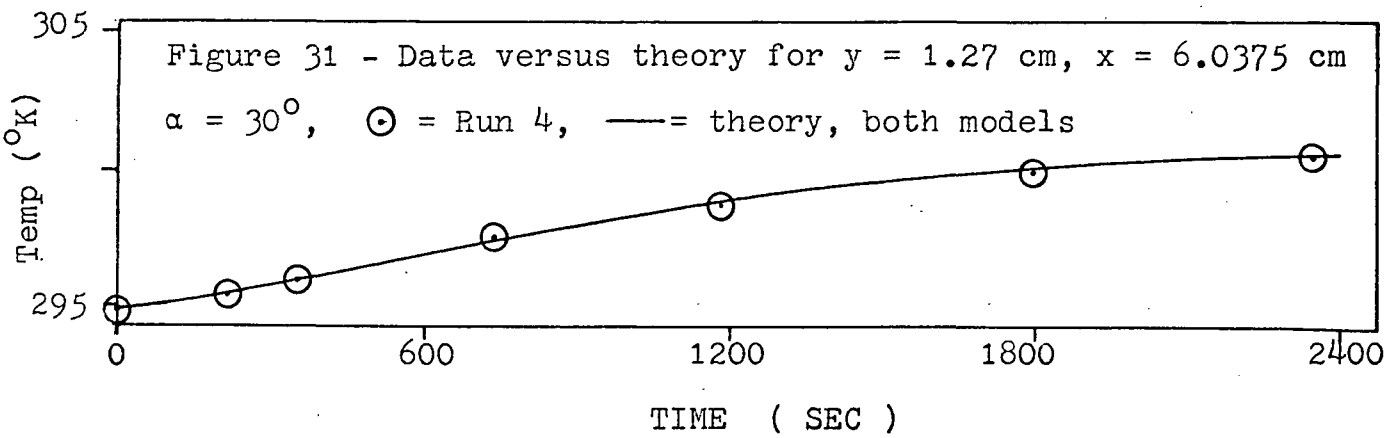
Figure 31 - Data versus theory for y = 1.27 cm, x = 6.0375 cm
α = 30°, ⊙ = Run 4, —— = theory, both models
305
295
Temp (°K)
0
600
1200
1800
2400
TIME (SEC)

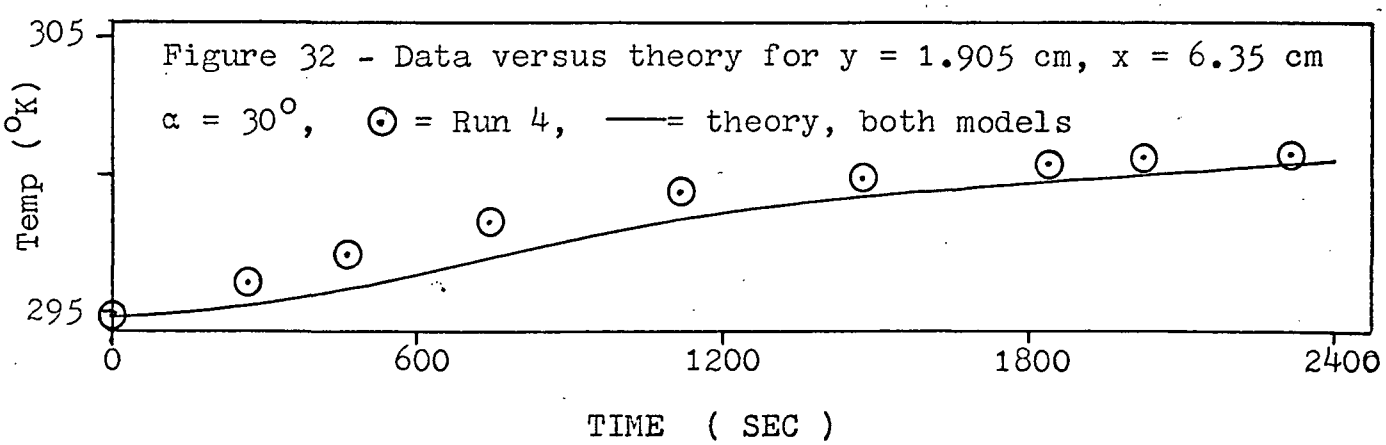
Figure 32 - Data versus theory for y = 1.905 cm, x = 6.35 cm
α = 30°, ⊙ = Run 4, —— = theory, both models
305
295
Temp (°K)
0
600
1200
1800
2400
TIME (SEC)

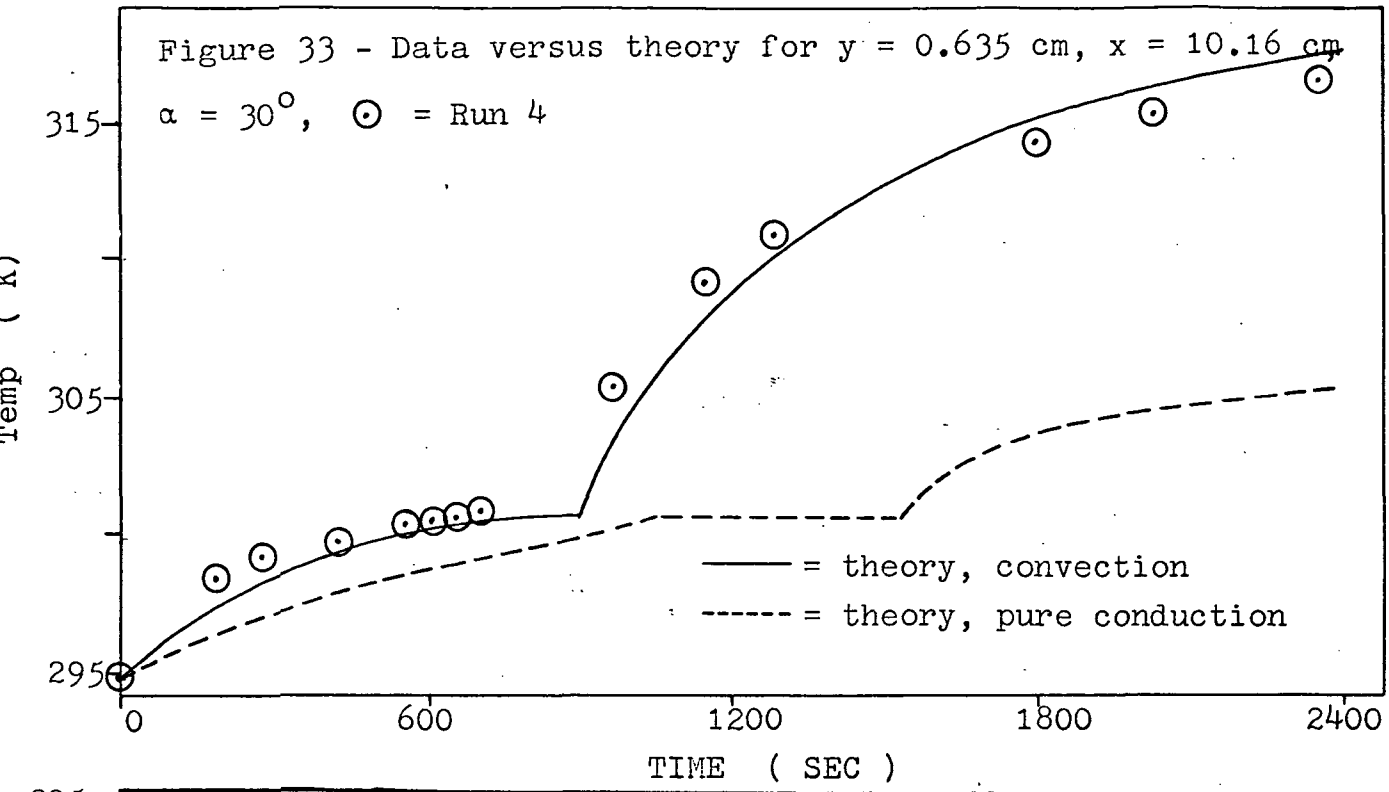
Figure 33 - Data versus theory for y = 0.635 cm, x = 10.16 cm
α = 30°, ⊙ = Run 4
315
305
295
Temp (K)
0
600
1200
1800
2400
TIME (SEC)
= theory, convection
= theory, pure conduction

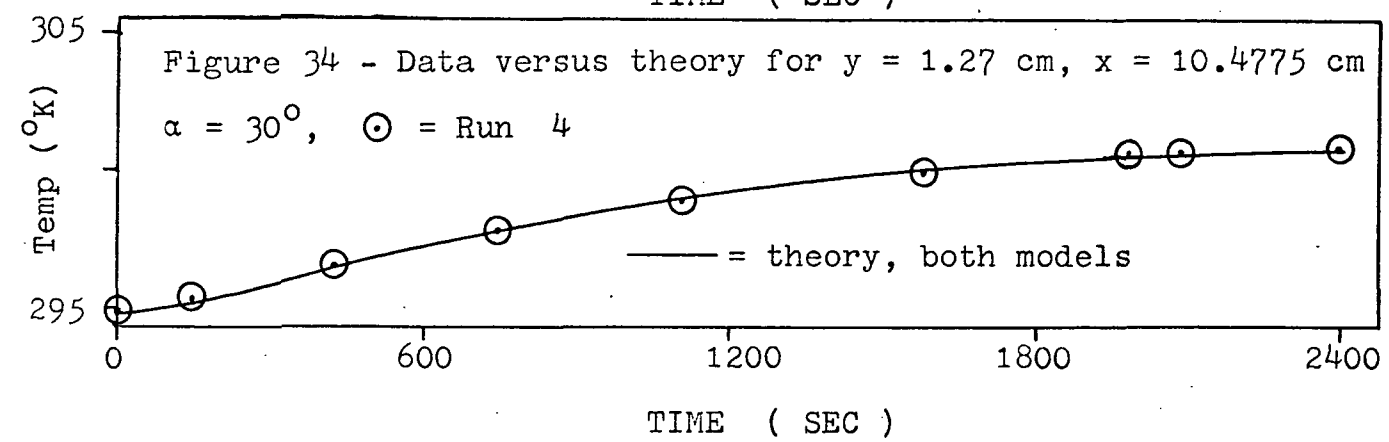
Figure 34 - Data versus theory for y = 1.27 cm, x = 10.4775 cm
α = 30°, ⊙ = Run 4
305
295
Temp (°K)
0
600
1200
1800
2400
TIME (SEC)
= theory, both models

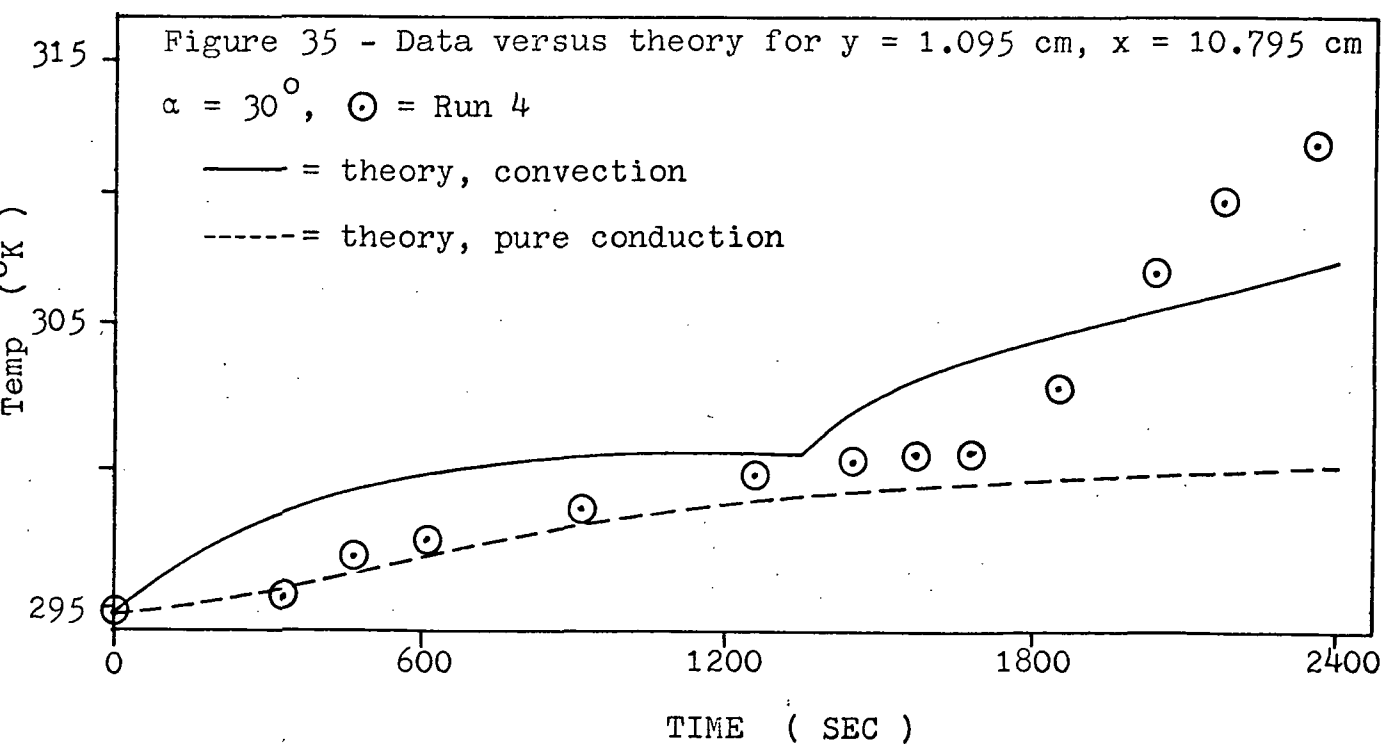
Figure 35 - Data versus theory for y = 1.095 cm, x = 10.795 cm
α = 30°, ⊙ = Run 4
= theory, convection
= theory, pure conduction
315
305
295
Temp (°K)
0
600
1200
1800
2400
TIME (SEC)

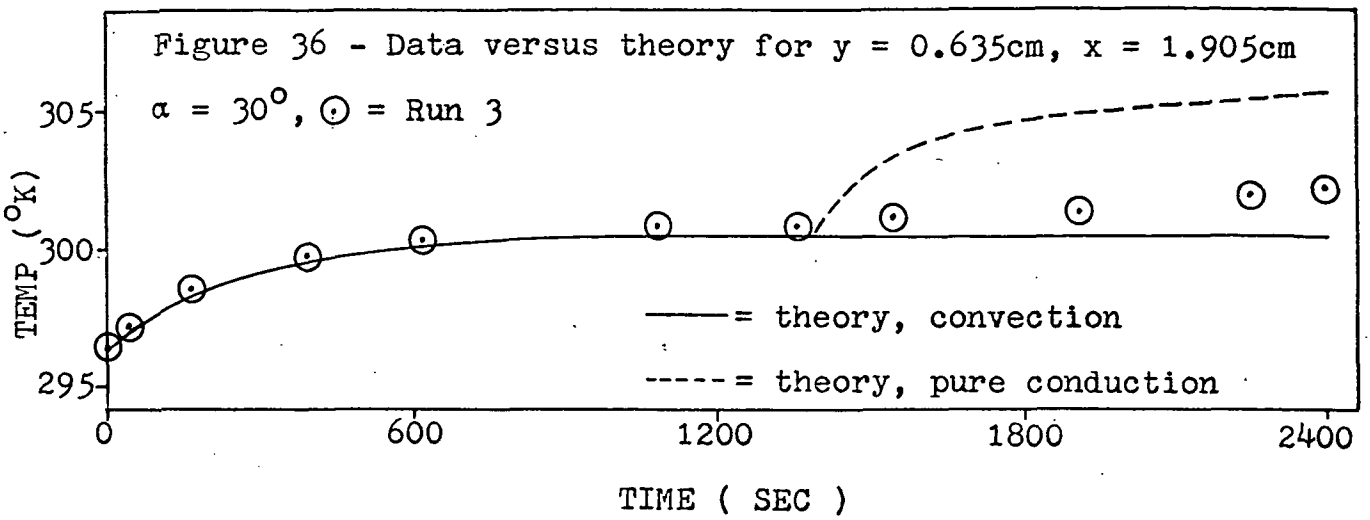
Figure 36 - Data versus theory for y = 0.635cm, x = 1.905cm
α = 30°, ⊙ = Run 3
305
300
295
TEMP (°K)
0
600
1200
1800
2400
TIME (SEC)
——— = theory, convection
----- = theory, pure conduction

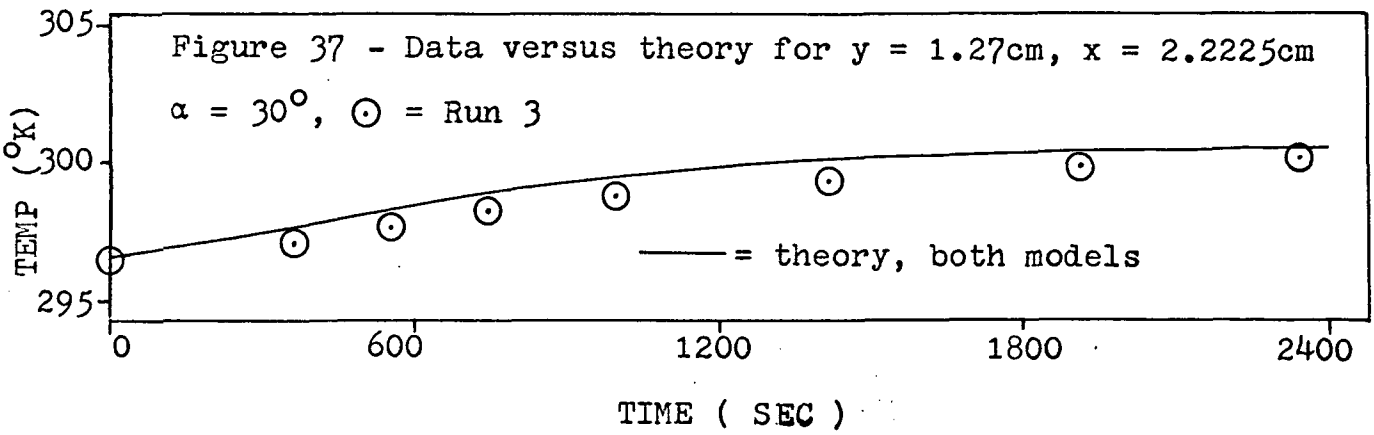
Figure 37 - Data versus theory for y = 1.27cm, x = 2.2225cm
α = 30°, ⊙ = Run 3
305
300
295
TEMP (°K)
0
600
1200
1800
2400
TIME (SEC)
——— = theory, both models

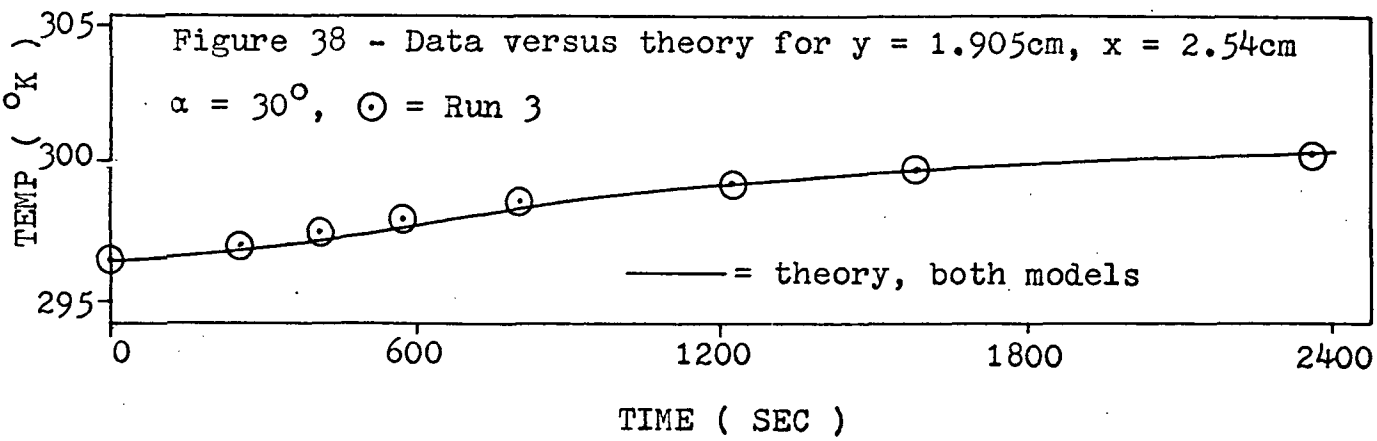
Figure 38 - Data versus theory for y = 1.905cm, x = 2.54cm
α = 30°, ⊙ = Run 3
305
300
295
TEMP (°K)
0
600
1200
1800
2400
TIME (SEC)
——— = theory, both models

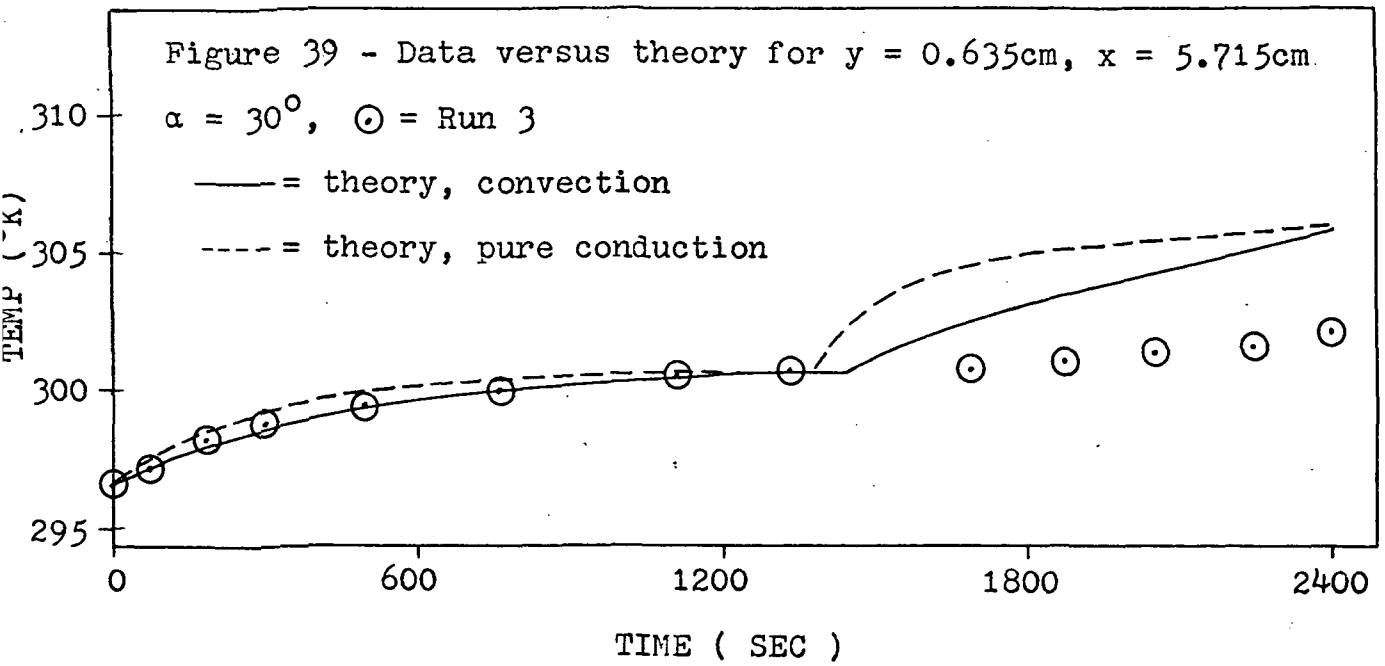
Figure 39 - Data versus theory for y = 0.635cm, x = 5.715cm
α = 30°, ⊙ = Run 3
——= theory, convection
----= theory, pure conduction
310
305
300
295
TEMP (°K)
0
600
1200
1800
2400
TIME (SEC)

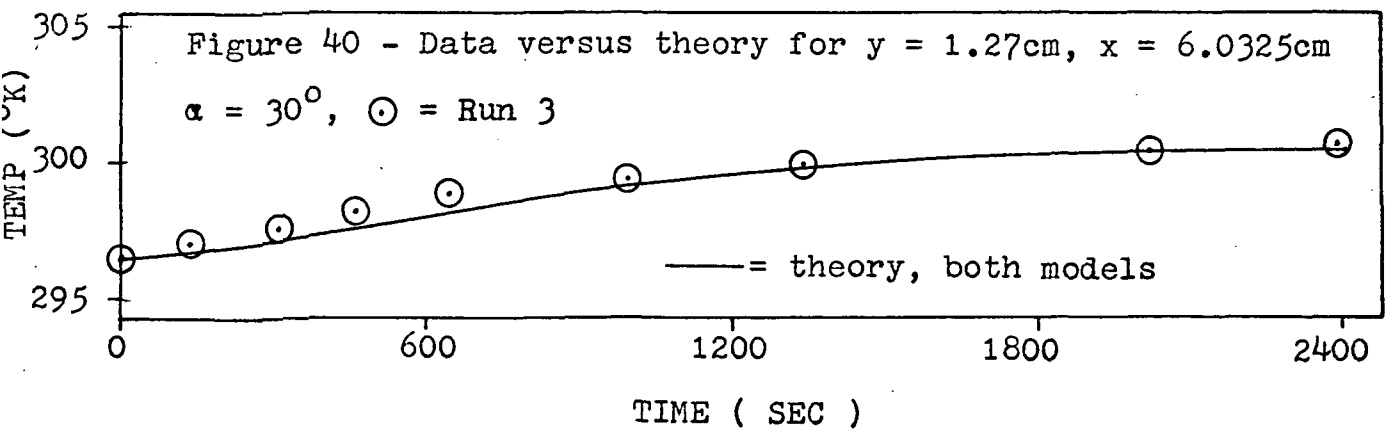
Figure 40 - Data versus theory for y = 1.27cm, x = 6.0325cm
α = 30°, ⊙ = Run 3
——= theory, both models
305
300
295
TEMP (°K)
0
600
1200
1800
2400
TIME (SEC)

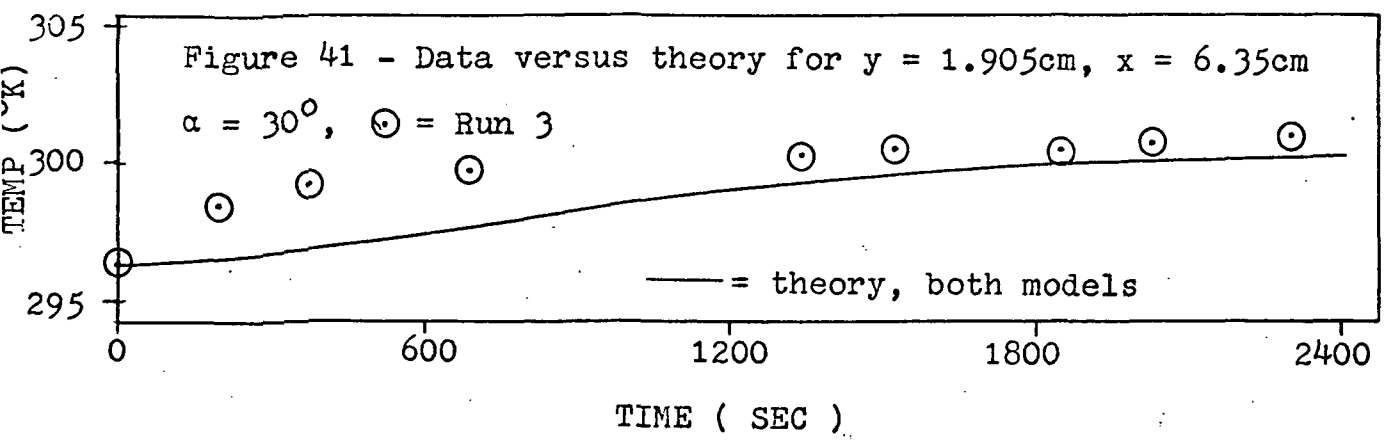
Figure 41 - Data versus theory for y = 1.905cm, x = 6.35cm
α = 30°, ⊙ = Run 3
——= theory, both models
305
300
295
TEMP (°K)
0
600
1200
1800
2400
TIME (SEC)

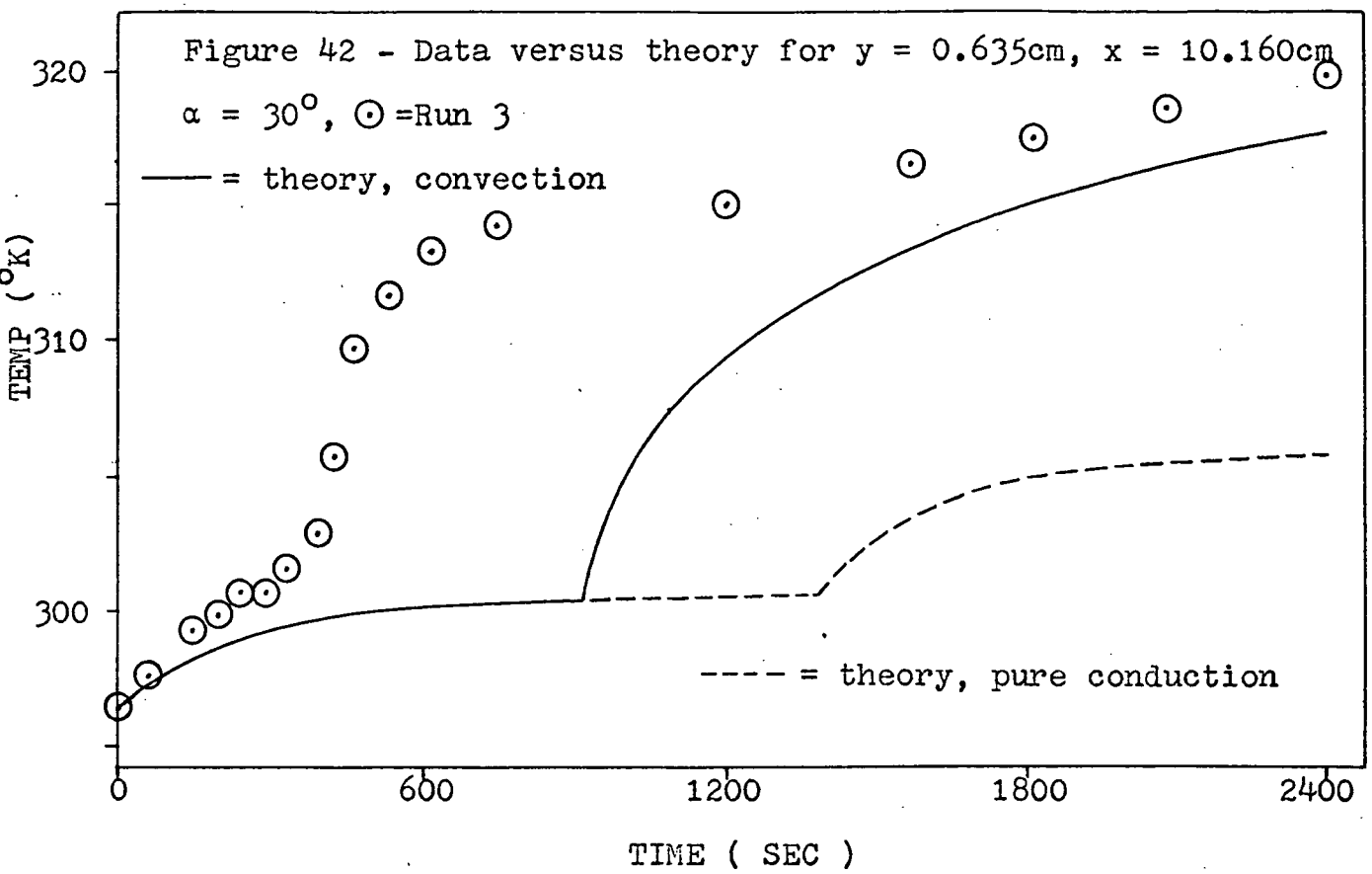
Figure 42 - Data versus theory for y = 0.635cm, x = 10.160cm
α = 30°, ⊙ =Run 3
—— = theory, convection
---- = theory, pure conduction
320
310
300
TEMP (°K)
0
600
1200
1800
2400
TIME (SEC)

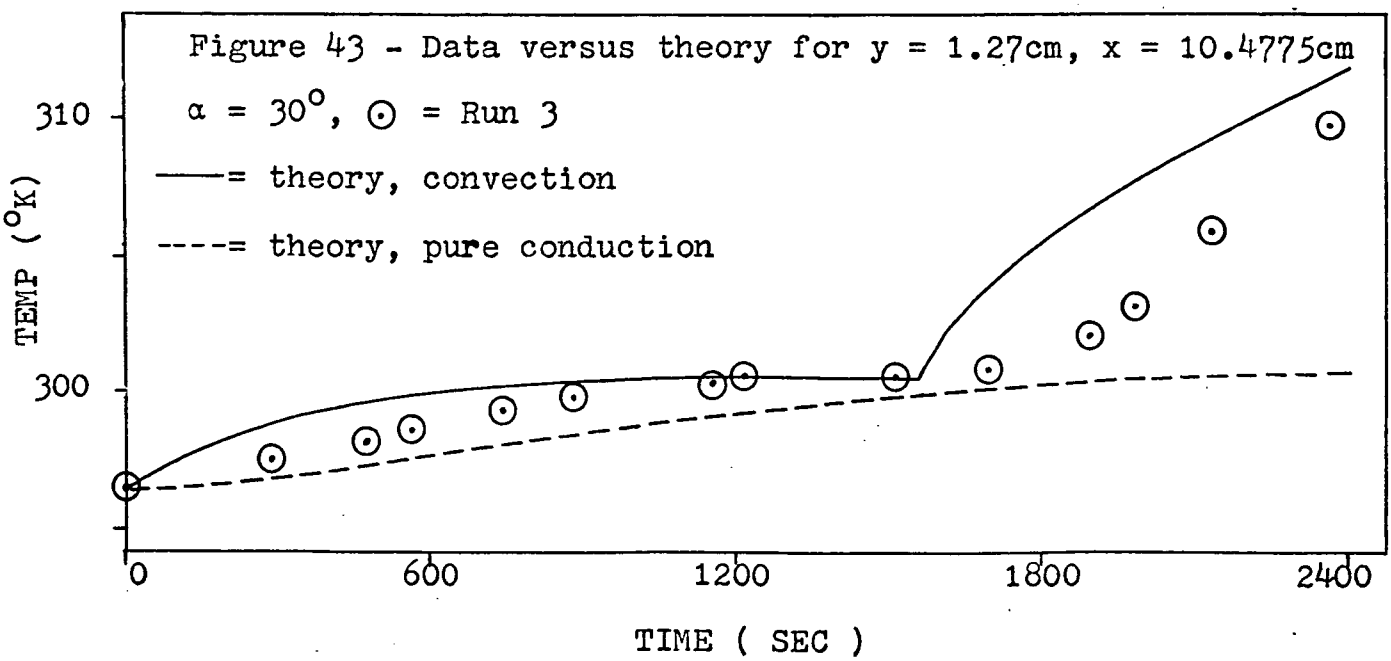
Figure 43 - Data versus theory for y = 1.27cm, x = 10.4775cm
α = 30°, ⊙ = Run 3
——= theory, convection
----= theory, pure conduction
310
300
TEMP (°K)
0
600
1200
1800
2400
TIME (SEC)

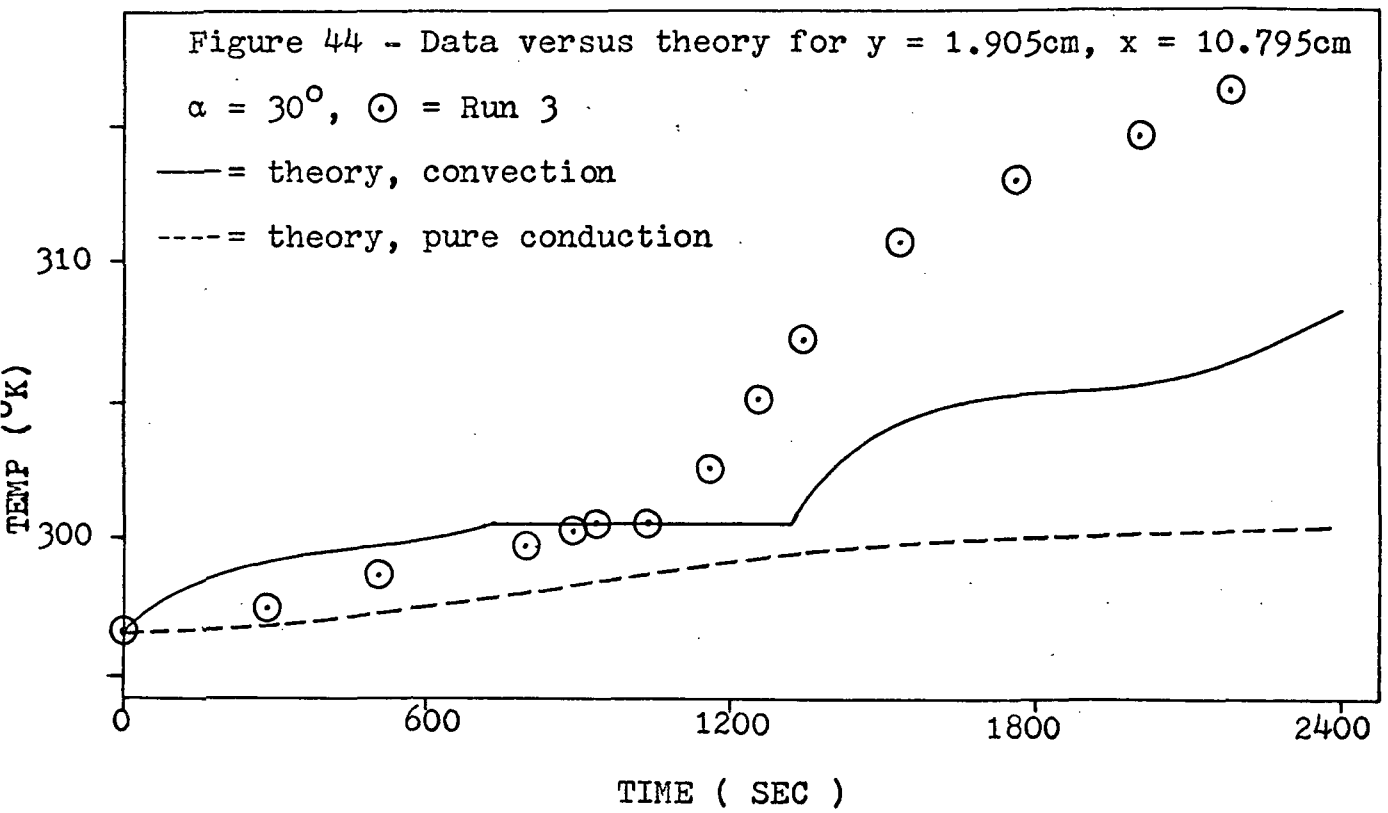
Figure 44 - Data versus theory for y = 1.905cm, x = 10.795cm
α = 30°, ⊙ = Run 3
——= theory, convection
----= theory, pure conduction
310
300
TEMP (°K)
0
600
1200
1800
2400
TIME (SEC)

Figure 45 - Theoretical interface distance from hot plate at v_{max}= 0.0107cm/sec for $\alpha = 60^{o}$

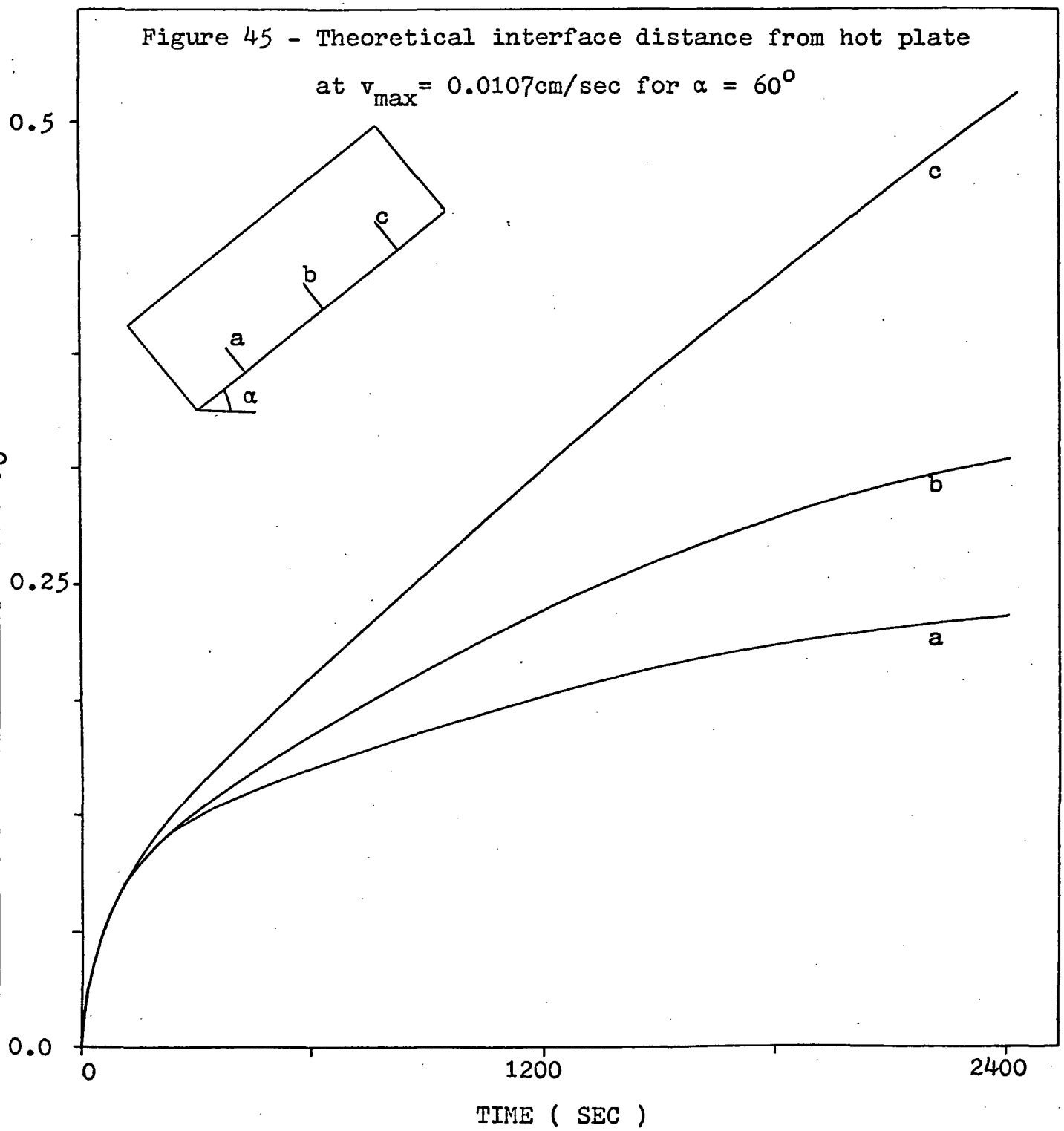

Figure 46 - Theoretical interface distance from hot plate at v_{max}= 0.00535cm/sec for $\alpha = 60^{o}$

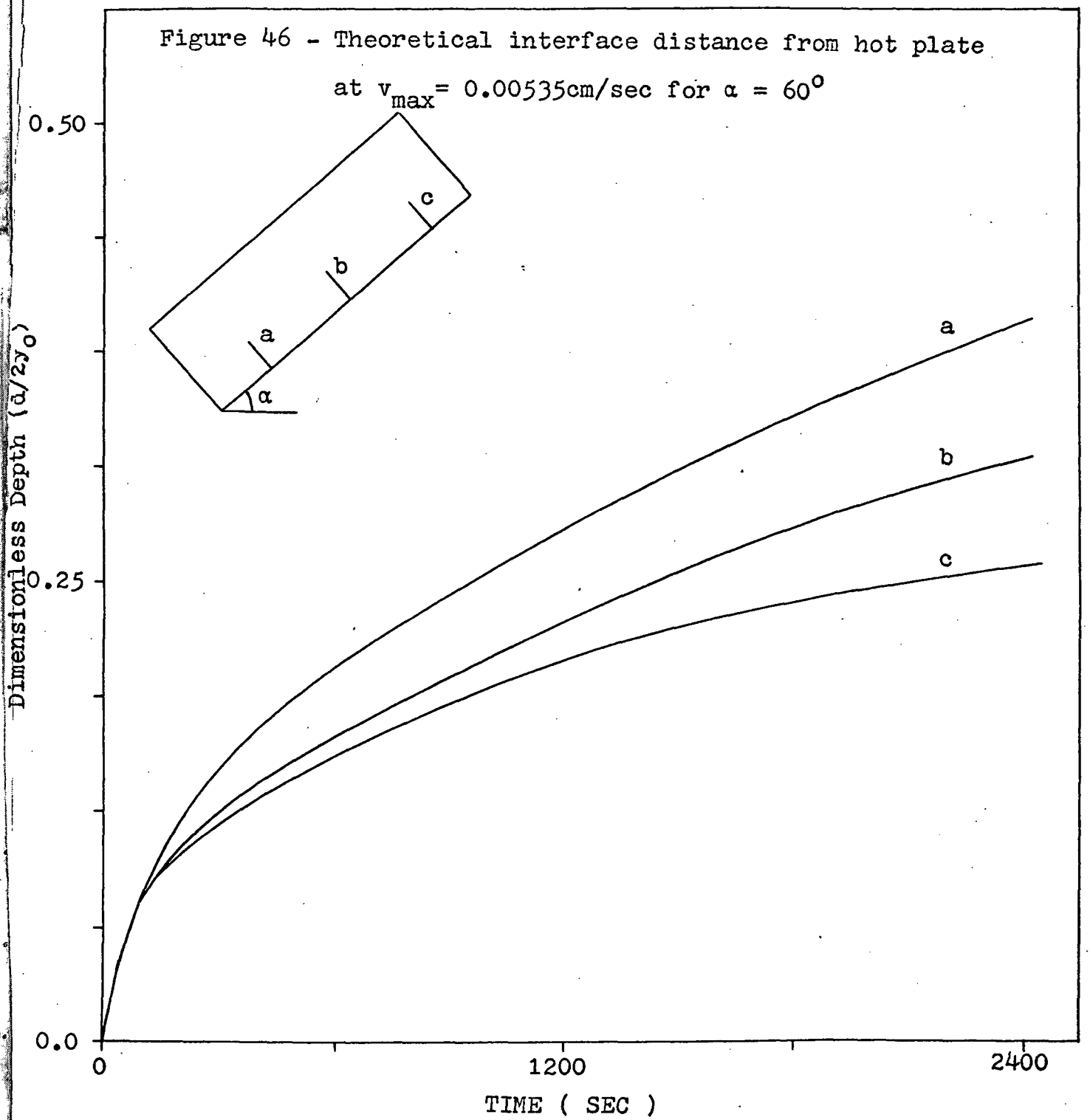

Figure 47 - Theoretical interface distance from hot plate at v_{max} = 0.002675cm/sec for $\alpha = 60^{o}$

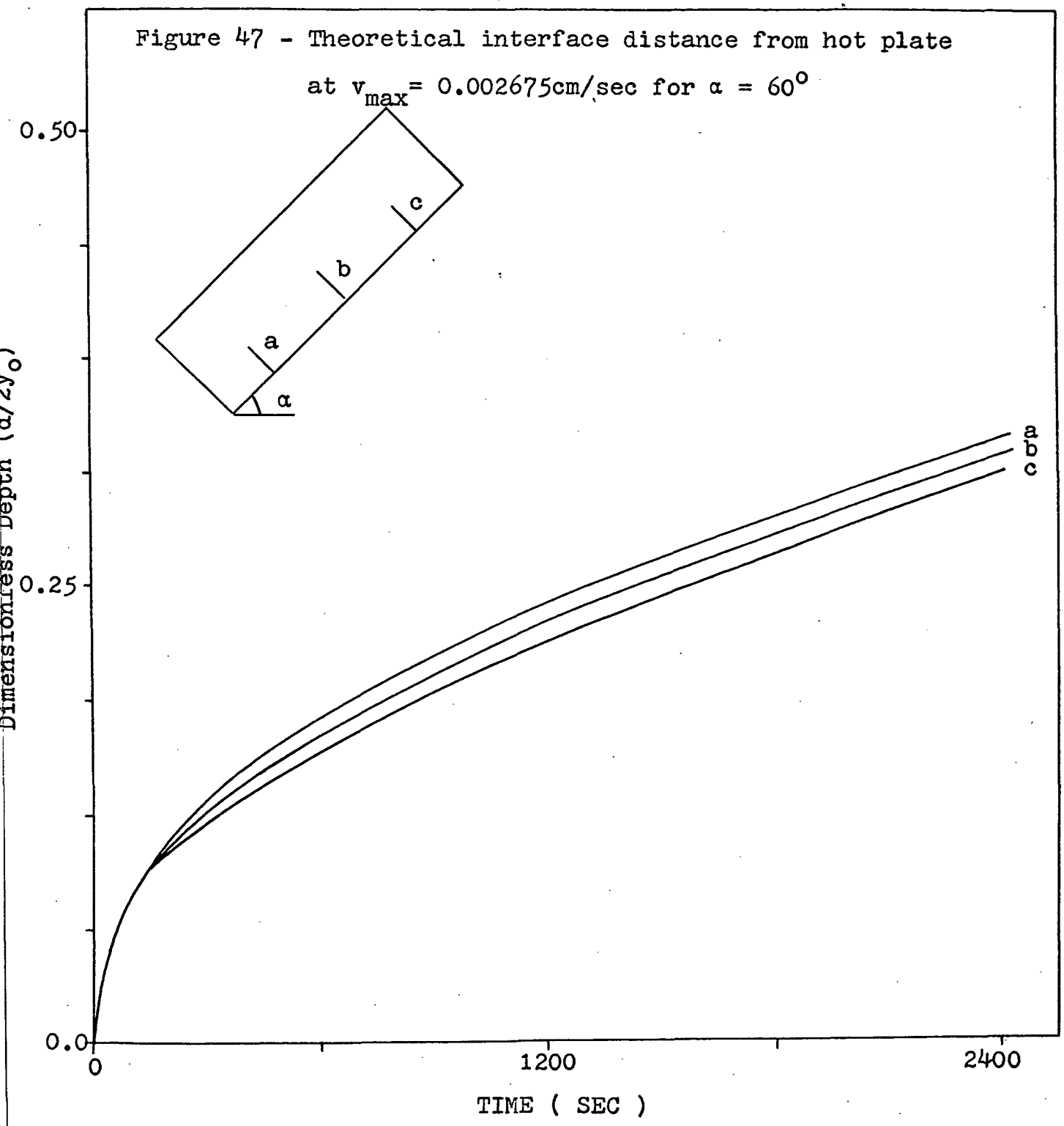

Figure 48 - Effect of velocity level on temperature profile

(a) at y = 0.635 cm, x = 10.160cm, α= 60°

(b) at y = 0.635 cm, x = 5.715cm, α= 60°

(c) at y = 0.635 cm, x = 1.905cm, α= 60°

Legend:

1 - convection model, v_{max}= 0.0107 cm/sec

2 - convection model, v_{max}= 0.00535 cm/sec

3 - convection model, v_{max}= 0.002675 cm/sec

4 - pure conduction model

⊙ - experimental data, Run 10

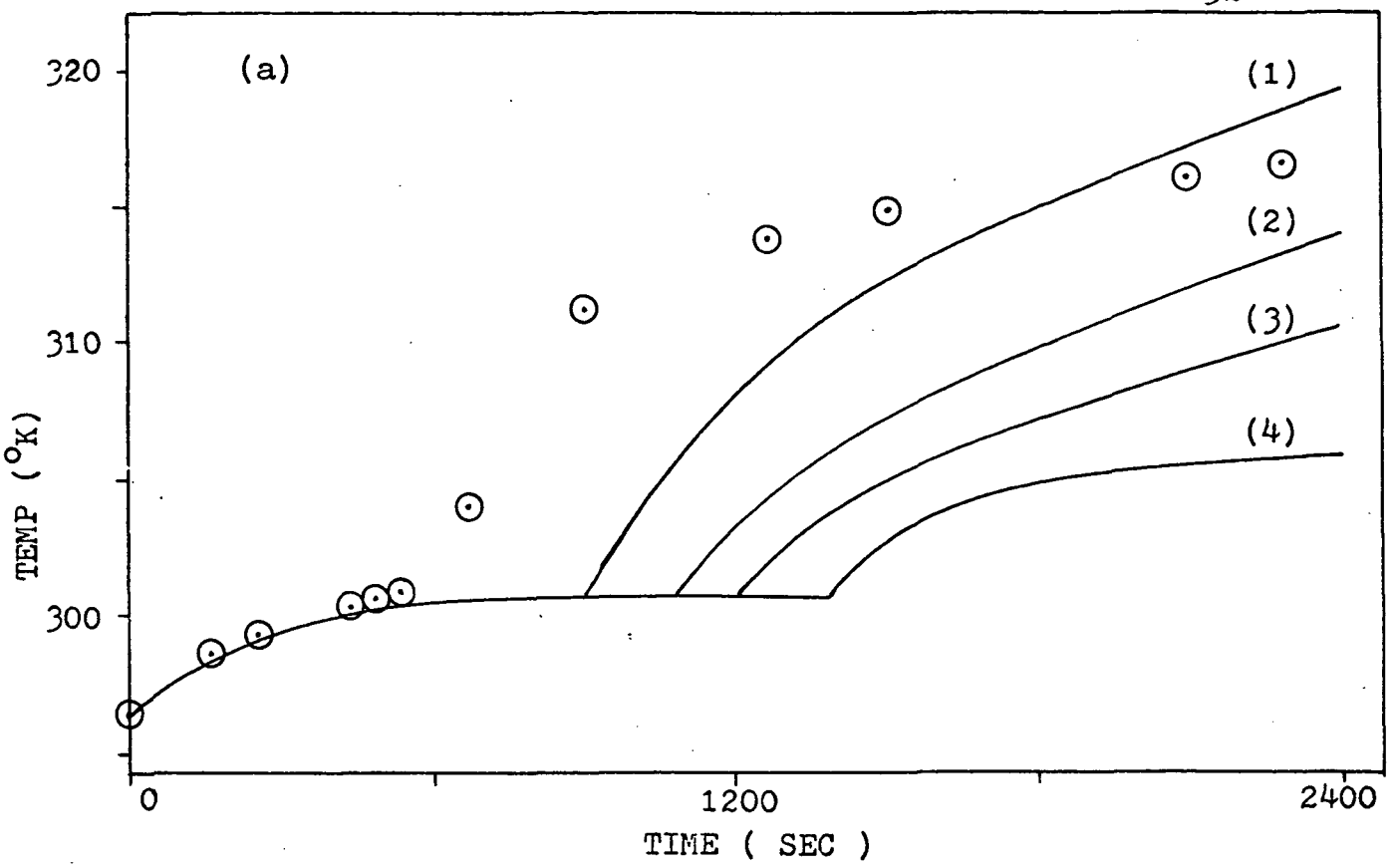
(a)
320
310
300
TEMP (°K)
(1)
(2)
(3)
(4)
0
1200
2400
TIME (SEC)

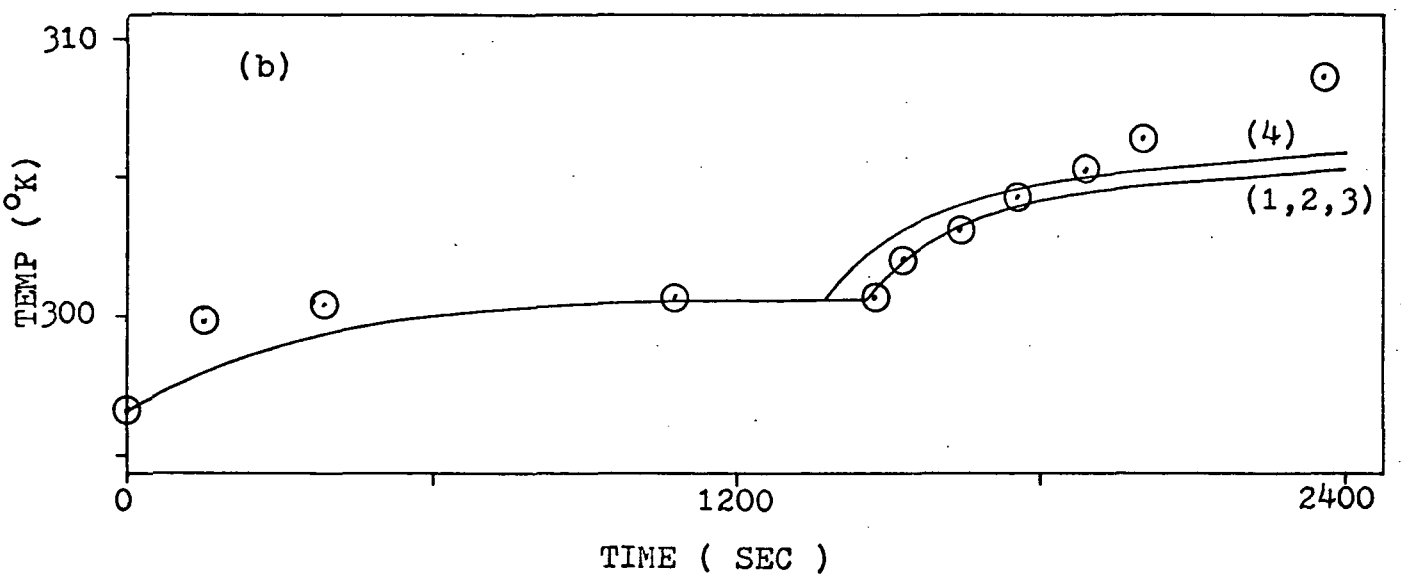
(b)
310
300
TEMP (°K)
(4)
(1,2,3)
0
1200
2400
TIME (SEC)

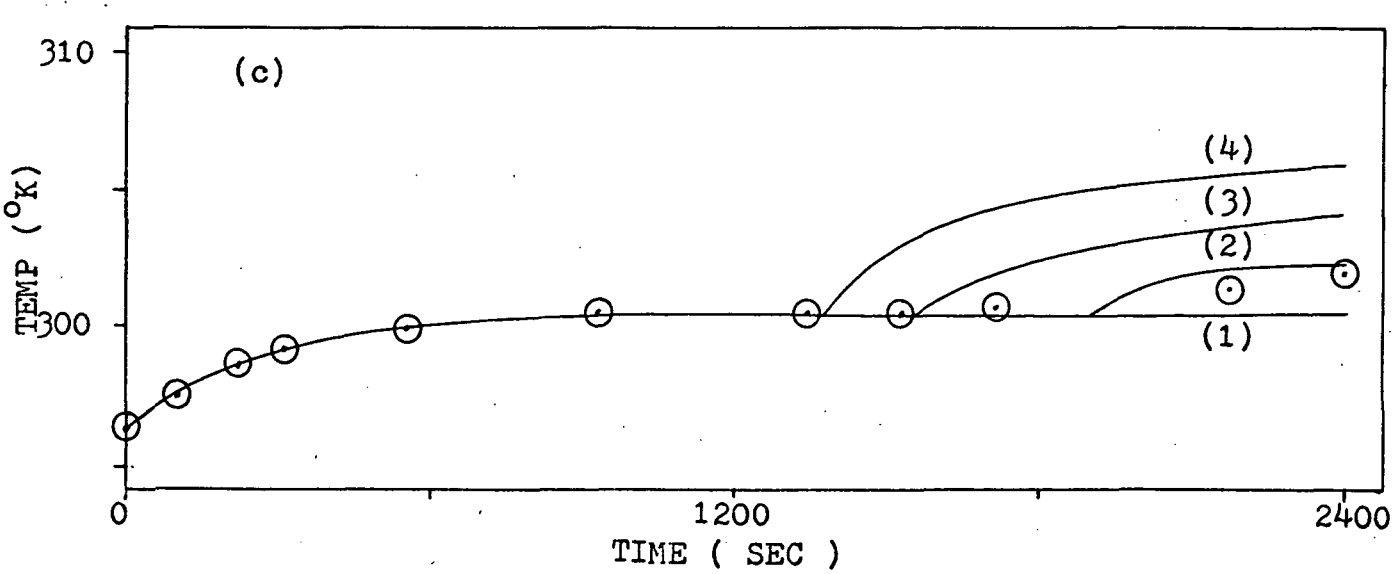
(c)
310
300
TEMP (°K)
(4)
(3)
(2)
(1)
0
1200
2400
TIME (SEC)

Figure 49 - Effect of numerical dispersion on temperature profile

(a) at y = 0.635 cm, x = 10.160 cm, $\alpha = 60^{\circ}$

(b) at y = 0.635 cm, x = 5.715 cm, $\alpha = 60^{\circ}$

(c) at y = 0.635 cm, x = 1.905 cm, $\alpha = 60^{\circ}$

Legend:

1 - v_{max} = 0.0107 cm/sec, Δt = 1.0 sec

2 - v_{max} = 0.0107 cm/sec, Δt = 1.5 sec

3 - v_{max} = 0.0107 cm/sec, Δt = 2.0 sec

⊙ - experimental data, Run 10

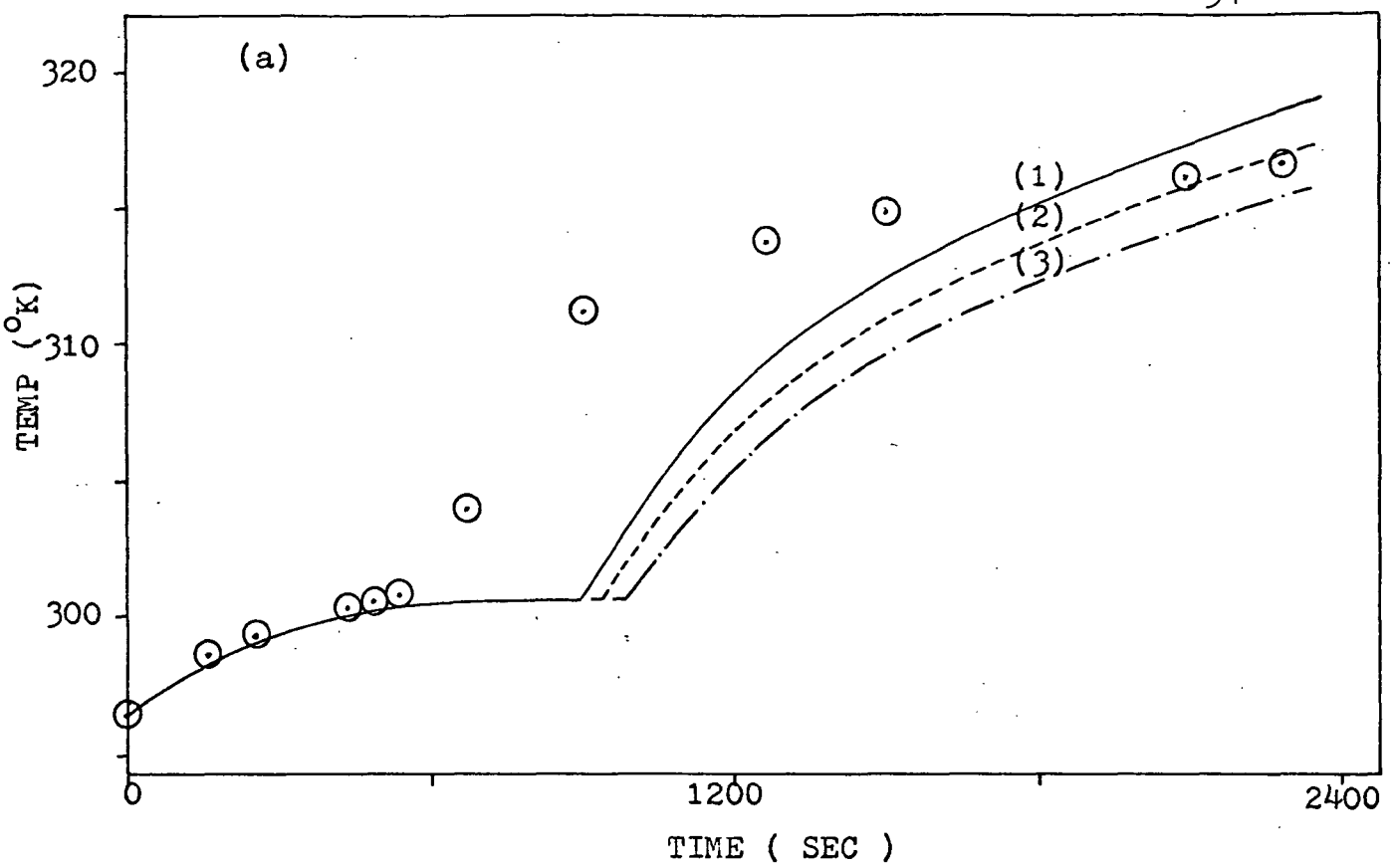
(a)
320
310
300
TEMP (°K)
(1)
(2)
(3)
0
1200
2400
TIME (SEC)

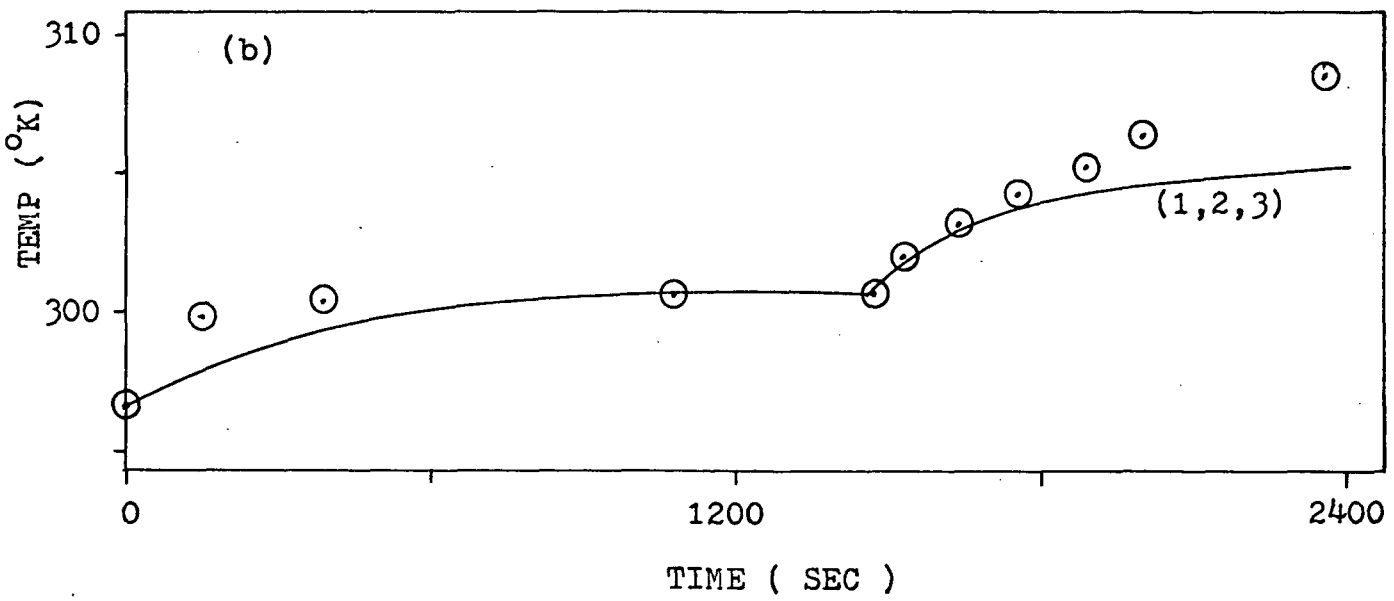
(b)
310
300
TEMP (°K)
(1,2,3)
0
1200
2400
TIME (SEC)

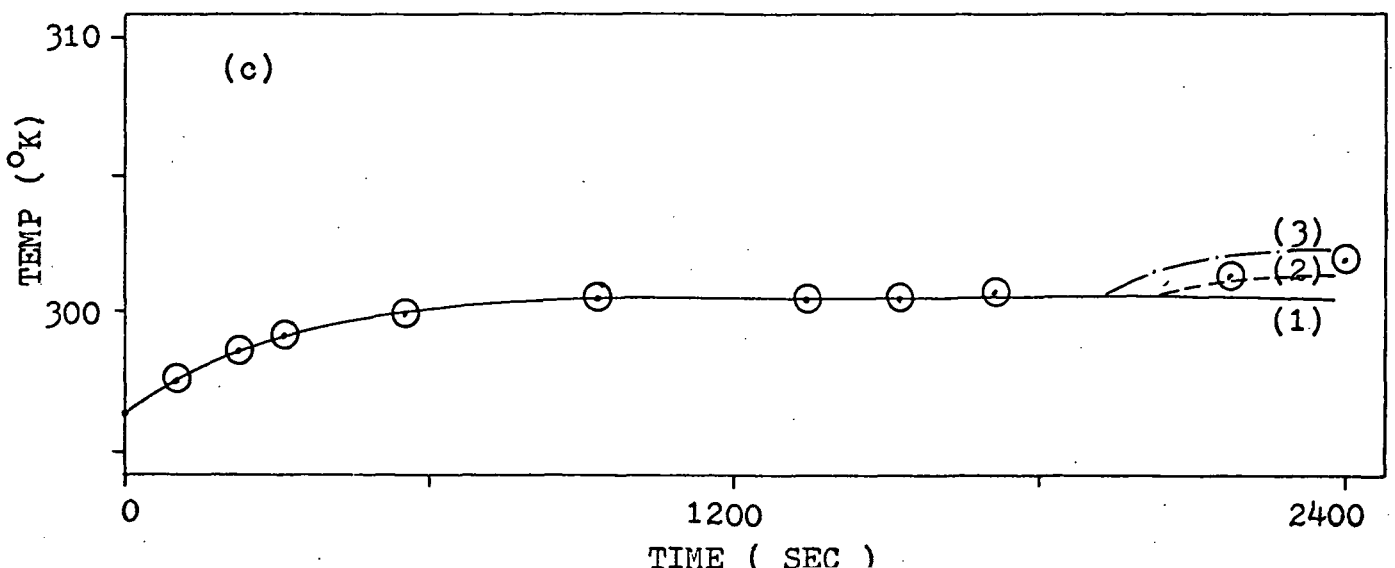
(c)
310
300
TEMP (°K)
(3)
(2)
(1)
0
1200
2400
TIME (SEC)

CONCLUSIONS

The following conclusions were drawn from this study:

1. The study has demonstrated that gravity-induced free convection greatly alters the melting interface profile and the temperature profiles of individual nodes within the phase change material.

2. The results show that the pure conduction model cannot predict gravity effects. In cases where convection is not present the pure conduction model does a good job of modeling the phase change process.

3. The convection model shows good agreement with experimental data. The velocity profile model is accurate enough to give temperature profiles to be used in the preliminary design of phase-change thermal control packages.

4. It was not possible to determine an approximate gravity level. Methods have been suggested[10] that relate a critical Rayleigh number to the velocity level. However, literature values for the critical Rayleigh number vary from 600 to 4000[31] for conditions similar to the one being studied. Therefore, any Rayleigh number in the range could be used to determine a gravity level which would justify the theoretical model. However, there is no basis for choosing a given Rayleigh number. Because of the uncertainty in the value of the Rayleigh number, we cannot state that the results correlate with a known gravity level. We can, however, evaluate convection effects in terms of the maximum velocity parameter and thus investigate convection effects in phase change devices.

5. Within the accuracy of numerical convection solutions obtained, the results indicate that gravity-induced free convection may be neglected at velocity levels less than 0.002675 cm/sec.

6. The experimental investigation has shown that air bubbles have a large effect upon the performance characteristics of the phase change material.

7. Sources of error in the numerical solution are:

   (a) numerical dispersion effects
   (b) arbitary flow profiles
   (c) stability limitations
   (d) constant maximum velocity

8. The method of solution is an initial solution to the phenomena of gravity-induced free convection in the liquefaction of a phase change material. The study has indicated problem areas in numerical solutions of the physical situation and has shown that further work is needed if complete solutions to the problem are to be realized.

RECOMMENDATIONS

The following recommendations are made as a result of this study.

1. Because of the large effect that air bubbles have upon the performance of the phase change material, further investigation should be made on methods of proper degassing of phase change materials.

2. A theoretical investigation should be made to determine the proper form of finite difference approximation needed to introduce an equation of state for density into the mathematical model for velocity.

3. An experimental study using tracer materials in the phase change system should be undertaken to determine the actual shape of convection induced velocity profiles in liquifaction and solidification phenomena. The measurement equipment should be photographic or microphotographic equipment.

4. A study should be made to determine the magnitude of gravity-induced free convection effects upon PCM performance in a PCM-filler system.

5. Because of the problems encountered in the theoretical modeling of the convection phenomena, a material investigation study should be made to determine whether or not low density polymers, which demonstrate a solid-solid phase change of proper magnitude in the proper temperature range, would make feasible phase-change materials. This type of material could be modeled using only a pure conduction model.

6. Further studies should be made, using a phase change material which has physical properties such that the stability criteria developed in the finite difference approximation for the vorticity equation is the governing stability criteria for the theoretical model. Then, given a computer with large enough memory capacity, the convection-conduction system could be accurately modeled.

LITERATURE CITED

1. Pujado, P. R., "Melting of a Finite Paraffin Slab," Thesis no. T-1215, Colorado School of Mines, Golden, Colorado (1968).

2. Bentilla, E. W., Stewart, K.F., and Kane, L.E., Final Report, Contract No. NAS-8-11163, Northrup Space Laboratories, Hawthorne, California, April, (1968).

3. Carslaw, H.S., and Jaeger, J.C., Conduction of Heat in Solida, Oxford University Press, (1959).

4. Rohsenow, , and Choi, , Heat, Mass, and Momentum Transfer, Prentice-Hall, Inc., Englewood Cliffs, N.J., (1961).

5. Schlicting, H., Boundary Layer Theory, McGraw-Hill Book Co., New York, N.Y., (1960).

6. Longwell, P.A., Mechanics of Fluid Flow, McGraw-Hill Book Co., New York, N.Y., (1966).

7. Dusinberre, G.M., Heat-Transfer Calculations by Finite Differences, International Textbook Corp., Scranton, P.A., (1961).

8. Bird, R.B., Stewart, W.E., and Lightfoot, E.N.; Transport Phenomena, John Wiley and Sons, Inc., New York, N.Y., (1960).

9. Vallentine, H. R., Applied Hydrodynamics, Butterworth and Co., Limited, London, England, (1959).

10. Grodzka, P.G., and Fan C., "Thermal Control by Freezing and Melting - Space Thermal Control Control Study," Lockheed Missles and Space Company, Huntsville, Alabama, Interim Report, Contract No. NAS-8-21123, March, (1968).

11. Bodoia, J. R., and Osterle, J. F., "Development of Free Convection between Vertical Heated Plates," Jour. Heat Transfer., Trans A.S.M.E., v 84, n 1, Feb. 1962, p. 40-44.

12. Dropkin, D., and Globe, S., "Natural Convection Heat Transfer in Liquids Confined by Two Horizontal Plates and Heated from Below, " Jour. Heat Transfer, Trans A.S.M.E., v 81, n 1, Feb. 1959, p. 24-28.

13. Dropkin, D., and Somerscales, E., "Heat Transfer by Natural Convection in Liquids Confined by Two Parallel Plates which are Inclined at Various Angles with Respect to Horizontal," Jour. Heat Transfer, Trans. A.S.M.E., v 90 n 1, Feb. 1968, p. 77-84.

14. Gebhart, B., "Transient Natural Convection from Vertical Element, "Jour. Heat Transfer, Trans. A.S.E.I., v 83, n 1, Feb. 1961, p. 61-70.

15. Koh, J.C., and Price, J.F., "Laminar Free Convection from a Non-Isothermal Cylinder," Jour. Heat Transfer, Trans. A.S.M.E., v 87, n 2, May 1965, p. 237-242.

16. Samuels, M.R., and Churchill, S.W., "Stability of a Fluid in a Rectangular Region Heated from Below," A.I.Ch.E. Jour, v 13, n 1, Jan. 1967, p. 77-85.

17. Wilkes, J.O., and Churchill, S. W., "The Finite-Difference Computation of Natural Convection in a Rectangular Enclosure," A.I.Ch.E. Jour, v 12, n 1, Jan. 1966, p. 161-166.

18. Peaceman, D. W., and Rachford, H. H., "The Numerical Solution of Parabolic and Elliptic Differential Equations," J. Soc. Indust. Appl. Math., v 3, n 1, March 1955, p. 28-41.

19. Bellamy-Knights, P.G., "An Unsteady Two-cell Vortex Solution of the Navier-Stokes Equations," J. Fluid Mechanics, v 41, 29 April, 1970, p. 673-687.

20. Fromm, J., "The Time Dependent Flow of an Incompressible Viscous Fluid," Methods In Computational Physics, Academic Press, New York, N.Y, 1964, p. 346-382.

21. Chi-Tien and Yim-Chao Yen, "Approximate Solution of a Melting Problem with Natural Convection," Chem. Eng. Prog. Symposium Ser., v 62, n 64 1966, p. 166-172.

22. Goodman, T.R., and Shea, J.J., "The Melting of Finite Slabs," J. Appl Mech., Trans. A.S.M.E., Feb., 1960, p. 16-24.

23. Bannister, T.C., and Bentilla, E.W., "Study on Thermal Control by Use of Fusible Materials," Proceedings of Annual Technical Meeting, Institute of Environmental Sciences, 1966, p. 593-607.

24. Ukanwa, A.O., Stermole, F.J., and Golden, J.O., "Phase Change Solidification Dynamics," Jour. of Spacecrafts and Rockets, v 8, n 2, Feb., 1971, p. 193-196.

25. Shah, A.P., "A Microscopic and Thermal Study of the Solidification of n-octadecane," Thesis No. T-1334, Colorado School of Mines, Golden, Colorado, 1970.

26. Emery, A.F., "The Effect of a Magnetic Field Upon the Free Convection of a Conducting Fluid," Jour Heat Transfer, Trans. A.S.M.E. v 85, n 2, May, 1963, p. 119-124.

27. Pearson, J.R.A., "On Convection Cells Induced by Surface Tension," Jour. Fluid Mechanics, v 4, 1958, p. 489-500.

28. Nield, D. A., "Surface Tension and Buoyancy Effects in Cellular Convection," Jour. Fluid Mechanics, v 19, 1964, p. 341-352.

29. Chandrasekhar, S., Hydrodynamic and Hydromagnetic Stability, Clarendon Press, Oxford, England, 1961.

30. Maxwell, J. B., Data Book on Hydrocarbons, Van Nostrand Co., Inc., New York, N.Y., 1950, p. 161.

31. Sparrow, E. N., Goldstein, R. J., and Jonsson, V. K., Jour. Fluid Mechanics, v 18, p 513 (1964).

Nomenclature

Definition:

Given that $s = f(x,y,t)$, then the following definitions are true:

$$s_t = \frac{\delta s}{\delta t},\ s_x = \frac{\delta s}{\delta x},\ s_y = \frac{\delta s}{\delta y},\ s_{tt} = \frac{\delta^2 s}{\delta t^2},\ s_{xx} = \frac{\delta^2 s}{\delta x^2},$$

$$s_{yy} = \frac{\delta^2 s}{\delta y^2},\ s_{xy} = \frac{\delta^2 s}{\delta x \delta y}$$

Parallel Flow Model:

b = one-half of distance between parallel walls, cm

g = acceleration of gravity, cm^2/sec

ΔT = temperature gradient between parallel walls, ^oK

y = distance from centerline, cm

η = y/b

β = coefficient of thermal expansion, $^oK^{-1}$

ρ = density, grams/cubic cm

μ = viscosity, gm $cm^{-1}sec^{-1}$

Ideal Flow Model:

a,b,c = real constants in ascending order of magnitude

A',B' = complex constants

t,w,z = complex planes

u = x-direction velocity, cm/sec

v = y-direction velocity, cm/sec

x = spatial dimension in complex z plane, cm

y = spatial dimension in complex z plane, cm

φ = potential function, sec^{-1}

ψ = stream function, sec^{-1}

Finite Difference Models:

c_p = heat capacity, watt·sec gm^{-1} $^oK^{-1}$

ΔH = latent heat of fusion, watts sec gm^{-1}

k = thermal conductivity, watts cm^{-1} $^oK^{-1}$

T = temperature, ^oK

$\mathbf{u}$ = x-direction velocity, cm/sec

$\mathbf{v}$ = y-direction velocity, cm/sec

x = spatial direction, cm

y = spatial direction, cm

α = angle of inclination, degrees

ρ = density, gm/cc

θ = time, sec

$\Delta\theta$ = time step, sec

ν = kinematic viscosity, centistokes

Subscripts:

f,i,l,o,p,s = fusion, initial, liquid, cold plate, hot plate, solid, respectively

Superscript:

* = at new time step

Pure Conduction Computer Program:

AHF = latent heat of fusion, Btu/lb

AKL = liquid phase thermal conductivity, Btu (ft sec $^{o}F)^{-1}$

AKS = solid phase thermal conductivity, Btu (ft sec $^{o}F)^{-1}$

CPL = liquid phase heat capacity, Btu (lb $^{o}F)^{-1}$

CPS = solid phase heat capacity, Btu (lb $^{o}F)^{-1}$

DT = time step, sec

DX = spatial increment, x-direction, inches

DY = spatial increment, y-direction, inches

RHOL = liquid phase density, lb/ cubic ft

RHOS = solid phase density, lb/ cubic ft

T = temperature, ^{o}F

TAU = initial time, sec

TE = excess degrees, ^{o}F

TF = fusion temperature, ^{o}F

TO = cold plate temperature, ^{o}F

TP = hot plate temperature, ^{o}F

Combined Model Computer Program:

AHF = latent heat of fusion, Btu/lb

AL = liquid phase thermal diffusivity, ft^2/sec

AS = solid phase thermal diffusivity, ft^2/sec

DX = spatial increment, x-direction, ft

DY = spatial increment, y-direction, ft

R = phase indicator

T = temperature at old time step, ^{o}F

TD = time increment, sec

TI = elapsed experimental time, sec

TF = phase change temperature, ^{o}F
TN = temperature at new time step, ^{o}F
TO = cold plate temperature, ^{o}F
TP = hot plate temperature, ^{o}F
UX = x-direction velocity, ft/sec
UY = y-direction velocity, ft/sec

APPENDIX A

The experimental data for this study is given in the following study:

> Bain, R. L., "The Effect of Gravity-Induced Free Convection Upon the Melting Phenomena of a Finite Paraffin Slab for Thermal Control," Thesis No. T 1319, Colorado School of Mines, Golden, Colorado, 1971.

APPENDIX B

Discussion of Other Theoretical Models

Other theoretical models were developed in this study, but due to stability requirements and other numerical difficulties it is not possible to use these models as solutions at the present time. Only one development is presented in this section; this model seems to have the best possible application to the problem of gravity-induced free convection effects in solid-liquid phase change.

The basic equations used in this development are the equations of motion, energy, and continuity.[8] These equations are given below:

Motion

$$u_t+uu_x+vu_y = \nu(u_{xx}+u_{yy})-q(T-T_a) \tag{29}$$

where

$$q=\frac{-ag\sin\alpha}{\rho_a}$$

and,

$$v_t+uv_x+vv_y = \nu(v_{xx}+v_{yy})-r(T-T'_a) \tag{30}$$

where

$$r=\frac{-ag\cos\alpha}{\rho_a}$$

Continuity

$$u_x+v_y = 0 \tag{31}$$

Energy

$$T_t+uT_x+vT_y = \frac{k}{\rho c_p}(T_{xx}+T_{yy}) \tag{32}$$

The stream function and vorticity, defined below, are introduced after the equations of motion are differentiated, the u equation with respect to y and the v equation with respect to x, and the equation of the difference between the two developed.

Stream function

$$\left.\begin{aligned} u &= \varphi_y \\ v &= -\varphi_x \end{aligned}\right\} \tag{33}$$

Vorticity

$$\lambda = -\varphi^2 = -u_y + v_x \tag{34}$$

The resulting vorticity equation is given below:

$$\lambda_t + (u\lambda)_x + (v\lambda)_y = (\lambda_{xx} + \lambda_{yy}) - qT_y - rT_x \tag{35}$$

The equation of continuity is inherently satisfied by the vorticity equation. Equations 32, 33, and 35 are then put into finite difference form; these equations are used, with appropriate boundary conditions, to model the liquid phase. Methods of finite difference formulation of these equations are presented by Wilkes[17] and Fromm.[32]

There are two problems present in the theoretical approach which make the solution meaningless at the present time. First, the base temperatures, T_a and T_a', in the gravity approximation are not well defined. Average values of the liquid phase temperature give temperature driving forces which cause velocities to exceed stability criteria after one time step. Therefore, before any finite difference solution using this gravity approximation can be made further investigation needs to be made in two areas. The first area to be studied is the correct determination of values of T_a and T_a' to be used in the gravity approximation. The second area to be studied is alternate finite difference formulations of the gravity approximation in order to reduce the magnitude of the gravity effect in the finite difference formulation.

An implicit finite difference technique can be used to eliminate stability requirements with respect to the magnitude of the time step; but a stability requirement still exists with respect to the maximum allowable velocity. The stability requirements for velocity in the energy equations are given by equations 12 and 13. The stability requirements for velocity in the vorticity equation are

$$u(n,m) - 2\nu/\Delta x \geq 0 \tag{36}$$

$$v(n,m) - 2\nu/\Delta x \geq 0 \qquad (37)$$

In the finite difference solution velocities velocities are calculated from the vorticity and stream function equations, then used in the solution of the energy equation. Therefore, to ensure a stable solution the properties of the test material must be such that

$$\nu > k/\rho c_p \qquad (38)$$

Otherwise, velocities may be calculated which are stable in the vorticity equation, but which cause the energy equation to be unstable. N-octadecane does not exhibit this property.

APPENDIX C

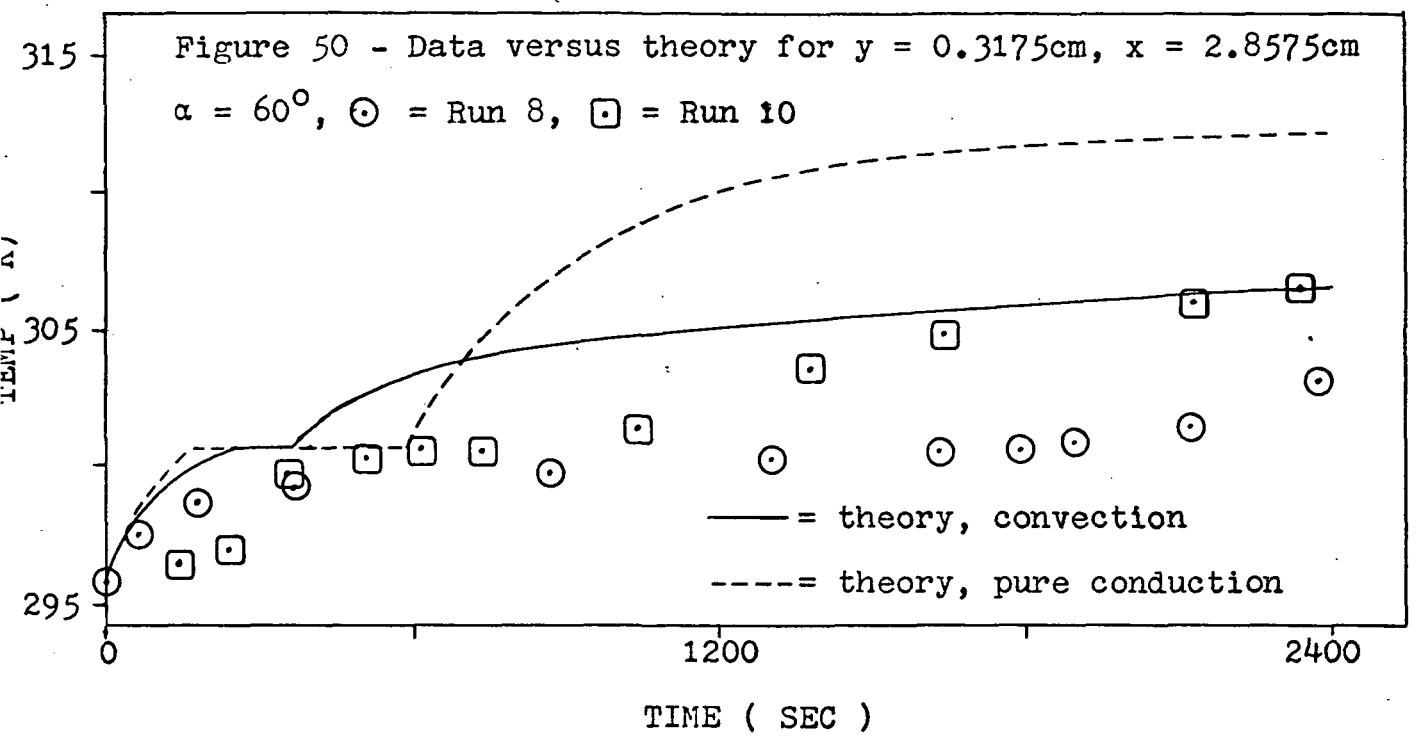

Figure 50 - Data versus theory for y = 0.3175cm, x = 2.8575cm
$\alpha = 60^{\circ}$, ⊙ = Run 8, ⊡ = Run 10

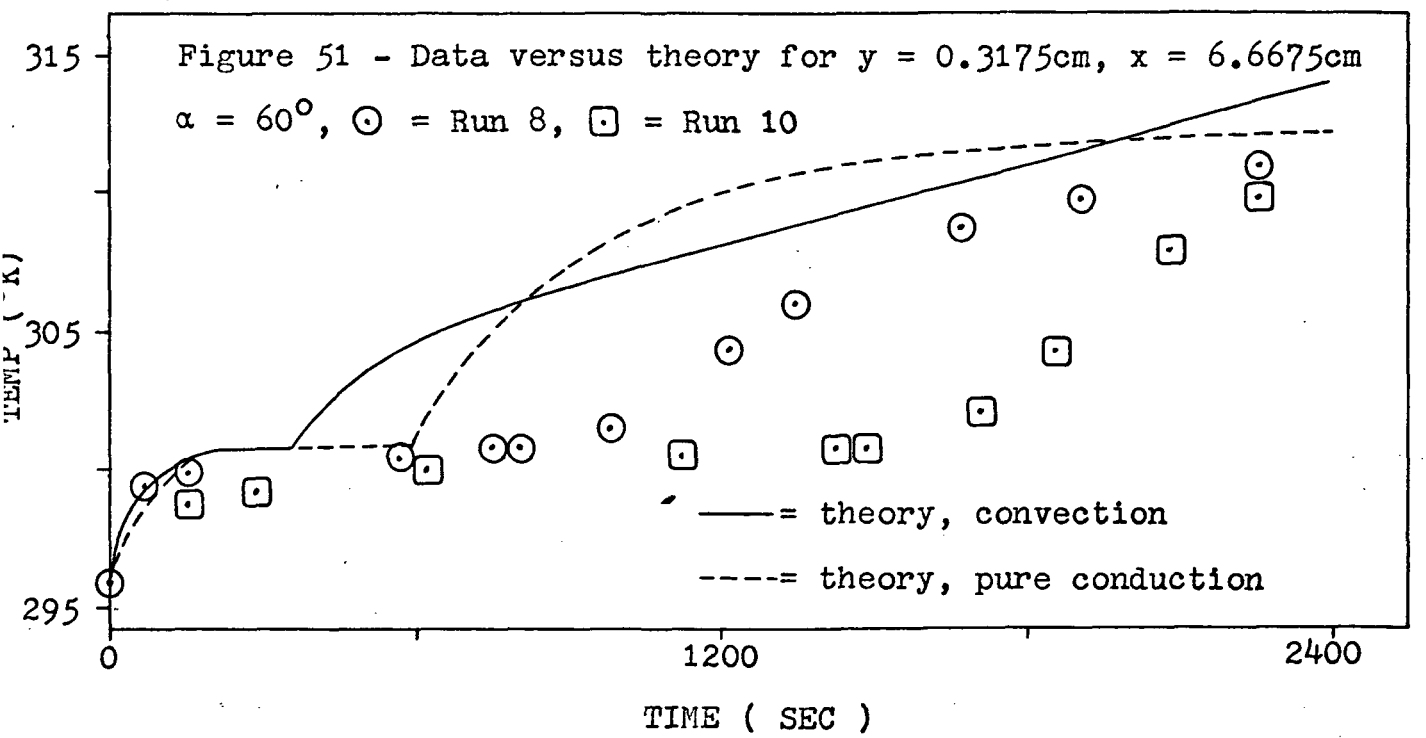

Figure 51 - Data versus theory for y = 0.3175cm, x = 6.6675cm
$\alpha = 60^{\circ}$, ⊙ = Run 8, ⊡ = Run 10

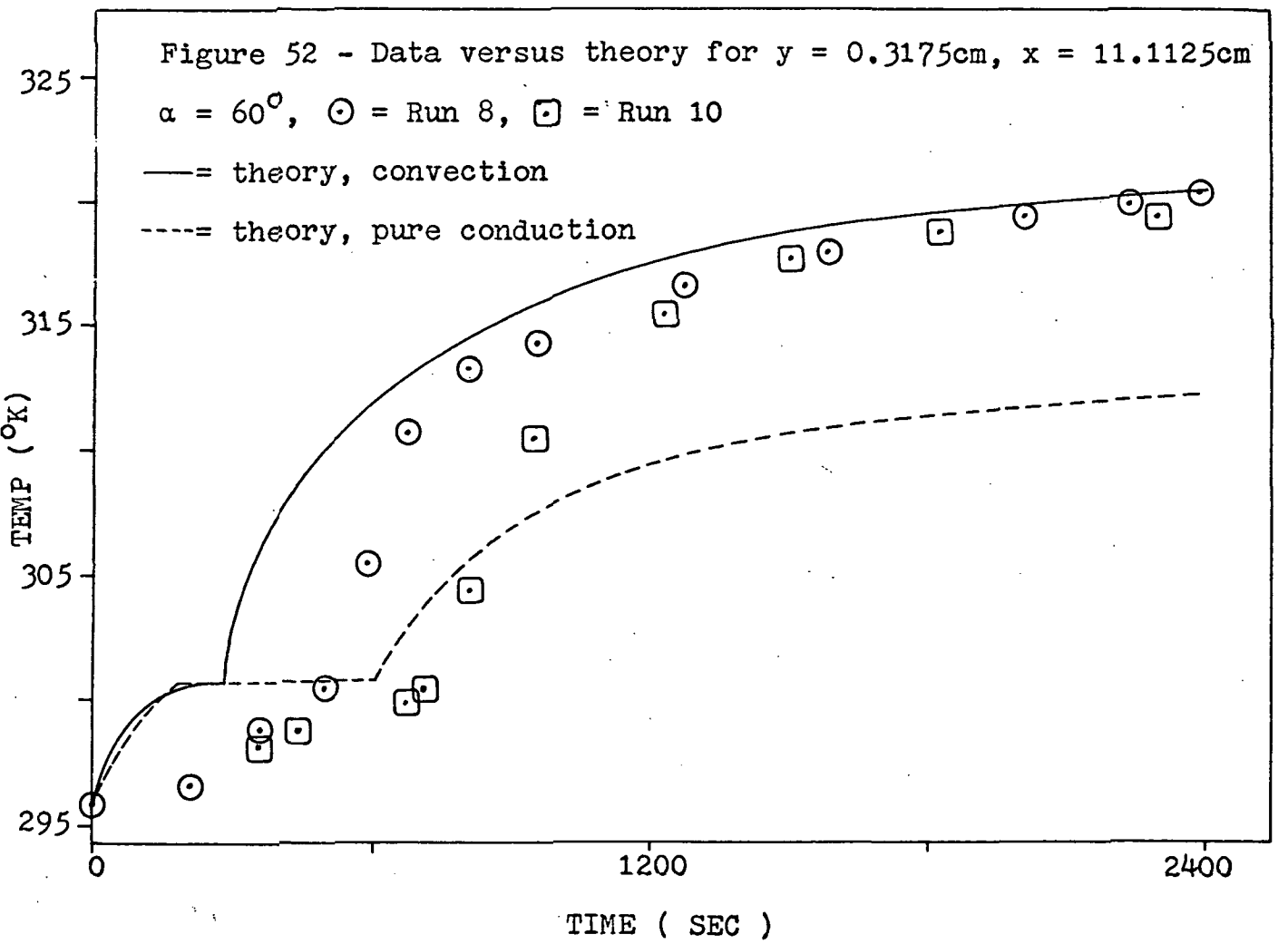
Figure 52 - Data versus theory for y = 0.3175cm, x = 11.1125cm
α = 60°, ⊙ = Run 8, ⊡ = Run 10
——= theory, convection
----= theory, pure conduction
325
315
305
295
TEMP (°K)
0
1200
2400
TIME (SEC)

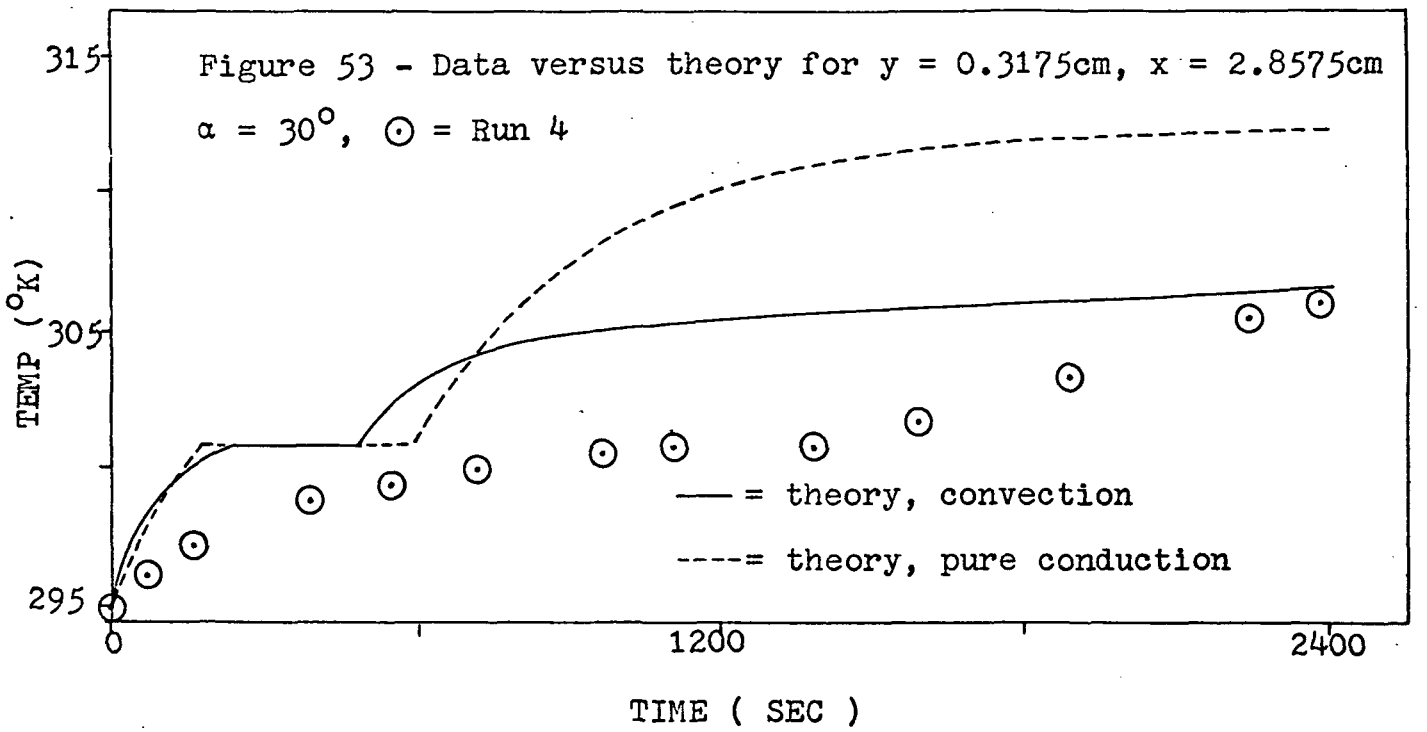

Figure 53 - Data versus theory for y = 0.3175cm, x = 2.8575cm
$\alpha = 30^{\circ}$, ⊙ = Run 4

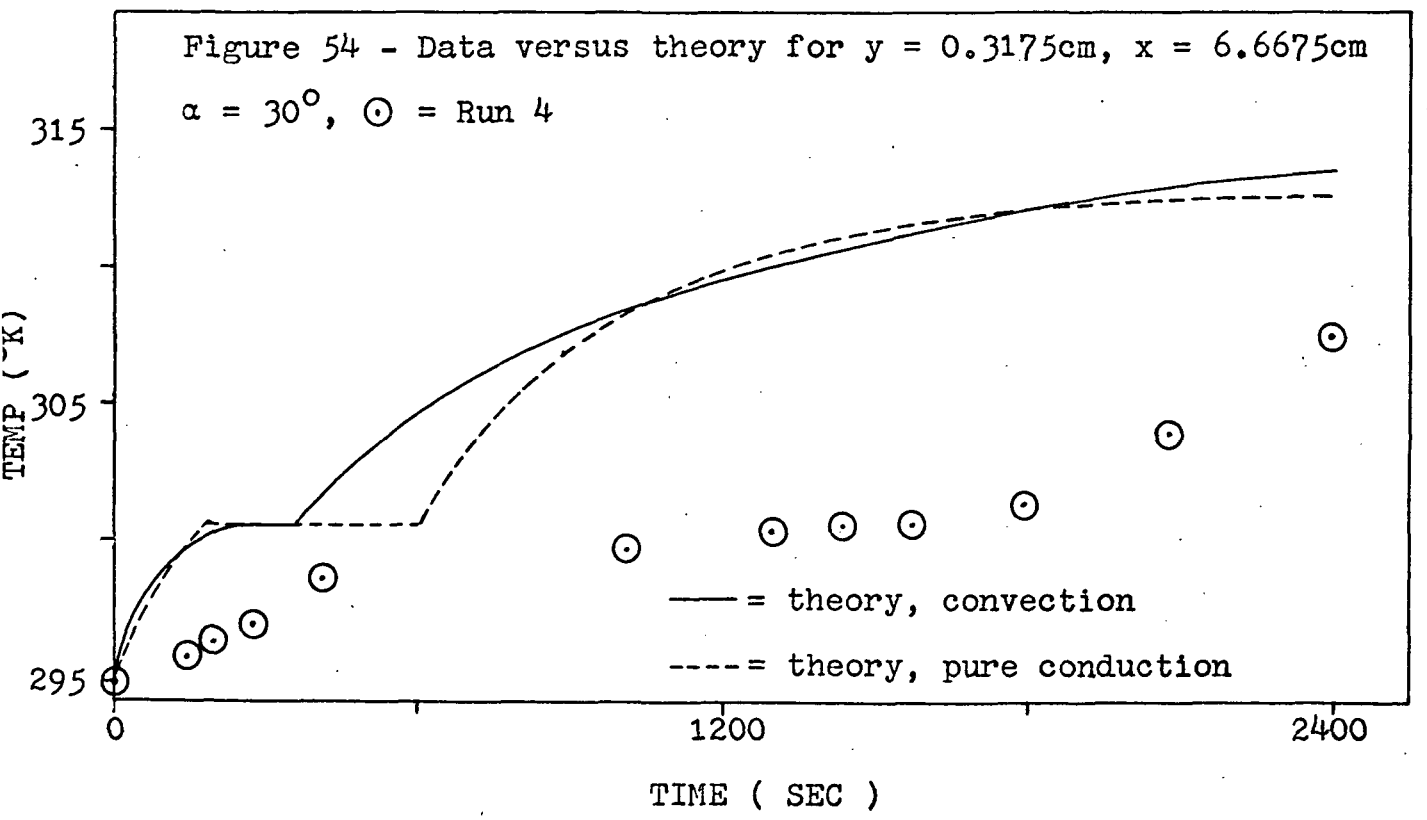

Figure 54 - Data versus theory for y = 0.3175cm, x = 6.6675cm
$\alpha = 30^{\circ}$, ⊙ = Run 4

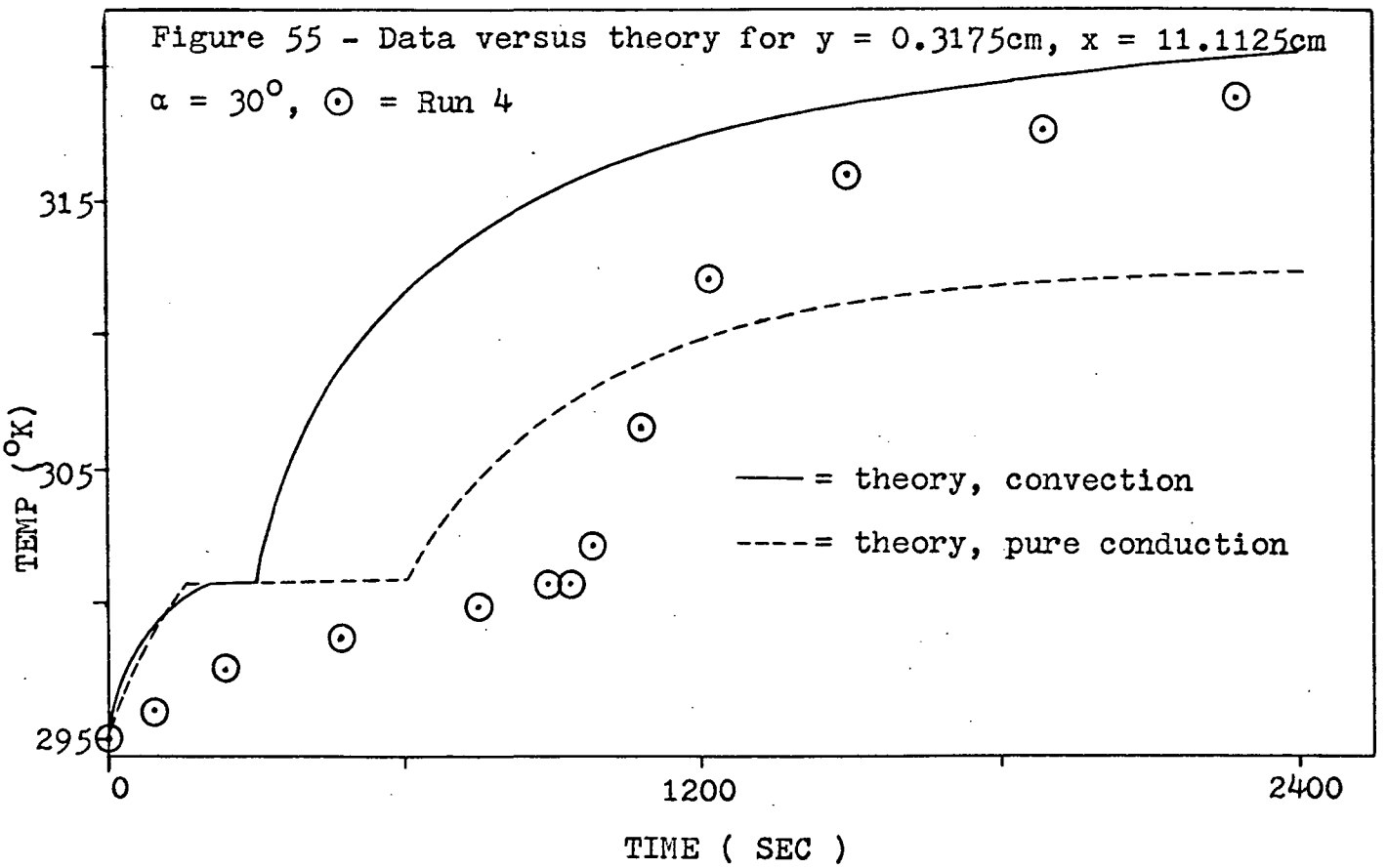
Figure 55 - Data versus theory for y = 0.3175cm, x = 11.1125cm
α = 30°, ⊙ = Run 4
315
305
295
TEMP (°K)
0
1200
2400
TIME (SEC)
—— = theory, convection
---- = theory, pure conduction

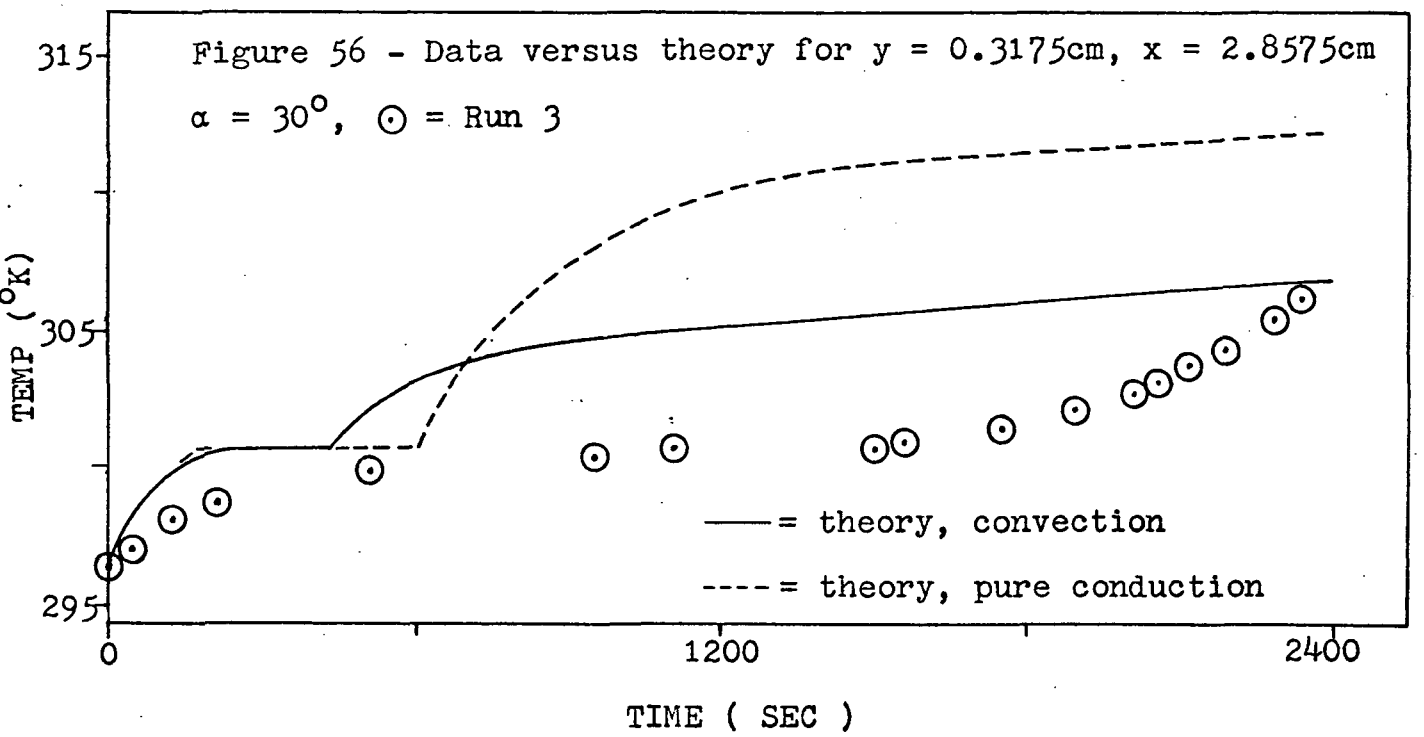

Figure 56 - Data versus theory for y = 0.3175cm, x = 2.8575cm
$\alpha = 30^{\circ}$, ⊙ = Run 3

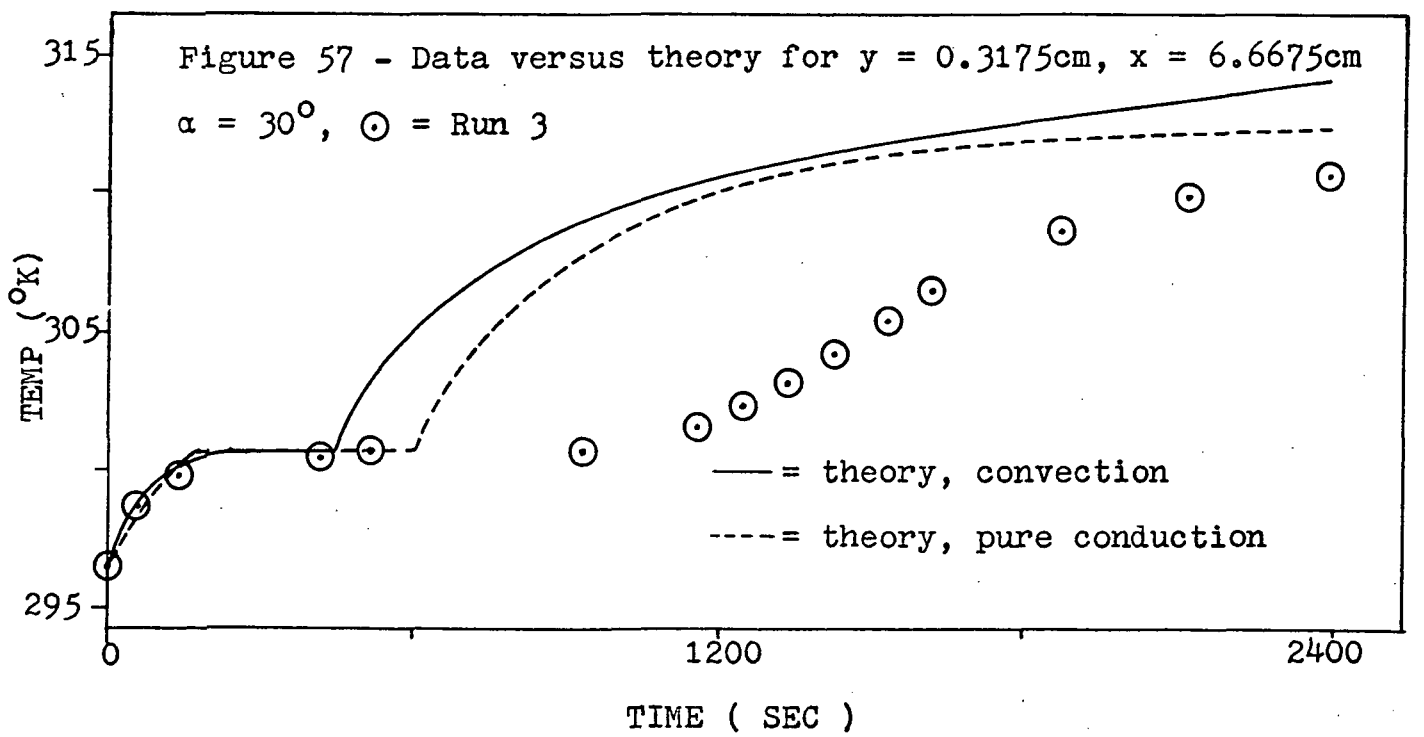

Figure 57 - Data versus theory for y = 0.3175cm, x = 6.6675cm
$\alpha = 30^{\circ}$, ⊙ = Run 3

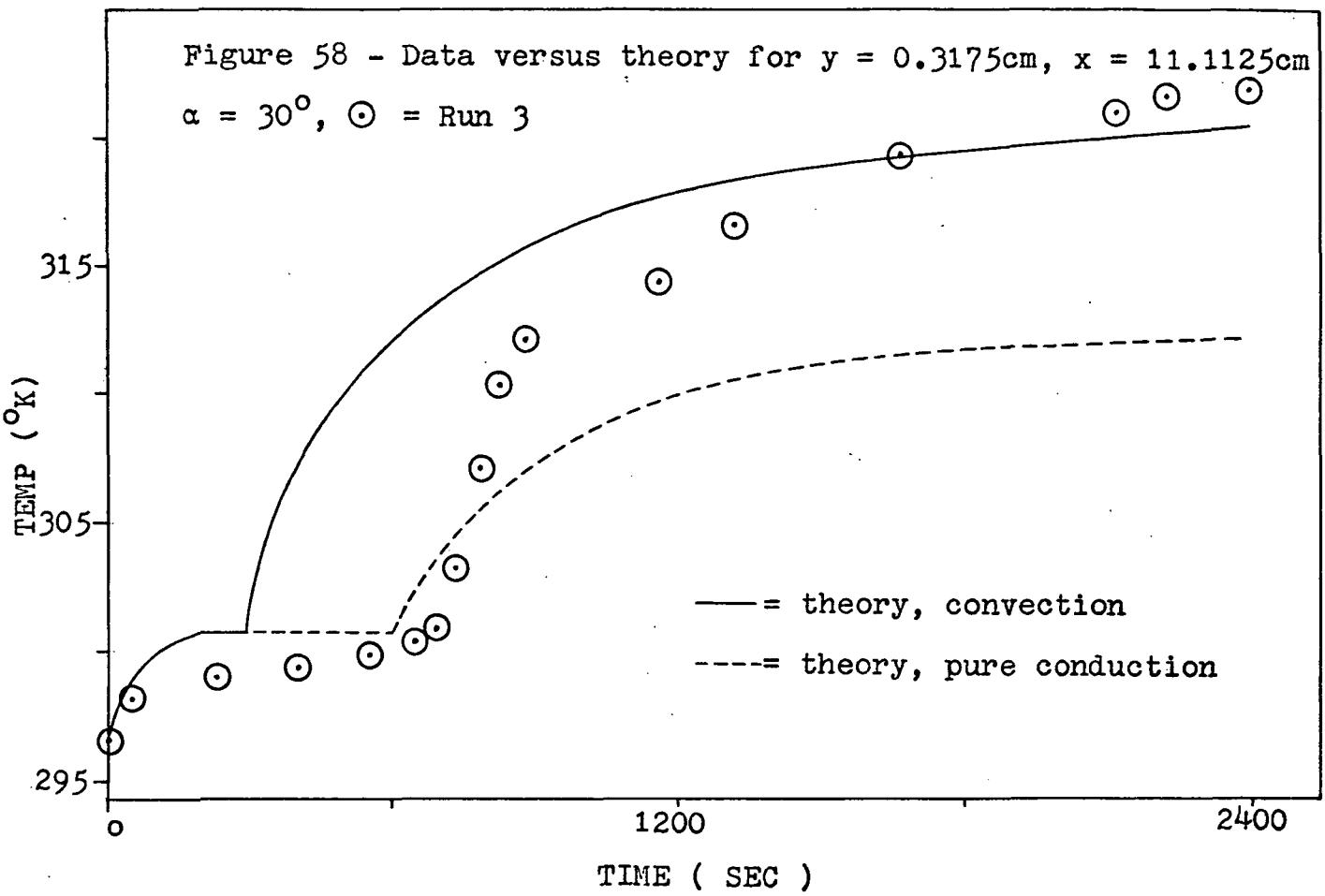
Figure 58 - Data versus theory for y = 0.3175cm, x = 11.1125cm
α = 30°, ⊙ = Run 3
315
305
295
TEMP (°K)
0
1200
2400
TIME (SEC)
—— = theory, convection
---- = theory, pure conduction

APPENDIX D

PURE CONDUCTION COMPUTER PROGRAM

This program was written in FORTRAN-II to solve a two-dimensional pure-conduction liquefaction problem. The program was run on a CDC-8090 computer. Consult nomenclature section for definition of terms.

Input file:

1. First card - DX, DY, TD, TAU, AHF, TF, TI
   where the format is (7F10.5), and

   DX [=] inches
   DY [=] inches
   TD [=] minutes
   TAU [=] minutes
   AHF [=] BTU/LB
   TF [=] ^{o}F
   TI [=] Min

2. Second card - AT, BT, CT, DT, ET, FT
   where the format is (5E16.8), and all variables are unitless. This is a dummy input file, to be used if a polynomial fit of hot plate temperature is desired; statement no 12 in the listing will have to be changed to polynomial form to use a polynomial fit. The polynomial is of the form

   $$T_p = AT * TAU^5 + BT* TAU^4 + CT * TAU^3 + DT * TAU^2 + ET * TAU + FT$$

3. Third card - ACT, BCT, CCT, DCT, ECT, FCT
   where the format is (5E16.8), and all variables are unitless. The polynomial is of the form

   $$T_o = ACT * TAU^5 + BCT * TAU^4 + CCT * TAU^3 + DCT * TAU^2 + ECT * TAU + FCT$$

4. Sample Input

   Card 1 - 0.250, 0.0625, 0.0, 104.90, 81.50, 0.98
   Card 2 - 0.1E-20, 0.1E-20, 0.1E-20, 0.1E-20, 0.1E-20, 0.1E-20
   Card 3 - -.109E-05, .11859E-03, -.4566E-02, .6941E-01, -.1157E + 00, .74487E + 02

Output file:

This program will print

1. Input variables
2. Time, t, at one minute intervals
3. Nodal Indicators for all nodes at time t
   Solid = +1
   Solid (at phase change temp.) = +3
   Liquid = -1

4. Temperatures ^{o}F , for all nodes at time t.

Note:

Subroutines TS1, TS2, and TL1 calculate the physical properties of n-octadecane as functions of temperature for solid, interface, and liquid phase nodes, respectively. For a different test material, these subroutines will have to be modified. The units used for physical properties in the subroutines are given below

C_p [=] Btu lb^{-1} $^{o}F^{-1}$

k [=] Btu (hr ft $^{o}F)^{-1}$

p [=] lb (cu. ft.)$^{-1}$

```
      DIMENSION T(22,18),CPS(22,18),CPL(22,18),AKS(22,18),AKL(22,18),RHO
     1S(22,18),RHOL(22,18),R(22,18),TE(22,18)
      COMMON TD,DX,DY
C READ DATA
      READ 1,DX,DY,TD,TAU,AHF,TF,TI
    1 FORMAT (7F10,5)
      PRINT 1,DX,DY,TD,TAU,AHF,TF,TI
      DX=DX/12,0
      DY=DY/12,0
      READ 2,AT,BT,CT,DT,ET,FT
      READ 2,ACT,BCT,CCT,DCT,ECT,FCT
    2 FORMAT (5E16,8)
      PRINT 2,AT,BT,CT,DT,ET,FT
      PRINT 2,ACT,BCT,CCT,DCT,ECT,FCT
C SET NODAL INDICATORS AND INITIAL CONDITIONS
      RMAX=0,0
      DO 8 M=1,18
      DO 8 N=1,22
      R(N,M)=1,0
      T(N,M)=FCT
      TE(N,M)=0,0
    8 CONTINUE
C CALCULATIONS
   10 TAU=TAU+TD
   12 TP=120,0
   13 TO=((((ACT*TAU+BCT)*TAU+CCT)*TAU+DCT)*TAU+ECT)*TAU+FCT
      DO 25 N=1,21
      T(N,1)=TP
   25 T(N,17)=TO
   24 FORMAT (2F10,5)
      IF (TP-TF) 29,29,27
   27 DO 28 M=2,16
      W=M
      T(1,M)=TF-(W/16,)*(TF-TO)
   28 T(21,M)=T(1,M)
      GO TO 99
   29 DO 39 M=2,16
      W=M
      T(1,M)=TP-(W/16,)*(TP-TO)
   39 T(21,M)=T(1,M)
   99 DO 50 M=2,16
      DO 40 N=2,20
      IF (R(N,M)) 30,100,15
   15 IF (R(N,M)-2,0) 31,100,35
      IF (T(N,M)-TF) 40,16,16
   31 CALL TS1(T,N,M,AS1,AS2,AS3,BS1,BS2,BS3)
      GO TO 36
   35 CALL TS2(T,N,M,AS1,AS2,AS3,BS1,BS2,BS3)
   36 T(N,M)=T(N,M)*(1,0-AS1*2,0-BS1*2,0)+AS2*T(N+1,M)+AS3*T(N-1,M)+BS2*
     1T(N,M+1)+BS3*T(N,M-1)
      IF(T(N,M)-TF) 40,16,16
   16 SUM=T(N,M)-TF
      SUM=SUM+TE(N,M)
      SA=(SUM-TF)*0,5170
      IF (SA-AHF) 18,17,17
   17 R(N,M)=-4,0
      GO TO 40
   18 T(N,M)=TF
      TE(N,M)=SUM
      R(N,M)=3,0
      IF (N-10) 40,37,40
```

```
   37 RMAX=M
      GO TO 40
   30 CALL TL1(T,N,M,AL1,AL2,AL3,BL1,BL2,BL3)
      T(N,M)=T(N,M)*(1,0-2,0*AL1-2,0*BL1)+AL2*T(N+1,M)+AL3*T(N-1,M)+BL2*
     1T(N,M+1)+BL3*T(N,M-1)
   40 CONTINUE
   50 CONTINUE
      IF (TAU-TI) 10,65,65
C PRINT RESULTS
   65 PRINT 66,TAU
   66 FORMAT (8H TIME = ,F10,5,1X,4H MIN)
   79 FORMAT (11F10,5)
      PRINT 78
   78 FORMAT (13H TEMPERATURE )
      PRINT 72
   72 FORMAT (11H0   N     M ,5X,5H TEMP)
      N=4
      M=5
      PRINT 73,N,M,T(N,M)
   73 FORMAT (2I5,F10,5)
      N=5
      M=9
      PRINT 73,N,M,T(N,M)
      N=5
      M=13
      PRINT 73,N,M,T(N,M)
      N=6
      M=3
      PRINT 73,N,M,T(N,M)
      N=10
      M=5
      PRINT 73,N,M,T(N,M)
      N=11
      M=9
      PRINT 73,N,M,T(N,M)
      N=11
      M=13
      PRINT 73,N,M,T(N,M)
      N=12
      M=3
      PRINT 73,N,M,T(N,M)
      N=16
      M=5
      PRINT 73,N,M,T(N,M)
      N=16
      M=9
      PRINT 73,N,M,T(N,M)
      N=17
      M=13
      PRINT 73,N,M,T(N,M)
      N=17
      M=3
      PRINT 73,N,M,T(N,M)
      IF (TI-39,9) 82,82,100
   82 TI=TI+1,00
      GO TO 10
  100 STOP
      END
      SUBROUTINE TS1(N,M,AS1,AS2,AS3,BS1,BS2,BS3)
      DIMENSION CPS(22,18),AKS(22,18),RHOS(22,18),T(22,18)
      COMMON TO,DX,DY
```

```
CPS(N,M)=0,517
CPS(N-1,M)=0,517
CPS(N+1,M)=0,517
CPS (N,M+1)=0,517
CPS(N,M-1)=0,517
RHOS(N,M)=0,0160*T(N,M)+54,65
RHOS(N+1,M)=0,0160*T(N+1,M)+54,65
RHOS(N-1,M)=0,0160*T(N-1,M)+54,65
RHOS(N,M+1)=0,0160*T(N,M+1)+54,65
RHOS(N,M-1)=0,0160*T(N,M-1)+54,65
AKS(N,M)=(-(,893E-4)*T(N,M)+0,0945)/60,0
AKS(N+1,M)=(-(,893E-4)*T(N+1,M)+0,0945)/60,0
AKS(N-1,M)=(-(,893E-4)*T(N-1,M)+0,0945)/60,0
AKS(N,M-1)=(-(,893E-4)*T(N,M-1)+0,0945)/60,0
AKS(N,M+1)=(-(,893E-4)*T(N,M+1)+0,0945)/60,0
AS1=(TD*AKS(N,M))/(DX*DX*RHOS(N,M)*CPS(N,M))
AS2=(TD*AKS(N+1,M))/(DX*DX*RHOS(N+1,M)*CPS(N+1,M))
AS3=(TD*AKS(N-1,M))/(DX*DX*RHOS(N-1,M)*CPS(N-1,M))
BS1=(TD*AKS(N,M))/(DY*DY*RHOS(N,M)*CPS(N,M))
BS2=(TD*AKS(N,M+1))/(DY*DY*RHOS(N,M+1)*CPS(N,M+1))
BS3=(TD*AKS(N,M-1))/(DY*DY*RHOS(N,M-1)*CPS(N,M-1))
RETURN
END
SUBROUTINE TS2(N,M,AS1,AS2,AS3,BS1,BS2,BS3)
DIMENSION CPS(22,18),AKS(22,18),RHOS(22,18),T(22,18)
COMMON TD,DX,DY
CPS(N,M)=0,517
CPS(N-1,M)=0,517
CPS(N+1,M)=0,517
CPS (N,M+1)=0,517
CPS(N,M-1)=,6057E-3*T(N,M-1)+0,4675
RHOS(N,M)=0,0160*T(N,M)+54,65
RHOS(N+1,M)=0,0160*T(N+1,M)+54,65
RHOS(N-1,M)=0,0160*T(N-1,M)+54,65
RHOS(N,M+1)=0,0160*T(N,M+1)+54,65
RHOS(N,M-1)=-0,0243*T(N,M-1)+50,5
AKS(N,M)=(-(,893E-4)*T(N,M)+0,0945)/60,0
AKS(N+1,M)=(-(,893E-4)*T(N+1,M)+0,0945)/60,0
AKS(N-1,M)=(-(,893E-4)*T(N-1,M)+0,0945)/60,0
AKS(N,M-1)=(-(,893E-4)*T(N,M-1)+0,0945)/60,0
AKS(N,M+1)=(-(,893E-4)*T(N,M+1)+0,0945)/60,0
AS1=(TD*AKS(N,M))/(DX*DX*RHOS(N,M)*CPS(N,M))
AS2=(TD*AKS(N+1,M))/(DX*DX*RHOS(N+1,M)*CPS(N+1,M))
AS3=(TD*AKS(N-1,M))/(DX*DX*RHOS(N-1,M)*CPS(N-1,M))
BS1=(TD*AKS(N,M))/(DY*DY*RHOS(N,M)*CPS(N,M))
BS2=(TD*AKS(N,M+1))/(DY*DY*RHOS(N,M+1)*CPS(N,M+1))
BS3=(TD*AKS(N,M-1))/(DY*DY*RHOS(N,M-1)*CPS(N,M-1))
RETURN
END
SUBROUTINE TL1(T,N,M,AL1,AL2,AL3,BL1,BL2,BL3)
DIMENSION CPL(22,18),AKL(22,18),RHOL(22,18),T(22,18)
COMMON TD,DX,DY
CPL(N,M)=,6057E-3*T(N,M)+0,4675
CPL(N+1,M)=,6057E-3*T(N+1,M)+0,4675
CPL(N-1,M)=,6057E-3*T(N-1,M)+0,4675
CPL(N,M+1)=,6057E-3*T(N,M+1)+0,4675
CPL(N,M-1)=,6357E-3*T(N,M-1)+0,4675
RHOL(N,M)=-,0240*T(N,M)+50,5
RHOL(N+1,M)=-0,0240*T(N+1,M)+50,5
RHOL(N-1,M)=-0,0240*T(N-1,M)+50,5
RHOL(N,M+1)=-0,0240*T(N,M+1)+50,5
```

```
AKL(N,M)=(-(,893E-4)*T(N,M)+0,0945)/60,0
AKL(N+1,M)=(-(,893E-4)*T(N+1,M)+0,0945)/60,0
AKL(N-1,M)=(-(,893E-4)*T(N-1,M)+0,0945)/60,0
AKL(N,M+1)=(-(,893E-4)*T(N,M+1)+0,0945)/60,0
AKL(N,M-1)=(-(,893E-4)*T(N,M-1)+0,0945)/60,0
AL1=(TD*AKL(N,M))/(DX*DX*RHOL(N,M)*CPL(N,M))
AL2=(TD*AKL(N+1,M))/(DX*DX*RHOL(N+1,M)*CPL(N+1,M))
AL3=(TD*AKL(N-1,M))/(DX*DX*RHOL(N-1,M)*CPL(N-1,M))
BL1=(TD*AKL(N,M))/(DY*DY*RHOL(N,M)*CPL(N,M))
BL2=(TD*AKL(N,M+1))/(DY*DY*RHOL(N,M+1)*CPL(N,M+1))
BL3=(TD*AKL(N,M-1))/(DY*DY*RHOL(N,M-1)*CPL(N,M-1))
RETURN
END
```

APPENDIX E

CONVECTION MODEL COMPUTER PROGRAM

This program was written in FORTRAN-IV to solve a liquefaction problem of n-octadecane under the influence of gravity-induced free convection. The program was run on a DEC, model PDP-10, computer. The program was written in specific, not general, terms for a given length to width ratio and a given number of nodes in spatial directions. See nomenclature section for definition of terms.

Input file:

1. For execution 4 = Input File or Input Device
2. First card -TD, DX, DY with a (3F) format where

   TD [=] sec
   DX [=] FT
   DY [=] FT

3. Second card - ACT, BCT, CCT, DCT, ECT, FCT, with a a (6E) format. See 3rd input card section in Appendix D for discussion of this input card.

Flag file:

1. For execution 6 = Flag File or Flag Device
2. Output -
   Time = (time in seconds)
   Input Flag (Hollerith Statement)
3. Input flag value - (F) format

   a. if flag < 10.0 -continue execution
   b. if flag ≥ 10.0 -stop execution

Output File:

1. For execution 5 = output file or device
2. Values of velocities for nodal system
3. time, t, at 120 second intervals
4. Temperatures of all nodes at 120 second intervals

Sample Input File:

First card - 1.0, .005208, .002604
Second card - -.109E-05, .11859E-03, -.4566E-02,
.6941E-01, -.1157E+00, .74487E+02

```
C       NOMENCLATURE-------
C               VMAX = MAXIMUM VELOCITY ALLOWABLE, FT/SEC
C               TD = TIME INCREMENT, SEC
C               DX = DELTA X, FT
C               DY = DELTA Y, FT
C               UX = X COMPONENT OF VELOCITY, FT/SEC
C               UY = Y COMPONENT OF VELOCITY, FT/SEC
C               T = TEMPERATURE AT OLD TIME STEP, DEG F
C               TN = TEMPERATURE AT NEW TIME STEP, DEG F
C               TP = TEMPERATURE OF HOT WALL, DEG F
C               TO = TEMPERATURE OF COLD WALL, DEG F
C               TF = PHASE CHANGE TEMPERATURE, DEG F
C               AS = SOLID PHASE THERMAL DIFFUSIVITY, FT**2/SEC
C               AL = LIQUID PHASE THERMAL DIFFUSIVITY, FT**2/SEC
C               AHF = LATENT HEAT OF FUSION, BTU/LB
C               TI = ELAPSED EXPERIMENTAL TIME, SEC
C               R = PHASE INDICATOR
C                       +1 IF LIQUID
C                       -1 IF SOLID
      DIMENSION UC(82,34),VC(82,34)
      DIMENSION T(82,34),TN(82,34),R(82,34),K(82,34),TE(82,34)
      DIMENSION UB(34),VO(82)
      DIMENSION VV(34),V(82,34),U(82,34),VB(34),SF(34),VO(34)
C   MAXIMUM VELOCITY CALCULATION
      DELT=10.0
      TD=0.2E-01
      VMAX=0.024*32.2*DELT*TD/50.5
      IF (ABS(VMAX).GE.0.250E-03) VMAX=0.250E-03
      V9=VMAX
C   COMBINED IDEAL-VISCOUS VELOCITY CALCULATION
      YV=-1.0
      B=1.0
      A=-1.0/SQRT(3.0)
      DO 10 I=2,32
      YV=YV+1.0/16.00
      C=YV/B
      RA=(C**3.-C)/(A**3.-A)
10    VV(I)=VMAX*RA
      PI=3.1415962
      Y=0.0
      DO 15 I=2,32
      Y=Y+1.0/32.00
      X=1.0
      SF(I)=SINH(PI*X)*SIN(PI*Y)
      UB(I)=-SINH(PI*X)*COS(PI*Y)*PI
15    VB(I)=COSH(PI*X)*SIN(PI*Y)*PI
      X=0.0
      Y=0.50
      DO 18 J=2,16
      X=X+1.0/32.0
18    VO(34-J)=PI*COSH(PI*X)*SIN(PI*Y)
      Y=0.50-1.0/32.0
      DO 36 M=17,32
      Y=Y+1.0/32.0
      X=0.0
      DO 36 N=2,16
      X=X+1.0/16.00
      SFT=SINH(PI*X)*SIN(PI*Y)
      U1=-SINH(PI*X)*COS(PI*Y)*PI
      DO 30 I=1,16
```

```
      KK=33-I
      IF (SFT.GE.SF(KK)) GO TO 30
      GO TO 31
30    CONTINUE
      KK=17
31    UMAX=UB(KK)
      UBO=VV(KK)
      U(N,M)=U1*UBO/UMAX
      VN=PI*COSH(PI*X)*SIN(PI*Y)
      V(N,M)=(1.0-ABS(VN/VB(KK)))*UBO
      IF (ABS(VN/VB(KK)).GE.1.00) V(N,M)=0.001*UBO
36    CONTINUE
      DO 40 M=2,16
      DO 40 N=2,16
      U(N,M)=-U(N,34-M)
      V(N,M)=V(N,34-M)
40    CONTINUE
      DO 50 M=2,32
      DO 50 N=17,65
      V(N,M)=0.1E-08
      U(N,M)=VV(M)
      IF (M.EQ.17) U(N,M)=0.1E-10
50    CONTINUE
      DO 60 M=2,32
      DO 60 N=66,80
      NN=N-65
      U(81-NN,M)=U(N-64,M)
      V(81-NN,M)=-V(N-64,M)
60    CONTINUE
C   PRINT COMBINED I-V VELOCITY VALUES
      DO 62 N=2,80
      DO 62 M=2,32
      AU=ABS(U(N,M))
      AV=ABS(V(N,M))
      IF (AU.GE.V9) GO TO 171
      IF (AV.GE.V9) GO TO 171
62    CONTINUE
      DO 65 M=2,32
      WRITE (5,63) M,(U(N,M),N=2,80)
63    FORMAT (I5,/,5X,(6E))
65    CONTINUE
      DO 70 M=2,32
      WRITE (5,68) M,(V(N,M),N=2,80)
68    FORMAT (I5,/,5X,(6E))
70    CONTINUE
      GO TO 71
171   WRITE (5,172)
172   FORMAT(' VELOCITY EXCEEDS STABLE VALUE ')
      GO TO 175
C   READ EXPERIMENTAL DATA AND INPUT PARAMETERS
71    READ (4,72) TO,DX,DY
72    FORMAT (3F)
      READ (4,74) ACT,BCT,CCT,DCT,ECT,FCT
74    FORMAT (6E)
C   SET INITIAL VALUES FOR TEMPERATURE AND FLAGS
      WRITE (5,72) TO,DX,DY
      WRITE (5,74) ACT,BCT,CCT,DCT,ECT,FCT
      TI=0.00
      ATI=119.90
      AHF=104.90
```

```
      TF=81.50
      TP=120.00
      TO=FCT
      DO 75 M=2,32
      DO 75 N=2,80
      NO(N)=1
      T(N,1)=TP
      T(N,33)=TO
      TN(N,M)=FCT
      TE(N,M)=0.000
      UC(N,M)=0.0000
      VC(N,M)=0.00
      T(N,M)=TO
      R(N,M)=-1.0
      K(N,M)=1
75    CONTINUE
180   TI=TI+TD
      TA=TI/60.0
      TO=((((ACT*TA+BCT)*TA+CCT)*TA+DCT)*TA+ECT)*TA+FCT
      DO 76 N=1,81
76    T(N,33)=TO
C     CALCULATE END WALL BOUNDARY VALUES
      J=33
      DO 78 M=2,32
      IF(R(2,M),GE,0,10) GO TO 78
      J=M
      GO TO 79
78    CONTINUE
79    DO 80 M=2,J
      W=J-1
      WT=M-1
80    T(1,M)=TP-(WT/W)*(TP-TF)
      IF (J,GE,33) GO TO 85
      JJ=J+1
      DO 81 M=JJ,32
      W=33-J
      WT=M-J
81    T(1,M)=TF-(WT/W)*(TF-TO)
      J=33
85    DO 82 M=2,32
      IF (R(80,M).GE,0.10) GO TO 82
      J=M
      GO TO 83
82    CONTINUE
83    DO 84 M=2,J
      W=J-1
      WT=M-1
84    T(81,M)=TP-(WT/W)*(TP-TF)
      IF (J,GE,33) GO TO 90
      JJ=J+1
      DO 86 M=JJ,32
      W=33-J
      WT=M-J
86    T(81,M)=TF-(WT/W)*(TF-TO)
C     SOLID PHASE CALCULATIONS
90    DO 110 N=2,80
      DO 110 M=2,32
      IF (R(N,M),GE,0.10) GO TO 110
      SUM=0.0
      AS=0.975E-06
```

```
      A=T(N,M)*(1.0-2.0*AS*TD/DX/DX-2.0*AS*TD/DY/DY)
      B=T(N+1,M)+T(N-1,M)
      C=AS*TD*0/DX/DX
      D=T(N,M+1)+T(N,M-1)
      E=AS*TD*0/DY/DY
      TN(N,M)=A+C+E
      IF (TN(N,M).GE.TF) GO TO 100
      GO TO 110
C     PHASE CHANGE CALCULATIONS
100   SUM=TN(N,M)-TF
      SUM=SUM+TE(N,M)
      SA=SUM*0.5170
      IF (SA-AHF) 101,101,102
101   TE(N,M)=SUM
      TN(N,M)=TF
      GO TO 110
102   R(N,M)=1.0
      K(N,M)=2
      TN(N,M)=TF+(SA-AHF)/0.5170
110   CONTINUE
C     LIQUID PHASE CALCULATIONS
      AL=0.950E-06
      DO 115 N=2,80
      DO 111 I=2,32
      J=I
      IF (R(N,I).LT.0.10) GO TO 112
111   CONTINUE
      NO(N)=33
      GO TO 115
112   NO(N)=J
115   CONTINUE
C     VELOCITY CONVERSION CALCULATIONS
120   DO 130 N=2,80
      L=NO(N)-1
      DO 130 I=2,L
      II=I-1
      JJ=NO(N)-1
      IF (JJ.LT.1) JJ=NO(N)
      S1=II/JJ
      IF (S1.GE.0.999) GO TO 128
      DO 125 J=2,32
      JK=J-1
      S2=JK/32
      IF (S2.LT.S1) GO TO 125
      UC(N,I)=U(N,J)
      VC(N,I)=V(N,J)
      GO TO 130
125   CONTINUE
      GO TO 130
128   UC(N,M)=0.1E-12
      VC(N,M)=0.1E-12
130   CONTINUE
C     L.P. CONVECTION ENERGY CALCULATIONS
      DO 135 N=2,80
      J=NO(N)-1
      IF (J.GE.33) J=32
      IF (J.LE.2) J=2
      DO 135 M=2,J
      IF (K(N,M).GT.1) GO TO 134
      IF (NO(N).LT.5) UC(N,M)=0.1E-12
```

```
      IF (NO(N),LT,5) VC(N,M)=0.1E-12
      A=T(N,M)*(1.0-2.0*AL*TD/DX/DX-2.0*AL*TD/DY/DY)
      B=T(N+1,M)*(AL*TD/DX/DX-UC(N,M)*TD/2.0/DX)
      C=T(N-1,M)*(AL*TD/DX/DX+UC(N,M)*TD/2.0/DX)
      D=T(N,M+1)*(AL*TD/DY/DY-VC(N,M)*TD/2.0/DY)
      E=T(N,M-1)*(AL*TD/DY/DY+VC(N,M)*TD/2.0/DY)
      TN(N,M)=A+B+C+D+E
      GO TO 135
134   K(N,M)=1
135   CONTINUE
161   DO 165 M=2,32
      DO 165 N=2,80
165   T(N,M)=TN(N,M)
C   PRINT TEMPERATURE PROFILES
      IF (ATI.GE.TI) GO TO 180
      WRITE (6,510) ATI
510   FORMAT (' TIME = ', F10.2/)
      ATI=ATI+120.0
      WRITE (5,166) TI
166   FORMAT (/,F,/)
      DO 170 M=2,32
      WRITE (5,168) M,(T(N,M),N=2,80)
168   FORMAT (I5,/,(6E))
170   CONTINUE
      WRITE (6,900) (T(N,2),N=1,81)
900   FORMAT (4E)
      WRITE (6,173)
173   FORMAT (' INPUT FLAG '/)
      READ (6,174) FLAG
174   FORMAT (F)
      IF (FLAG.GE.10.0) GO TO 175
      IF (TI.LE.2395.0) GO TO 180
175   STOP
      END
```